SIMULATION OF VISCOUS FLUID FLOWS USING A CONTROL VOLUME FINITE ELEMENT-MULTIGRID METHOD

CHUAN WANG

SIMULATION OF VISCOUS FLUID FLOWS USING A CONTROL VOLUME FINITE ELEMENT-MULTIGRID METHOD

BY

© CHUAN WANG

A thesis submitted to the School of Graduate Studies
in partial fulfillment of the requirements for the degree of
Master of Engineering

Faculty of Engineering & Applied Science
Memorial University of Newfoundland

September, 1995

St. John's Newfoundland Canada

ISBN 0-612-06155-8

Abstract

The formulation and implementation of an equal-order colocated control volume finite element-multigrid (CVFE-MG) method for steady, two-dimensional, viscous incompressible flows is presented in this thesis. In the proposed CVFE-MG, the calculation domain is discretized using three-node triangular elements. Each element is further divided in such a way that control volumes are formed around each node in the calculation domain. The proposed method is formulated using the velocity components and pressure as dependent variables, and interpolation functions for these dependent variables are all based on an elemental level. The pressure and the diffused scalars are interpolated linearly; the convected scalars are interpolated using mass weighted interpolation which guarantees positive contributions to the coefficients in the algebraic discretization equation; and the transporting velocities are interpolated using a linear interpolation of pseudo-velocities and pressure coefficients, in which the pressure gradients appear explicitly. This feature allows the formulation of an equal-order colocated method valid for incompressible flows. Using these interpolation functions, the discretized forms of the governing equations are obtained by deriving algebraic approximations to integral conservation equations for each control volume. These nonlinear, coupled, algebraic equations are then solved by a segregated solution algorithm. This solution method is implemented in the context of FMV- and V-cycle multigrid algorithms in an attempt to improve its convergence behaviour.

The proposed CVFE-MG method was found to generate solutions that could

capture the physical behaviour of the fluid flows used as test problems. The multigrid methods were found to accelerate the convergence rate 2.18 to 7.43 times for the outflow and recirculating flow test problems presented. The effectiveness of the multigrid algorithm was reduced for higher Reynolds numbers, due to the interpolation schemes used in the control volume finite element method (CVFEM).

The successful implementation of multigrid algorithms in the context of a primitive variables, viscous flow CVFEM is very encouraging. Further research will be performed to improve the effectiveness of CVFE-MG implementations.

Acknowledgments

I would like to express my deep gratitude to my supervisor, Dr. N.A.Hookey, for his assistance throughout this research program, especially in regard to his criticism of this thesis.

Financial support for this research was provided by the Natural Sciences and Engineering Research Council of Canada, the School of Graduate Studies and the Faculty of Engineering and Applied Science of Memorial University of Newfoundland. Also, fr omputing time was provided by the Center for Computer Aided Engineering.

Contents

List of Figures

List of Tables

Nomenclature

Symbol	Description
$\mathbf{A}$	matrix of a system of linear equations
A_e	area of a triangular element
a_i, a_n, d_i	coefficients in the discretized forms of the x, y momentum and continuity equations
a, b, c	coefficients in the interpolation functions for p, ϕ^d
c_p	specific heat at constant pressure
C_1, C_2, C_3	coefficients in the algebraic approximation of the integrated convection-diffusion flux across a control volume face
d^u, d^v	pressure coefficients derived from momentum equations
E_1, E_2, E_3, B	coefficients in the algebraic approximation of the integrated mass flux across a control volume face
det	value of determinant
ds	differential area
$\vec{\mathbf{e}}$	algebraic error vector
f	constant used in MAW scheme
$\vec{\mathbf{f}}$	constant vector of a system of linear equations
$\vec{g}$	mass flux vector
$\vec{i}, \vec{j}$	unit vectors in the x and y directions, respectively
I	interpolation or injection operator
$\vec{J}$	combined convection-diffusion flux vector
k	thermal conductivity

$\dot{m}$	a mass flux across a control volume face
N	total number of nodes in a discretized domain
$\vec{n}$	outward unit vector normal to the differential area $d\boldsymbol{s}$, or to a boundary
p	pressure
$\vec{\mathbf{r}}$	residual vector
S	volumetric source term
$\mathcal{S}$	generalized source term that includes S and pressure gradients
S_c, S_p	coefficients in the linearized expression for the source terms
Δs	area of a control volume surface
T	temperature
$\hat{u}$	pseudo-velocity, defined from momentum equations
u, v	velocity components in the x and y directions, respectively
$\vec{\mathbf{u}}$	exact solution vector of a system of linear equations
$\vec{v}$	velocity vector
$\vec{\mathbf{v}}$	approximation to the exact solution of a system of linear equations
$\Delta V, \partial V$	control volume, and surface of the control volume, respectively
x, y	axes and coordinates in the Cartesian coordinate system

Greek Symbols

α	under-relaxation parameter
Γ	diffusion coefficient for ϕ
μ	dynamic viscosity
Φ	nodal value of ϕ

ρ	mass density
ϕ	scalar dependent variable
Ω	calculation domain

Subscripts

av	average value within an element
H	value at the midpoint of a control volume face of an element
i	value at node i
$ip1, ip2$	integration points 1 and 2 used in the MAW scheme
M	value at the midpoint of a side of a triangular element
max, min	maximum and minimum values, respectively
n	neighbour node of node i
$spec$	specified value
u, v, p, T, ϕ	identify the coefficients in the u, v, p, T, ϕ interpolation functions, respectively
x, y	components in the x and y directions, respectively

Superscripts

c	pertains to discretization of convection terms
d	pertains to discretization of diffusion terms
$h, 2h...$	level of grids
k	control volume face k, where $k = 1, 2$
$*$	calculated value from a previous iteration

Chapter 1

Introduction

1.1 Aims and Motivation of the Thesis

Prediction of heat transfer and fluid flow processes can be obtained by two main methods: experimental investigation and theoretical calculation. This thesis concentrates on the latter. The main goal of this thesis is to develop, implement, and test a control volume finite element-multigrid (CVFE-MG) method for the simulation of steady, two-dimensional, viscous incompressible fluid flow problems. Such flows are frequently encountered in the aeronautical, power generation and environmental fields. Specific examples include internal combustion engines, nuclear reactors, heat exchangers, and effluent discharge into the environment.

The formulation of the proposed CVFE-MG is an extension of that used in earlier CVFE's [3, 4, 5, 7, 18, 19, 20, 30, 31, 32] for incompressible fluid flows. In the proposed control volume finite element method (CVFEM), triangular elements are used to discretize the calculation domain, and polygonal control volumes are constructed around each node in the domain. The mathematical model of the fluid flow is based on the so-called primitive variables, the velocity components, u and v, and the pressure p. Element-based interpolation functions for these dependent variables, and the method of weighted residuals (MWR) [15], are then used to de-

rive algebraic approximations to the governing equations. In this MWR, for each node in the calculation domain, the weighting function is set equal to one over the control volume associated with the node, and zero elsewhere. Thus, the proposed CVFEM for fluid flow and heat transfer involves the imposition of physical conservation principles on finite control volumes in the calculation domain,and hence its solutions satisfy global conservation requirements, even for coarse grids. In addition, this control volume based formulation facilitates physically meaningful interpretation of the various terms in the algebraic discretization equations.

The proposed CVFEM is an equal-ordered colocated method, in which pressure and velocity are evaluated at all grid points. Momentum and continuity equations are discretized using the same set of control volumes, and the pressure equation is solved by the same equation solver used for the other dependent variables. With this method, oscillatory solution fields are prevented by using so-called "mass conserving" velocity interpolation functions, in which the pressure gradient terms appear explicitly. When these functions are used to discretize the continuity equation, they lead to a set of strongly velocity-pressure-coupled algebraic equations from which the oscillatory solution fields could not appear.

The proposed CVFEM is limited to steady two-dimensional situations, however, its basic formulation can be easily extended to unsteady and three-dimensional problems using the procedures described in [29, 24, 25].

Thus far, CVFEM research has concentrated on the development of methods to simulate problems, without great concern for their efficiency. In this thesis, greater priority is given to algorithm and implementation efficiencies, and hence the multigrid techniques are employed. By introducing several grids and exchanging information between them in a sophisticated way, multigrid methods can solve large

sparse matrix elliptic problems in a dramatically more efficient way compared to conventional iterative algorithms on a single grid. In the proposed CVFE-MG, a multigrid method, along with a segregated iterative solution algorithm, is employed to solve the system of discretized governing equations.

1.2 Outline of the Thesis

This thesis consists of six chapters. In this chapter the aims and motivations of the thesis were presented. The remainder of this thesis describes the development, implementation, and testing of the proposed CVFE-MG.

Chapter 2 presents a synopsis of available CVFEM's for the solution of incompressible fluid flow problems. The formulation of the proposed two-dimensional CVFEM is presented in detail in Chapter 3. In Chapter 4, the fundamental principles of multigrid methods are briefly discussed, then details of the implementation of the multigrid algorithm into the CVFE-MG method are presented. Results generated by the proposed CVFE-MG method in the solution of several test problems are presented in Chapter 5. These results are compared with those of benchmark numerical studies available in the literature, and with results generated by the proposed CVFEM using one solution mesh. Finally, in Chapter 6, the contributions of this thesis are summarized, and suggestions for further work are presented.

Chapter 2

A Review of Available Solution Methods

2.1 Introduction

Many solution methods have been developed for incompressible fluid flow problems. The choice of a particular solution procedure is strongly dependent upon the shape of the problem domain (regular, irregular), the nature of the fluid (viscid, inviscid), and the type of flow (steady, unsteady). Due to space restrictions, and the vast number of available methods, only some basic solution algorithms are discussed in this chapter. A brief overview of available numerical methods is given in section 2.2. In sections 2.3 and 2.4, the available CVFEM's for convection-diffusion and fluid flow problems are discussed. Finally, in section 2.5, a brief survey of multigrid solution methods in the context of CVFEM's is presented.

2.2 A Synopsis of Available Solution Methods

The goal of a computational method is to obtain values of the dependent variables, such as temperature, velocity, and pressure at discrete locations within a physical domain. What differentiates one numerical method from another is the manner in

which the algebraic discretization equations are obtained. Two of the most popular classes of methods for obtaining these equations are Finite Element Methods (FEM's) [2, 12], and Control Volume Finite Difference Methods (CVFDM's) or Finite Volume Methods (FVM's) [29]. Both of these methods are subsets of the Method of Weighted Residuals (MWR) [3-4]. The formulation of a MWR-FEM involves the following steps [37]:

1. Discretization of a calculation domain into elements of a specific shape.
2. Prescription of appropriate element based interpolation functions.
3. Derivation of discretized equations using a suitable form of the MWR.
4. Element by element assembly of the coefficients in the discretized equations.
5. Solution of the resulting discretized equations.

Conventional FEM's for fluid flow and heat transfer [2, 12] employ the Galerkin MWR [23] to derive the algebraic discretization equations, where the weighting function is the same as the interpolation function.

CVFDM's can be described as subdomain-type methods of MWR [29, 34]. Their formulations are as follows:

1. Discretization of a calculation domain into control volumes, and nodes associated with these control volumes.
2. Prescription of appropriate functions for the estimation of gradients and values of the dependent variables.
3. Derivation of discretization equations, which are algebraic approximations to the governing differential equations. Here, the MWR as it applies to control volume, or subdomain, formulations is used.

4. A node by node assembly of the discretization equations.

5. Prescription of a procedure to solve the resulting discretization equations.

For each node, the weighting function is set to unity over the associated control volume, and zero elsewhere [29]. The most outstanding feature of CVFDM's is that they satisfy the exact numerical conservation of mass, momentum and energy over each control volume, and hence over the entire calculation domain [29].

The CVFDM's can be further subdivided into Orthogonal Grid (OG) and Non-Orthogonal Grid (NOG) formulations [34]. However, CVFDM's are found to be most suitable for mildly complex domains for which fairly orthogonal, and smooth grids can be generated [34]. This is because in NOG's, the grid lines are not normal to the control volume faces, and hence the accuracy of the algebraic approximations to the flux integrals across the control volume faces suffers. It should be noted that FEM's do not suffer from this limitation. Indeed, the strength of FEM's lies in their ability to discretize complex calculation domains, especially in irregular-shaped and three-dimensional geometries.

Control Volume Finite Element Methods (CVFEM's) combine the attractive features of both FEM's and CVFDM's. They allow solution on irregular shaped domains, similar to FEM's, and they use the subdomain MWR to apply conservation principles to control volumes constructed around nodes in the calculation domain, similar to CVFDM's. Therefore, CVFEM's also satisfy global conservation requirements for mass , momentum and energy.

CVFDM's and CVFEM's both use subdomain-type MWR, but they are different in a few aspects. One difference between them is in the way the dependent variables are interpolated. In CVFDM's, the dependent variables are usually interpolated by locally one-dimensional functions defined either along grid lines, or

flow-oriented lines. On the other hand, in CVFEM's, the dependent variables are usually interpolated by multi-dimensional functions defined over the finite elements. Another difference between the two methods, is the choice of the co-ordinate system used to define the velocity components. For co-ordinate systems other than the Cartesian system, curvature related terms arise in the governing differential equations. In both OG and NOG formulations, the curvature terms can be complicated, and may lead to a loss of accuracy in the numerical solution of the governing equations [34]. Most CVFEM's are formulated in the Cartesian co-ordinate system, and hence curvature related terms are not involved. It is because of these fundamental differences, that CVFEM's can provide accurate solutions to the governing equations in complex domains. A detailed discussion of the differences and similarities between CVFDM's and CVFEM's is available in Prakash and Baliga [34].

In the following two sections, some recent advances in CVFEM's for both convection-diffusion and fluid flow problems will be reviewed.

2.3 CVFEM's for Convection-Diffusion Problems

Convection-diffusion problems involve the solution for a dependent variable in the presence of a known flow field. The dependent variable of interest is convected with the flow, while its gradients cause a diffusion transport. A satisfactory solution procedure for convection-diffusion problems is a prerequisite for the formulation of methods to solve fluid flows.

A CVFEM for convection-diffusion problems was originally introduced by Baliga

and Patankar [3, 4, 5]. They discretized the domain using three-node triangular elements. Within each element, the transported scalar (in both convection and diffusion terms) was interpolated using a flow-oriented function that considers the relative strengths of convection and diffusion in the mean flow direction, as well as, diffusion normal to that direction. This interpolation function was derived from a simplified version of the appropriate governing equation, written with respect to an element-based flow-oriented coordinate system. The aligning of one of the axes in the local element-based coordinate system with the mean flow direction in the element helps to reduce false diffusion [35]. Prakash [32] later modified this interpolation function to include source related variations of the dependent variable in the flow direction. Hookey and Baliga [18, 19] introduced a source related term that accounted for influences both parallel and normal to the mean flow direction. The interpolation function proposed by Prakash [32] is a special case of the function proposed by Hookey and Baliga. For the problems tested in [18, 19, 32], an improvement in accuracy over results obtained with other CVFEM's was reported.

Ramadhyani and Patankar [36], and later, Schneider and Raw [38, 39, 40] introduced CVFEM's for quadrilateral finite elements. In [38], Schneider and Raw introduced a positive-coefficient upwinding procedure, in which the coefficients arising due to the algebraic approximation of the convection fluxes are assured to be positive at an elemental level, and hence at control volume level. In [39], an upwinding formulation was presented that was similar in form to the positive coefficient scheme, however, the directionality of the flow was more closely approximated, reducing false diffusion, but allowing for the appearance of some negative coefficients. For the problems they tested [39], it was found that the magnitude of the negative coefficients were small enough that they did not pose any difficulties.

The effects of diffusion, both parallel and normal to the mean flow direction, and source terms were also explicitly accounted for in the interpolation function for the convected scalar [39]. In this method, the pressure gradients were included in the interpolation functions for velocities at an elemental level, this interpolation scheme allowed for the development of an equal-order colocated formulation of incompressible fluid flow problems.

In the context of CVFEM's with triangular elements, Prakash introduced the donor-cell scheme as a means of ensuring positive coefficients [33]. This approach stated that the value of a dependent variable convected out of a control volume must be the value of the dependent variable at the node within the control volume. This approach guarantees positive coefficients, but takes little account of the directionality of the flow, and takes no account of the effects of diffusion and source terms on the interpolation of the convected scalar. The positive coefficient scheme proposed by Schneider and Raw [38] is a more attractive approach to eliminate negative coefficients, even though it involves more computations.

2.4 CVFEM's for Fluid Flow Problems

In the original CVFEM, Baliga and Patankar [3, 5] proposed an unequal-order incompressible CVFEM in which the domain is first discretized by six-node triangular elements, and these "macroelements" are then divided into four three-node "subelements" by joining the midpoints of each side. Pressure is stored at the vertices of the macroelements, and velocity is stored at the vertices of all subelements, which results in an unequal-order scheme that avoids solution harmonics. This formulation also employs a mixed interpolation scheme: pressure is interpo-

lated linearly in the macroelements, and the velocity components are interpolated by flow-oriented upwind type functions within the subelements. Polygonal control volumes used in the discretization of the continuity equation are constructed around the vertices of the macroelements, while those used in the discretization of the momentum equations are constructed around the vertices of the subelements. This method has been used in conjunction with SIMPLE, SIMPLER, and SIMPLEC [3, 5, 18, 20, 6] solution algorithms. However, this scheme has several limitations related to the use of two types of elements and control volumes. Since the momentum and continuity equations are discretized using two different control volumes, mass conservation is not strictly satisfied over the momentum control volumes. Also, the discretization equation for pressure is quite different from the discretization equation for the other dependent variables and a separate equation solver is needed. Finally, since the unequal-order method uses a much coarser grid for pressure, it may not be very accurate for problems in which the pressure gradients are large.

The first equal-order CVFEM with three-node triangular elements was proposed by Prakash and Pantankar [30, 31]. In this method, pressure and velocity are computed at all grid points, and the discretization of the continuity and momentum equations uses the same control volumes. The velocities used in the momentum equations are interpolated by the flow-oriented upwinding type functions proposed in [3, 5], pressure is interpolated linearly, and the mass flow field in each element is obtained from linear interpolation of a pseudo-velocity field and pressure. The use of the pseudo-velocity and pressure in the discretization of the continuity equation provides the necessary coupling between velocity and pressure, which effectively prevents the appearance of pressure harmonics. This method was

formulated in the context of the SIMPLER solution algorithm [29], and it has been extended to three-dimensions by LeDain-Muir and Baliga [24, 25].

In an attempt to refine his previous equal-order method, Prakash [32] proposed a second method. In this method, the interpolation functions for the scalar dependent variables include source-related terms, in order to provide for a source influence on the distribution of the dependent variable within an element. The appropriate pressure gradients are included in the source related terms used in the velocity interpolation functions, and it is this explicit inclusion of the pressure gradients that prevents the appearance of spurious oscillations of velocity and pressure. A solution algorithm similar to SIMPLER is used to solve the discretized momentum and continuity equations [32].

Hookey and Baliga [18, 20] modified the interpolation functions and solution algorithms of the equal-order CVFEM in [32]. They employed an improved interpolation function which included source term effects in directions both parallel and normal to the mean flow within each element. Furthermore, a SIMPLEC type solution algorithm was used, and the velocity-correction formulation was more completely specified than in [32]. However, the resulting pressure-correction equation involved up to twenty-five neighbouring nodes in two-dimensional problems, and this would make extensions to three-dimensional problems impractical. Recently, Hookey [21] successfully reduced the number of neighbouring nodes in the discretized equations. For two-dimensional problems, the maximum neighbouring nodes was eight for both pressure and velocity equations. This method was, therefore, better suited for three-dimensional formulations. The discretized momentum and continuity equations were solved in a coupled manner using a Coupled Equation Line Solver (CELS). The CELS solves the coupled equations simultaneously

along a grid line in the calculation domain, and iteratively improves the overall solution by successively sweeping the domain line by line, in alternating directions, until a desired level of convergence is obtained [21].

Schneider and Raw [39] have also extended their convection-diffusion CVFEM to flow problems. The key feature of their method is that the interpolation functions used for convection terms in the momentum equations explicitly include the pressure gradients, therefore, the velocity and pressure fields are coupled. In their method, the calculation domain is discretized using quadrilateral elements instead of triangular elements. The use of triangles is believed to be more efficient for irregular shaped domains and adaptive grid methods, because triangular elements allow more freedom in the placement of nodes within the calculation domain. Schneider and Raw used a direct banded solver for the solution of the algebraic discretization equations of two-dimensional problems. In three-dimensions, the cost of such a solution method is prohibitive.

Recently, Saabas [37] has developed an equal-order CVFEM for the simulation of three-dimensional turbulent incompressible fluid flow. To overcome problems with outflow boundaries inherent with the method developed by Hookey [21], he has used "mass conserving" velocities, derived from the discretized momentum equations, to discretize the continuity equation. For example, the x-component of the "mass conserving" velocity at a node i, u_i^m, can be expressed as:

$$u_i^m = \hat{u}_i + d_i^u \frac{\partial p}{\partial x} \tag{2.1}$$

where the pseudo-velocity, $\hat{u}_i$, is the summation of all terms on the right hand side of the discretized x-momentum equation, except for the pressure gradient term, divided by the coefficient multiplying u_i. The pressure coefficient term, d_i^u, is the area of the control volume, divided by the coefficient multiplying u_i. A similar

expression can be developed for the y-component, c_i^m. The nodal values of $\dot{u}$, $\dot{v}$, d^u and d^v are interpolated linearly within an element in order to provide algebraic approximations to the mass flux at the control volume faces. Also, the d^u and d^v terms are used in conjunction with the elemental pressure gradients to prevent the possibility of pressure harmonics. This method forms the basis for the CVFEM to be implemented in this thesis.

2.5 Multigrid Solution Methods

Multigrid methods have been developed only recently. In what probably was the first multigrid publication, Fedorenko [13] formulated a multigrid algorithm for the standard five-point finite difference discretization of the Poisson equation. This work was then generalized to the central difference discretization of the general linear elliptic partial differential equations by Bachvalov [1]. The first practical results were reported by Brandt [9, 10], in which he outlined the main principles and the practical utility of multigrid methods. The multigrid method was also discovered independently by Hackbusch [17], who laid firm mathematical foundations and provided reliable methods. The common property of these multigrid methods is their ability to obtain optimal convergence rates, in terms of computing effort, which are linearly dependent on the number of grid points.

Much work has been done in the 1980's on extending these methods to the Euler and Navier Stokes equations. Studies related to laminar flow in simple rectilinear geometries by Lonsdale [26], Vanka [41] and Becker et al. [8] reported that favorable convergence rates were reached by using multigrid techniques. In these papers, the speed-up factors were of the order 10−100, depending on grid density, type of flow

and the precise manner of multigrid implementation. Although rigorous proofs of the rates of convergence of multigrid methods are complicated, there is no doubt about the efficiency of these methods when compared to iterative solutions on one grid. A more detailed multigrid bibliography can be found in [11].

Of particular interest to researchers in the field of CVFEM's is the work of McCormick [27]. McCormick [27] independently developed a CVFEM as he thought it would be the ideal method for MG and multilevel adaptive techniques. In [27] McCormick describes the implementation of a CVFEM for diffusion problems in a MG algorithm. Also described is initial work on the implementation of a CVFEM for viscous flows based on a stream function-vorticity formulation of the governing equations. This work has been the inspiration for the work in this thesis. The successful application of MG to CVFEM's in [27] has led to the attempt to implement MG in the context of a CVFEM based on the primitive variable formulation of the viscous fluid flow problem. Hookey [22] has implemented a CVFE-MG method for primitive variable formulation of viscous flows using the CVFEM in [21] with the CELS. In this thesis, the CVFEM of Saabas [37] will be implemented in the context of a multigrid algorithm.

2.6 Summary

This chapter has presented a brief overview of some of the numerical methods available for the solution of incompressible flows. Emphasis has been placed on the CVFEM's that have been developed for the simulation of viscous fluid flows. In the next chapter, the formulation of the proposed CVFEM for steady, viscous, incompressible, two-dimensional fluid flow will be discussed.

Chapter 3

Formulation of the Proposed Two-Dimensional CVFEM

3.1 Introduction

The formulation of a CVFEM for steady, viscous, two-dimensional, incompressible fluid flows is presented in this chapter. The proposed CVFEM is an equal-order colocated method and it was originally presented by Saabas [37] for three-dimensional turbulent flows. The presentation is divided into sections on the following topics: (1) definition of the governing equations; (2) domain discretization details; (3) derivation of control volume integral conservation equations; (4) specification of element-based interpolation functions for the dependent variables; (5) derivation of the discretized forms of the conservation equations and boundary conditions; and (6) algorithms used to solve the discretized equations.

3.2 Governing Equations

The partial differential equations governing steady, two-dimensional, viscous, incompressible fluid flow are the following [43]:

Continuity:

$$\frac{\partial}{\partial x}(\rho u) + \frac{\partial}{\partial y}(\rho v) = 0 \tag{3.1}$$

x-momentum:

$$\frac{\partial}{\partial x}(\rho uu) + \frac{\partial}{\partial y}(\rho vu) = -\frac{\partial p}{\partial x} + \frac{\partial}{\partial x}\left(\mu\frac{\partial u}{\partial x}\right) + \frac{\partial}{\partial y}\left(\mu\frac{\partial u}{\partial y}\right) + S^u \tag{3.2}$$

y-momentum:

$$\frac{\partial}{\partial x}(\rho uv) + \frac{\partial}{\partial y}(\rho vv) = -\frac{\partial p}{\partial y} + \frac{\partial}{\partial x}\left(\mu\frac{\partial v}{\partial x}\right) + \frac{\partial}{\partial y}\left(\mu\frac{\partial v}{\partial y}\right) + S^v \tag{3.3}$$

Energy:

$$\begin{aligned}\frac{\partial}{\partial x}(\rho uT) + \frac{\partial}{\partial y}(\rho vT) &= \frac{\partial}{\partial x}\left(\frac{k}{c_p}\frac{\partial T}{\partial x}\right) + \frac{\partial}{\partial y}\left(\frac{k}{c_p}\frac{\partial T}{\partial y}\right) + \frac{S^T}{c_p} \\ &+ \frac{1}{c_p}\left(u\frac{\partial p}{\partial x} + v\frac{\partial p}{\partial y}\right) + \frac{1}{c_p}\Phi\end{aligned} \tag{3.4}$$

General convection-diffusion equations:

$$\frac{\partial}{\partial x}(\rho u\phi) + \frac{\partial}{\partial y}(\rho v\phi) = \frac{\partial}{\partial x}\left(\Gamma\frac{\partial \phi}{\partial x}\right) + \frac{\partial}{\partial y}\left(\Gamma\frac{\partial \phi}{\partial y}\right) + S^\phi \tag{3.5}$$

where u and v are the velocity components in the x and y directions, respectively, p the pressure, μ the dynamic viscosity, T the absolute temperature, k the thermal conductivity, c_p the specific heat at constant pressure, Φ the viscous dissipation term, ϕ a scalar dependent variable, Γ its associated diffusion coefficient, and S^u, S^v, S^T, and S^ϕ are the volumetric source, or generation, terms for the appropriate equation.

These partial differential equations may be cast in the following conservative forms [29]:

$$\vec{\nabla}\cdot\vec{J} = S \tag{3.6}$$

$$\vec{\nabla} \cdot \vec{g} = 0 \tag{3.7}$$

Where , $\vec{J}$ is the combined convection-diffusion flux vector, S is the source term, and $\vec{g}$ is the mass flux vector $\rho\vec{v}$. Equation 3.6 represents the x-momentum equation when:

$$\vec{J} = \rho\vec{v}u - \mu\vec{\nabla}u \tag{3.8}$$

$$S = S^u - \frac{\partial p}{\partial x} \tag{3.9}$$

the y-momentum equation when:

$$\vec{J} = \rho\vec{v}v - \mu\vec{\nabla}v \tag{3.10}$$

$$S = S^v - \frac{\partial p}{\partial y} \tag{3.11}$$

the energy equation when:

$$\vec{J} = \rho\vec{v}T - \frac{k}{c_p}\vec{\nabla}T \tag{3.12}$$

$$S = \frac{S^T}{c_p} + \frac{1}{c_p}\left(u\frac{\partial p}{\partial x} + v\frac{\partial p}{\partial y}\right) + \frac{1}{c_p}\Phi \tag{3.13}$$

and the governing equation for the scalar dependent variable ϕ when:

$$\vec{J} = \rho\vec{v}\phi - \Gamma\vec{\nabla}\phi \tag{3.14}$$

$$S = S^\phi \tag{3.15}$$

Integrating the governing Eqs. 3.6 and 3.7 over a control volume V, which is fixed in space, gives:

$$\int_V \vec{\nabla} \cdot \vec{J}\, dV = \int_V S\, dV \tag{3.16}$$

$$\int_V \vec{\nabla} \cdot \vec{g}\, dV = 0 \tag{3.17}$$

Applying Gauss' Divergence Theorem to Eqs. 3.16 and 3.17, the integral forms of the governing equations can be obtained:

$$\int_{\partial V} \vec{J} \cdot \vec{n}\, ds = \int_V S\, dV \tag{3.18}$$

$$\int_{\partial V} \vec{g} \cdot \vec{n}\, ds = 0 \tag{3.19}$$

where ∂V is the surface of the control volume, and $\vec{n}$ is a unit outward vector normal to the differential area ds.

3.3 Domain Discretization

In the proposed CVFEM, the calculation domain is discretized by a line-by-line structured grid. Triangular elements are constructed by drawing one of the two possible diagonals in each quadrilateral formed by the intersection of the grid lines resulting from the domain discretization. All the dependent variables are stored at all the nodes in the domain, giving rise to the so-called colocated scheme. The discretization of a representative irregularly shaped calculation domain is illustrated in Fig. 3.1a. An advantage of using triangular elements is that they do not require isoparametric transformations [44], which are needed by general quadrilateral elements.

Once the calculation domain is discretized with the triangular elements, polygonal control volumes are constructed around each node in the calculation domain, by joining the midpoint of the longest side of the element with the midpoints on the two remaining sides. This results in two control volume faces within each element. The polygonal control volumes constructed in an irregularly shaped calculation domain discretized by triangular elements are shown by dashed lines in Fig. 3.1b.

These polygonal control volume faces have the following characteristics: (1) they do not overlap; (2) collectively they fill the entire calculation domain; (3) their boundaries do not involve interelement edges; and (4) they can be used with any triangulation. These characteristics facilitate the formulation of a CVFEM that possesses the conservative property [3, 29, 44].

As stated previously, the discretization scheme employed arranges the nodes in a line-by-line pattern. Such an arrangement of the nodes greatly facilitates the assembly of the coefficients in the discretized equations, and permits solution of these equations with iterative line-by-line solvers. Further, a structured mesh of this kind is perfectly suited to the use of multigrid techniques.

3.4 Integral Conservation Equations for a Control Volume

Using the control volumes defined in the previous section, the integral conservation equations, Eqs. 3.18 and 3.19, can be specified for a control volume as follows. With reference to the polygonal control volume associated with a typical node 3 within the calculation domain, Fig. 3.2, Eqs. 3.18 and 3.19 can be cast in the following forms:

$$\left[\int_{M_1}^{M_3} \vec{J}\cdot\vec{n}^1\,ds - \int_{M_3}^{M_2} \vec{J}\cdot\vec{n}^2\,ds - \int_V S\,dV\right]$$
$$+ \quad [\text{similar contributions from other elements associated with node 3}]$$
$$+ \quad [\text{boundary contributions, if applicable}] \quad = \quad 0 \qquad (3.20)$$

$$\left[\int_{M_1}^{M_3} \vec{g}\cdot\vec{n}^1\,ds - \int_{M_3}^{M_2} \vec{g}\cdot\vec{n}^2\,ds\right]$$

$$+ \quad [\text{similar contributions from other elements associated with node 3}]$$

$$+ \quad [\text{boundary contributions, if applicable}] \quad = \quad 0 \qquad (3.21)$$

where M_k is the midpoint of the corresponding side of the triangular element, see Fig. 3.2. The first bracketed terms in Eqs. 3.20 and 3.21 represent the contributions of element 123 to the control volume conservation equations for the control volume surrounding node 3. The control volumes in this two-dimensional formulation are assumed to be of unit depth, therefore, the surface and volume integrals in Eqs. 3.20 and 3.21 reduce to line and area integrals, respectively.

3.5 Interpolation Functions

Interpolation functions are required for all dependent variables, source terms, and fluid properties that appear in the integral conservation equations, Eqs. 3.20 and 3.21. It should be noted that all the interpolation functions are defined at the element level. Each interpolation function is discussed in this section.

3.5.1 Interpolation of Thermophysical Properties

All thermophysical properties, such as viscosity μ, density ρ, and all other diffusion coefficients Γ are supplied at the three nodes of each element, and an arithmetic mean of these nodal values is assumed to prevail over the corresponding element.

3.5.2 Interpolation of Source Terms

The source terms, S^u, S^v, S^T, and S^ϕ in the conservation equations are linearized using Taylor's expansion [29], if required, and expressed as follows:

$$S^u = (S_c^u)_i + \left(S_p^u\right)_i u_i \tag{3.22}$$

$$S^v = (S_c^v)_i + \left(S_p^v\right)_i v_i \tag{3.23}$$

$$S^T = \left(S_c^T\right)_i + \left(S_p^T\right)_i T_i \tag{3.24}$$

$$S^\phi = \left(S_c^\phi\right)_i + \left(S_p^\phi\right)_i \phi_i \tag{3.25}$$

where S_c represents terms independent of the superscripted variable, and S_p provides for a linear dependence of S on the corresponding variable. The values of S_c and S_p are supplied at the three nodes of each element, and these nodal values are assumed to prevail over the corresponding subcontrol volumes. The appropriate dependent variable, used in the linearized source term, is also assumed to be the nodal value associated with the corresponding subcontrol volume.

3.5.3 Interpolation of Pressure

Within an element, the pressure is interpolated linearly:

$$p = a_p x + b_p y + c_p \tag{3.26}$$

The coefficients a_p, b_p, and c_p in Eq. 3.26 are defined by the nodal values of pressure, and the geometry of the corresponding triangular element. The pressure gradients can be expressed as follows:

$$\frac{\partial p}{\partial x} = a_p = \frac{1}{det} \sum_{i=1}^{3} ymul_i\, p_i \tag{3.27}$$

$$\frac{\partial p}{\partial y} = b_p = -\frac{1}{det} \sum_{i=1}^{3} xmul_i\, p_i \tag{3.28}$$

A complete derivation of the coefficients in the above equations is given in Appendix A. It should be noted that the pressure gradients within each element are constant.

3.5.4 Interpolation of Velocity

Introduction

In the proposed CVFEM, three different interpolation functions for velocities are used: (1) mass weighted interpolation (MAW) is used when velocity is treated as a convected scalar; (2) linear interpolation is used when velocity is treated as a diffused scalar; and (3) linear interpolation of a pseudo-velocity is used when velocity appears in the mass flux terms ($\rho\vec{v}\cdot\vec{n}$) in the continuity and momentum equations. The first two interpolation functions are discussed in this subsection and the third will be described in section 3.6.2.

Mass Weighted Interpolation for the Convected Scalar

The MAW scheme is an adaption of a positive coefficient scheme, introduced by Schneider and Raw [38] for quadrilateral elements, to the case of triangular elements with control volumes as described in section 3.3. The essence of this scheme is to ensure positive contributions, at an element level, to the coefficients in the algebraic discretization equations. This will ensure that the coefficients in the completely assembled algebraic discretization equation for a control volume will be positive. This will help to overcome difficulties with negative coefficients in some of the previous CVFEM's.

Consider the element shown in Fig. 3.3a. The midpoint of a control volume

face, or integration surface is called the integration point [38], and is represented by the subscript *ip*. The value of the convected scalar at the integration point is assumed to prevail over the surface.

The mass flux across a particular subcontrol volume surface within an element is taken as positive when the velocity vector at the integration point is in the same direction as the assumed normal to the surface. With reference to Fig. 3.3a, the mass flux across face 1 is given by:

$$\dot{m}_1 = \rho \vec{v}^1 \cdot \vec{n}^1 \tag{3.29}$$

A similar expression can be written for the mass flux across the other subcontrol volume face within an element.

Given the assumed flow direction shown in Fig. 3.3b, the MAW scheme approximates the values of a convected scalar, ϕ, at the integration points on control volume faces 1 and 2 as follows [37]:

$$\phi_{ip_1} = f\,\phi_{ip_2} + (1 - f)\,\Phi_3 \tag{3.30}$$

$$\phi_{ip_2} = \Phi_2 \tag{3.31}$$

where

$$f = min\left[max\left(\frac{\dot{m}_2}{\dot{m}_1}, 0\right), 1\right] \tag{3.32}$$

and Φ refers to the nodal values, and ϕ indicates a value at an integration point.

Considering the subcontrol volume surrounding node 3 in Fig. 3.3b, the integral of the convective flux out of the subcontrol volume can be written as follows:

$$\int_{M_1}^{M_3} \rho\vec{v}\phi \cdot \vec{n}^1\, ds - \int_{M_3}^{M_2} \rho\vec{v}\phi \cdot \vec{n}^2\, ds = \dot{m}_1\left[f\,\Phi_2 + (1 - f)\,\Phi_3\right] - \dot{m}_2\,\Phi_2 \tag{3.33}$$

which can be rewritten as:

$$\int_{M_1}^{M_1} \rho \vec{v} \phi \cdot \vec{n}^1 \, ds - \int_{M_1}^{M_2} \rho \vec{v} \phi \cdot \vec{n}^2 \, ds = \dot{m}_1 (1 - f) \Phi_3 - (\dot{m}_2 - \dot{m}_1 f) \Phi_2 \quad (3.34)$$

In this case both $\dot{m}_1$ and $\dot{m}_2$ are positive, because they are in the same direction as the assumed unit normals $\vec{n}^1$ and $\vec{n}^2$, respectively. Therefore, negative coefficients due to the algebraic approximation of the convection terms cannot occur at a subcontrol volume level, or at the control volume level. The more general case where either or both mass fluxes are negative will be studied later. The "price" that is paid to have positive coefficients is a less faithful accounting of the directionality of the flow, and the distribution of the scalar over the element. This may result in increased false diffusion in the numerically predicted solutions.

The integration point value of the convected scalar at ip_1, which is assumed to prevail over surface 1, can depend on the value of the convected scalar at ip_2, as well as the nodal values of ϕ. In turn, the integration point value of ϕ_{ip_2}, can depend on the value of ϕ at ip_1, and at the nodes. Consequently, a 2×2 system of simultaneous linear algebraic equations, within each element, must be solved in order to express the integration point values in terms of nodal values. For the element and associated nomenclature shown in Fig. 3.4b, the following rules can be used to determine the integration point value ϕ_k^c, where k is the index for the control volume face, and the superscript c indicates a convected scalar.

For control volume face 1:

$$\text{If } \dot{m}_1 > 0 \qquad \phi_1^c = f_1 \phi_2^c + (1 - f_1) \Phi_3 \quad (3.35)$$

$$\text{If } \dot{m}_1 < 0 \qquad \phi_1^c = \Phi_1 \quad (3.36)$$

where

$$f_1 = min \left[max \left(\frac{\dot{m}_2}{\dot{m}_1}, 0 \right), 1 \right] \quad (3.37)$$

For control volume face 2:

$$\text{If } \dot{m}_2 > 0 \qquad \phi_2^c = \Phi_2 \tag{3.38}$$

$$\text{If } \dot{m}_2 < 0 \qquad \phi_2^c = f_2 \phi_1^c + (1 - f_2)\,\Phi_3 \tag{3.39}$$

where

$$f_2 = min\left[max\left(\frac{\dot{m}_1}{\dot{m}_2}, 0\right), 1\right] \tag{3.40}$$

Solving these equations, the integration point values can be expressed as follows:

$$\phi_k^c = \sum_{i=1}^{3} CM_i^k\,\Phi_i \tag{3.41}$$

The derivation of the CM_i^k terms is given in Appendix A.

It should be noted that if there are only two control volume faces within each element, which is the case of the proposed CVFEM, the CM_i^k terms in Eq. 3.41 can be obtained directly from Eqs. 3.35 and 3.36 or Eqs. 3.38 and 3.39.

Linear Interpolation of a Diffused Scalar

In the proposed CVFEM, the diffusive flux is approximated using a linear interpolation of the diffused scalar ϕ^d, within an element. The interpolation function has the following form:

$$\phi^d = a_\phi^d\, x + b_\phi^d\, y + c_\phi^d \tag{3.42}$$

where the coefficients a_ϕ^d, b_ϕ^d, and c_ϕ^d are determined as presented in Appendix A. These coefficients are only functions of the element geometry and the nodal values of ϕ.

3.6 Derivation of the Discretized Equations

To obtain algebraic approximations of the integral conservation equations for a control volume, Eqs. 3.18 and 3.19, approximations of the element contributions to Eqs. 3.20 and 3.21 are derived and assembled in an appropriate manner. Algebraic approximations of the boundary conditions are then derived, if applicable, and added to the element contributions. These approximations and assembly procedures are discussed in this section.

3.6.1 Momentum Equations

Integration of the Convection-Diffusion Flux across a Control Volume Face

To determine the element contributions to the integral conservation equation, Eq. 3.20, it is necessary to integrate the flux of momentum across the two control volume faces in each element.

$$[\text{Integrated flux across control volume face } k] = \int_{face\,k} \vec{J}^k \cdot \vec{n}^k \, ds \qquad (3.43)$$

Within each element, the combined convection-diffusion flux of x-momentum, Eq. 3.8, across face k can be separated into its component parts in the x and y directions:

$$\vec{J}^k = J_x^k \vec{i} + J_y^k \vec{j} \qquad (3.44)$$

where

$$J_x^k = \rho u u - \mu \frac{\partial u}{\partial x} \qquad (3.45)$$

$$J_y^k = \rho v u - \mu \frac{\partial u}{\partial y} \qquad (3.46)$$

The unit normal to the control volume face k is defined by:

$$\vec{n}^k = (n_x^k \vec{i} + n_y^k \vec{j})/l^k \tag{3.47}$$

where

$$n_x^k = y_M^k - y_{M_3} \tag{3.48}$$

$$n_y^k = x_{M_3} - x_M^k \tag{3.49}$$

$$l^k = [(x_M^k - x_{M_3})^2 + (y_M^k - y_{M_3})^2]^{\frac{1}{2}} \tag{3.50}$$

In the proposed CVFEM, the integral of the combined convection-diffusion flux, Eq. 3.43, is approximated using Simpson's Rule [7]. Thus,

$$\int_{face\,k} \vec{J}^k \cdot \vec{n}^k \, ds = \frac{n_x^k}{6}\left[(J_x)_M^k + 4\,(J_x)_H^k + (J_x)_{M_3}\right] \tag{3.51}$$

$$+ \frac{n_y^k}{6}\left[(J_y)_M^k + 4\,(J_y)_H^k + (J_y)_{M_3}\right] \tag{3.52}$$

where the subscripts H and M indicate that the subscripted quantity is evaluated at the positions shown in Fig. 3.4, for face k.

Using the definitions of the interpolation function coefficients given in Appendix A, the integrated flux across a control volume face k can be written in the following compact form:

$$\int_{face\,k} \vec{J}^k \cdot \vec{n}^k \, ds = C_1^k u_1 + C_2^k u_2 + C_3^k u_3 \tag{3.53}$$

where the subscripted numbers refer to the node numbering scheme in Fig. 3.4.

The integral of the source term in Eq. 3.20 is approximated as:

$$\int_{V_j} \mathcal{S}^u \, dV = A_j \left[(S_c^u)_j + \left(S_p^u\right)_j u_j - \frac{1}{det} \sum_{i=1}^{3} ymul_i \, p_i\right] \tag{3.54}$$

where $\mathcal{S}^u$ indicates the x-momentum source term and the pressure gradient $\partial p/\partial x$. For a complete derivation of Eqs. 3.53 and 3.54, the reader is referred to Appendix

B. The det and $ymul_i$ terms in Eq.3.54 result from the geometry of the element, and are described in Appendix A.

Final Form of the Discretized Momentum Equations

Expressions similar to Eq. 3.53 can be derived for the integrated convection-diffusion flux across the two control volume faces in each element. When these expressions are added appropriately with similar expressions from other elements which make a contribution to the control volume surrounding a node i, along with the applicable boundary contributions and integrated source terms, Eq. 3.54, the algebraic approximation of the integral conservation equation for a control volume, Eq. 3.20, is obtained. The resulting discretized x-momentum equation can be cast in the following form:

$$a_i^u u_i = \sum_n a_n^u u_n + e_i^u \tag{3.55}$$

where the summation is taken over all the nodes neighbouring node i. Appendix C and Fig. 3.4 demonstrate the complete assembly of Eq. 3.55, and the neighbouring nodes that are involved in the equation.

A similar procedure can be followed to derive the algebraic approximation of the y-momentum equation. The final form of the discretized y-momentum can be written as:

$$a_i^v v_i = \sum_n a_n^v v_n + e_i^v \tag{3.56}$$

The assembly of Eq. 3.56 is performed in the same manner as that of Eq. 3.55.

3.6.2 Continuity Equation

Introduction

As mentioned previously, a "mass conserving" velocity is used in the mass flux terms ($\rho\vec{v}\cdot\vec{n}$) in the continuity and momentum equations. The approach taken here is to use a particular form of the discretized momentum equations to define four new nodal fields, which will be used in the prescription of suitable interpolation functions for the "mass conserving" velocities. To derive these functions the discretized x-momentum Eq. 3.55 can be written in the following form:

$$a_i^u u_i = \sum_n a_n^u u_n - (\partial p/\partial x)_{av}\Delta V + b_i^u \tag{3.57}$$

In this expression, the e_i^u term of Eq. 3.55 has been separated into two terms. The first of these terms is related to the volume integral of an average pressure gradient $(\partial p/\partial x)_{av}$ which is assumed to prevail over a control volume. Equation 3.57 can be rearranged as follows:

$$u_i = \frac{\sum_n a_n^u u_n + b_i^u}{a_i^u} - \frac{(\partial p/\partial x)_{av}\Delta V}{a_i^u} \tag{3.58}$$

Defining $\hat{u}_i$ and d_i^u as follows:

$$\hat{u}_i = \frac{\sum_n a_n^u u_n + b_i^u}{a_i^u} \tag{3.59}$$

$$d_i^u = \frac{\Delta V}{a_i^u} \tag{3.60}$$

Eq. 3.58 can be written as:

$$u_i^m = \hat{u}_i - d_i^u \left(\frac{\partial p}{\partial x}\right)_{av} \tag{3.61}$$

where u_i^m is a mass conserving velocity component, and $\hat{u}$ is a pseudo-velocity. The pseudo-velocity field, $\hat{u}$, and the pressure coefficient field, d_i^u can be defined

using Eq. 3.59 and 3.60. It should be noted that the pseudo-velocity and pressure coefficient fields should be evaluated before the discretized momentum equations are under-relaxed. Furthermore, the Dirichlet boundary conditions on the velocity components (if any) are implemented as follows: at the points where the velocity is specified, the appropriate $\hat{u}_i$ or $\hat{v}_i$ is set equal to the specified velocity, and the corresponding d_i^u or d_i^v term is set to zero.

Interpolation of Mass Conserving Velocity

Within an element, each "mass conserving" velocity component is interpolated by assuming a linear variation of the corresponding pseudo-velocities and pressure coefficients used in conjunction with the local elemental pressure gradient. Consequently, one can write the following expression for the "mass conserving" velocities (in the x direction) at each node within an element:

$$u_i^m = \hat{u}_i - d_i^u \left(\frac{\partial p}{\partial x}\right)_e \tag{3.62}$$

where the $\hat{u}_i$ and d_i^u terms result from the discretized momentum equation for the appropriate node. The subscript, e, on the pressure gradient indicates that the elemental pressure gradient, and not the average pressure gradient over the control volume surrounding node i is being used. This is done, even though the pressure coefficients d_i^u are defined based on the momentum discretization equation for the control volume surrounding node i, Eq. 3.61. If the average pressure gradient acting on the control volume surrounding the node were used in the interpolation of "mass conserving" velocity, it would have two disadvantages: (1) physically unrealistic checkerboard type pressure fields could result; and (2) the resulting discretization equation for pressure would contain a large number of neighbours,

that could lead to an unwieldy and non-robust CVFEM [37]. The proposed interpolation appears inconsistent, but it does not suffer from the above-mentioned disadvantages. Moreover, in the limit, as the grid becomes very fine, the average pressure gradient acting on the control volume and the elemental pressure gradient approach the same value [37].

The pseudo-velocities, $\hat{u}_i$, and the pressure coefficients d_i^u, are known at the nodal points. In order to determine the values of these quantities at the integration points on the control volume faces within the elements, a linear interpolation of the nodal values is used:

$$\hat{u}_i = a_u x + b_u y + c_u \tag{3.63}$$

$$d_i^u = a_{d^u} x + b_{d^u} y + c_{d^u} \tag{3.64}$$

The a_u through c_u coefficients are functions of the element geometry, and the nodal pseudo-velocities, whereas the a_{d^u} through c_{d^u} coefficients depend on geometry and the nodal pressure coefficients. A complete derivation of these coefficients and similar expressions for "mass conserving" velocities in y direction is given in Appendix A.

Integration of the Mass Flux across a Control Volume Face

The integral of the mass flux across a control volume face k may be expressed as:

$$[\text{Integrated mass flux across control volume face k}] = \int_{face\,k} \vec{g}^* \cdot \vec{n}^k \, ds \tag{3.65}$$

where

$$\vec{g}^* = \rho \vec{v}^* \tag{3.66}$$

Substituting Eqs. 3.47 and 3.62 into Eq. 3.65 gives:

$$\int_{face\,k} \vec{g}^k \cdot \vec{n}^k \, ds \;=\; \frac{1}{l^k} \int_{face\,k} \rho^k \left\{ \left[\hat{u} - d^u \left(\frac{\partial p}{\partial x} \right)_c \right]^k n_x^k + \left[\hat{v} - d^v \left(\frac{\partial p}{\partial y} \right)_c \right]^k n_y^k \right\} ds \quad (3.67)$$

Substituting Eqs. 3.27 and 3.28 for the element pressure gradients into Eq. 3.67, and using Simpson's Rule to approximate the integral, one can obtain the following compact form of the integrated mass flux in terms of nodal pressures:

$$\int_{face\,k} \vec{g}^k \cdot \vec{n}^k \, ds \;=\; E_1^k p_1 + E_2^k p_2 + E_3^k p_3 + B^k \quad (3.68)$$

A complete derivation of the E_i^k and B^k terms is given in Appendix B.

Final Form of the Discretized Continuity Equation

Expressions similar to Eq. 3.68 can be derived for the mass flow across the two control volume faces in an element. When these expressions are added appropriately with similar expressions from other elements which make a contribution to the control volume surrounding a node i, along with the applicable boundary contributions, the algebraic approximation of the integral mass conservation equation for a control volume is formed. The resulting equation can be cast in the following form:

$$a_i^p p_i \;=\; \sum_n a_n^p p_n + e_i^p \quad (3.69)$$

where the summation is taken over all the nodes neighbouring node i. Appendix C, and Fig. 3.4, demonstrate the complete assembly of Eq. 3.69, and the neighbouring nodes that are involved in the equation.

3.6.3 Boundary Conditions

Introduction

If the node under consideration is located in the calculation domain, no boundary conditions are present, and the specification of the discretized equations discussed previously is complete. For nodes located on boundaries, however, the discretized equations are incomplete until the flux across the side of element 123, from M_1 to 3, in Fig. 3.2b, is specified to complete the contribution of element 123 to the control volume surrounding node 3. The transport of the scalar dependent variable, ϕ, out of the control volume from M_1 to node 3 can be specified as:

$$\left[\begin{array}{c} \text{Integrated flux of } \phi \text{ out of} \\ \text{control volume side } M_1 \text{ to } 3 \end{array} \right] = \int_{M_1}^{3} \vec{J} \cdot \vec{n}\, ds \qquad (3.70)$$

where $\vec{n}$ is the outward unit normal vector to the element side ds. The equations in this subsection are written for the general scalar dependent variable, ϕ, however, they may be interpreted as equations for the other dependent variables, u, v, T, and p, where indicated. The derivation of the algebraic approximations of the three types of boundary conditions, which are: (1) specified value boundary; (2) specified flux boundary; and (3) outflow boundary, and the incorporation of these boundary contributions into the discretized equations are described in the following subsections.

Specified Value Boundary

The specified value boundary conditions is the simplest to apply; when the value of ϕ_i is to be given a specific value, ϕ_{spec}, the discretized equation for node i is

written in the following form:

$$\phi_i = \phi_{spec} \tag{3.71}$$

It is implemented by setting all the calculated coefficients in the applicable discretized equation equal to zero, and defining:

$$a_i^{\phi} = 1 \; : \qquad r_i^{\phi} = \phi_{spec} \tag{3.72}$$

where ϕ can be replaced by u, v, T, or p, as required.

It should be noted that for the specified velocity boundary, both velocity and pseudo-velocity boundary conditions are implemented. The specified velocity boundary conditions for pseudo-velocities have been discussed in section 3.6.2.

Specified Flux Boundary

This boundary condition is used when the flux, of the quantity of interest, across a boundary is specified. If the specified flux out of the control volume is denoted by q, equation 3.70 can be written as:

$$\int_{M_1}^{3} \vec{J} \cdot \vec{n} \, ds = \int_{M_1}^{3} q \, ds \tag{3.73}$$

where, q may be a constant or a function that can be integrated in closed form over the boundary surface. When q is available only at the nodes, then linear interpolation is used between the nodes, and the integral of Eq. 3.73 is written as:

$$\int_{M_1}^{3} \vec{J} \cdot \vec{n} \, ds = \int_{M_1}^{3} q \, ds = \Delta s_{M_1-3}(3\, q_3 + q_1) \,/\, 4 \tag{3.74}$$

where Δs_{M_1-3} is the length of the side of the element from position M_1 to node 3, in Fig. 3.2b.

Outflow Boundary

At outflow boundaries, if the dependent variable is not specified, the diffusion transport is made equal to zero by setting the dot product of the gradient of ϕ and the outward unit normal vector to the boundary, $\vec{n}$, equal to zero:

$$\vec{\nabla}\phi \cdot \vec{n} = 0 \tag{3.75}$$

This boundary condition is used to disconnect the calculation domain from external influences across outflow boundaries. There will, however, be a convective flux across outflow boundaries. This flux is integrated as follows:

$$\left[\begin{array}{c}\text{Integral of convective flux out of}\\ \text{control volume side } M_1 \text{ to } 3\end{array}\right] = \int_{M_1}^{3} \rho\vec{v}\phi \cdot \vec{n}\, ds \tag{3.76}$$

In the proposed CVFEM, an algebraic approximation of this integral is obtained by assuming that ϕ_i prevails over the control volume for node i. The mass flowing out of the control volume :

$$\left[\begin{array}{c}\text{Integrated mass flux out of}\\ \text{control volume side } M_1 \text{ to } 3\end{array}\right] = \int_{M_1}^{3} \rho\vec{v} \cdot \vec{n}\, ds \tag{3.77}$$

is approximated by assuming linear interpolation of ρ, u, and v between two nodes on the boundary, such as nodes 1 and 3 in Fig. 3.2b. It should be noted that in Eqs. 3.76 and 3.77, $\vec{v}$ is a "mass conserving" velocity.

To complete the specification of the momentum, continuity, and general convection-diffusion equations at outflow boundaries the integrated convective flux across the boundary has to be incorporated into the forms of the discretized equations that have been obtained from element contributions alone. This is done by adding the integrated mass flux, Eq. 3.77, to the appropriate coefficient for ϕ_i, where ϕ is replaced by u, v, or T for the appropriate equation.

3.7 Solution of the Discretized Equations

3.7.1 Solution Algorithm

In the proposed CVFEM, a coupled set of nonlinear algebraic equations for velocity, pressure, and other transported scalars are obtained as approximations of the corresponding integral conservation equations. The nonlinearities in the equations are solved by an iterative successive substitution procedure, in which the coefficients in these equations are evaluated using the most updated available values. A segregated solution method with multigrid techniques is used to solve these algebraic equations in this thesis. The overall solution procedure proceeds in the following steps:

1. Guess the pressure field, velocity fields, and any other dependent variables.

2. Evaluate all the coefficients in the discretized momentum equations, Eqs. 3.55 and 3.56, excluding those resulting from the integral of the element pressure gradient over the control volume.

3. Evaluate the pseudo-velocity and pressure coefficient fields using Eqs. 3.59 and 3.60. Apply the boundary conditions, if the specified value boundaries exist.

4. Evaluate the coefficients in the discretized continuity equation, Eq. 3.69. Apply the appropriate boundary conditions, and solve the algebraic equations to obtain the pressure field using a line-by-line tridiagonal matrix algorithm (TDMA) [29].

5. Evaluate the contribution of the volumetric integral of the appropriate pressure gradient to the control volume discretization equations for momentum,

and add it to the constant term c_i of Eqs. 3.55 or 3.56. Apply any boundary conditions, if needed.

6. Under-relax the discretized momentum equations, and solve them to obtain the velocity fields using a TDMA.

7. Evaluate the coefficients for the other dependent variables that are coupled to the flow field. Apply the appropriate boundary conditions, underrelax the equations, and solve.

8. Repeat steps (2) – (7), until a suitably converged solution is obtained.

9. Solve for other dependent variables of interest that do not influence the flow field.

It should be noted that the above algorithms do not include the multigrid techniques, which are discussed in the next chapter.

3.7.2 Under-relaxation of the Discretized Equations

The discretization equations are nonlinear and coupled algebraic equations. The nonlinearities are resolved by iteration. If the change in the solution field from one iteration to another is too large, the solution may begin to oscillate, and eventually may diverge. This problem is controlled by using the under-relaxation techniques of Pantankar [29]. The discretized x-momentum equation, Eq. 3.55, is underrelaxed as follows:

$$\frac{a_i^u}{\alpha_u} u_i = \sum_n a_n^u u_n + d_i^u + (1 - \alpha_u) \frac{a_i^u}{\alpha_u} u_i^* \qquad (3.78)$$

where u_i^* is the value of u_i from a previous iteration, and α^u is the under-relaxation parameter ($0 < \alpha^u < 1$). A comparison of Eq. 3.78 with Eq.3.55, shows that the coefficient multiplying u_i has been modified, and a new term has been added to the right side. When convergence is reached, $u_i = u_i^*$, and Eq. 3.78 reduces to Eq. 3.55.

A similar method is used to underrelax the y-momentum equation, using the parameter α_v. The continuity equation is not relaxed, as this would imply mass source or sink terms in the discretized equation.

3.7.3 Solver used for the Linear Algebraic Equations

In the proposed CVFEM, a line-by-line Tridiagonal Matrix Algorithm (TDMA) [29] is used to solve the algebraic discretization equations. The TDMA solver used in this thesis allowed for sweeps in alternative directions, i.e. in both x and y directions, which strongly enhances the convergence rate of the solution to the algebraic equations.

3.8 Summary

The CVFEM described in this chapter may be used to simulate steady-state viscous incompressible fluid flows. Some sample solutions are included in Chapter 5. The goal of this thesis, however, is to improve the convergence rate of this CVFEM using multigrid techniques. The multigrid methods used, and details regarding their implementation in the context of CVFEM's are discussed in the following chapter.

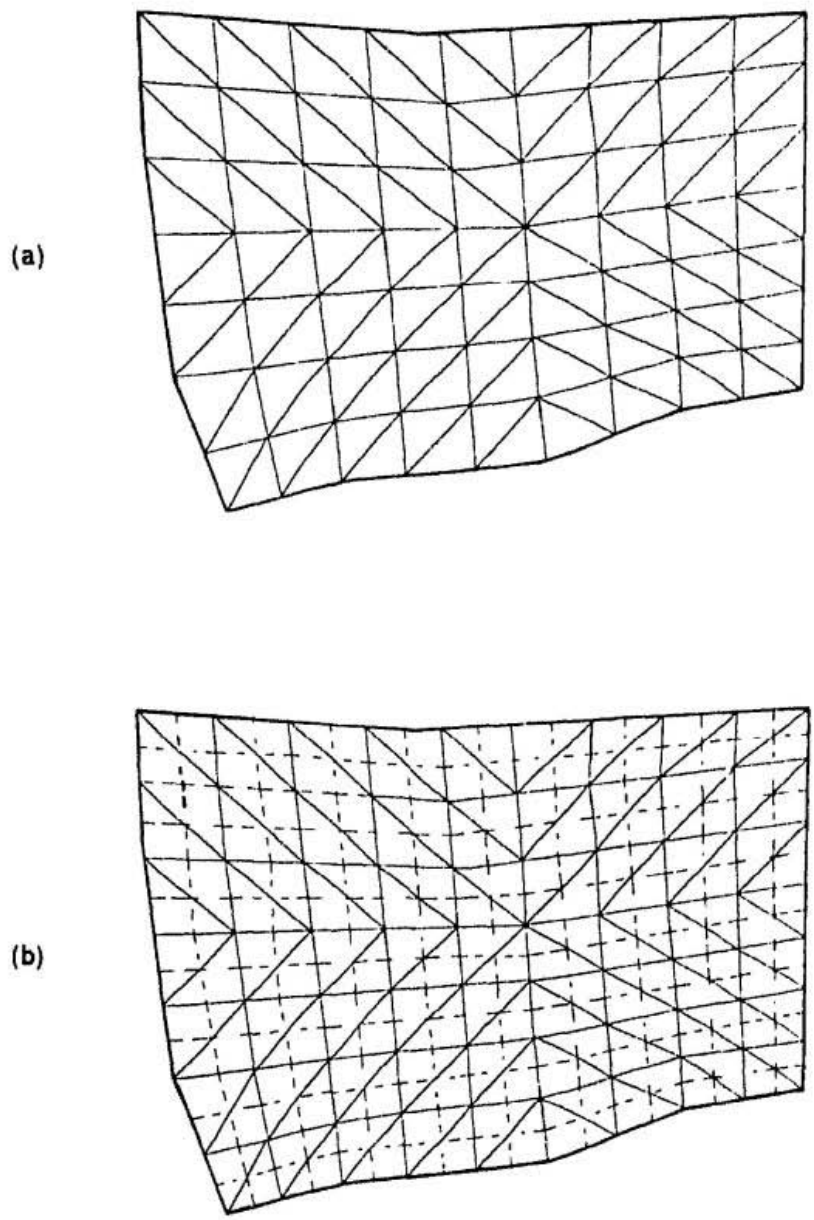

Figure 3.1: Discretization of an irregular shaped calculation domain by the proposed two-dimensional CVFEM: (a) three-node triangular elements; and (b) polygonal control volumes.

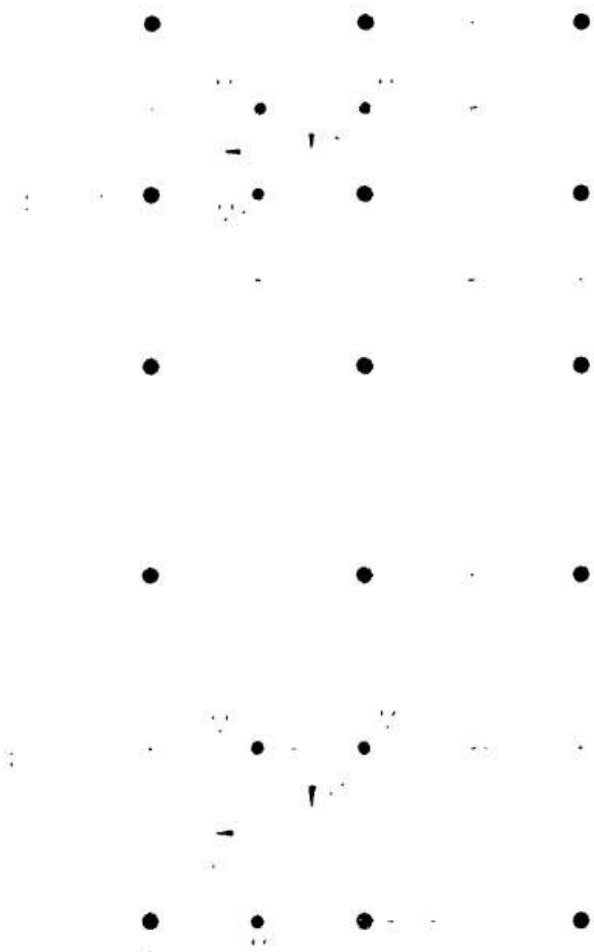

Figure 3.2: Details of the domain discretization, and related nomenclature: (a) an internal node; and (b) a boundary node.

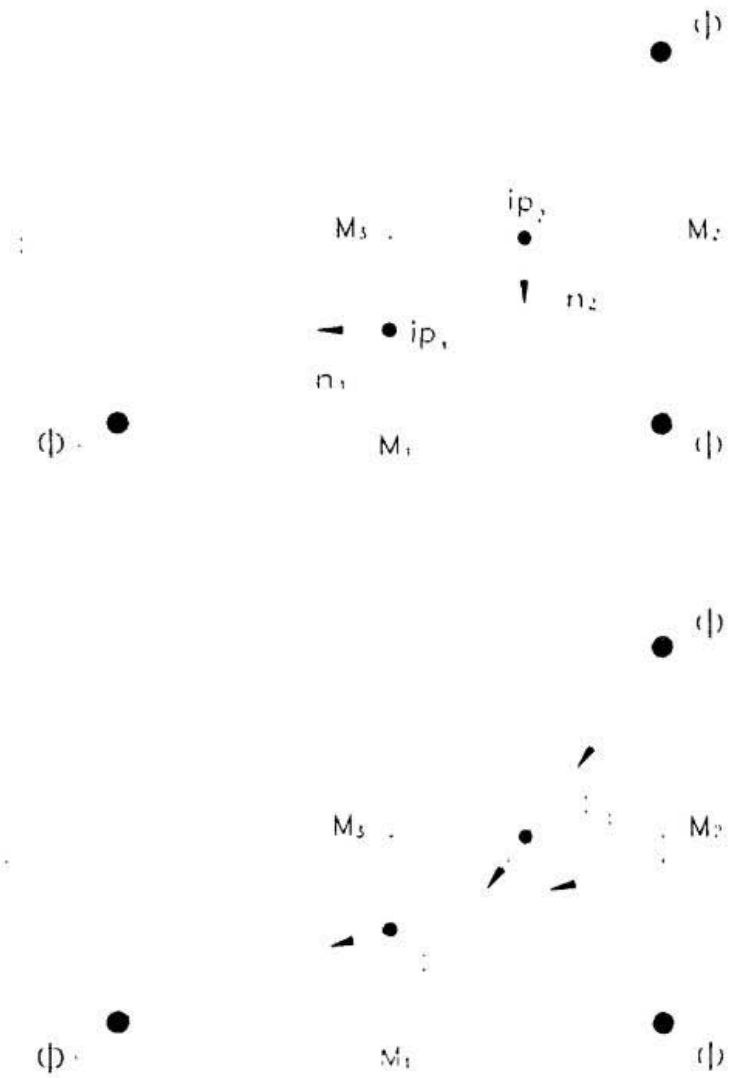

Figure 3.3: Element used in discretization of MAW scheme: (a) associated nomenclature; (b) assumed flow directions

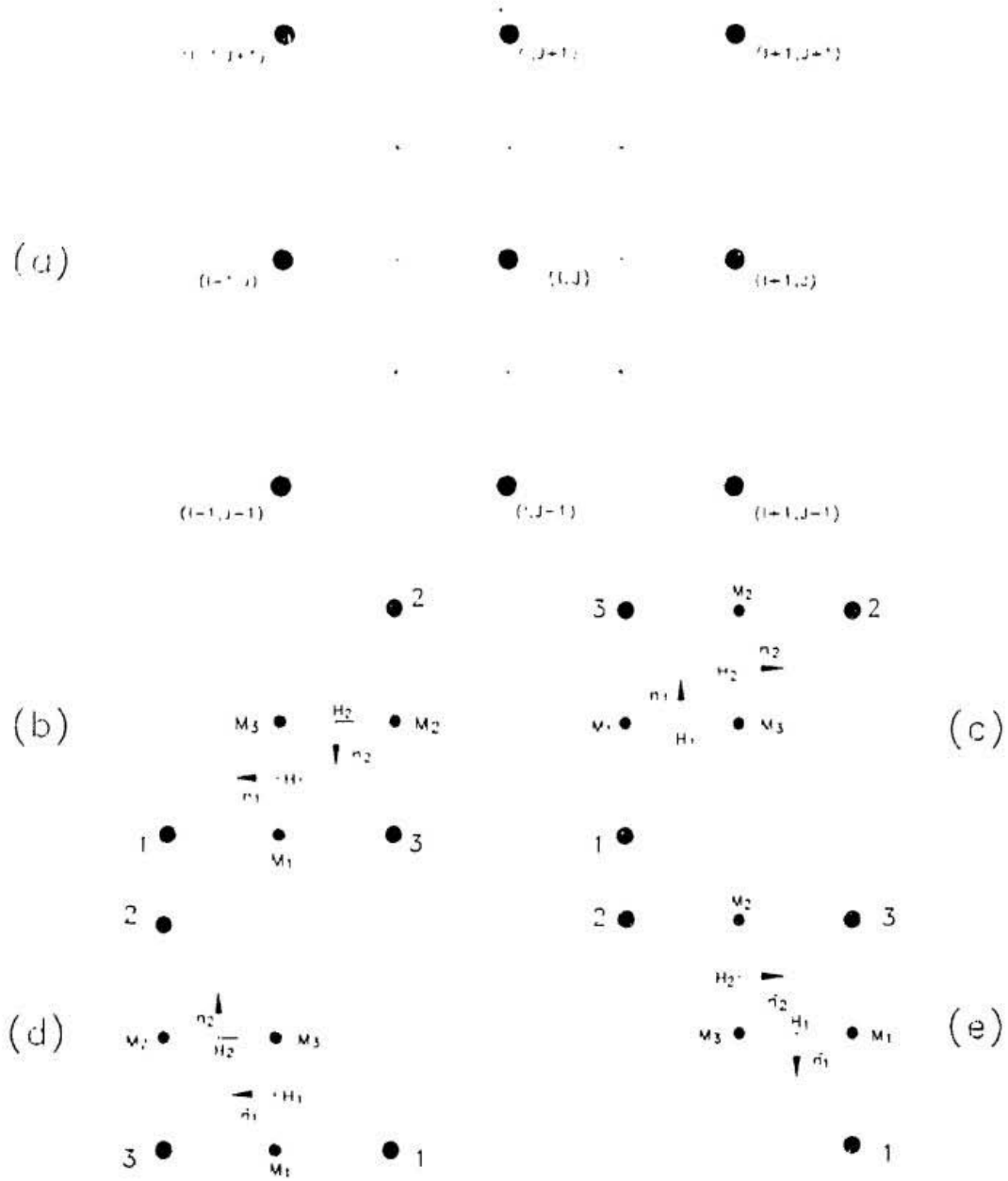

Figure 3.4: The node cluster involved in the discretization equation for a node (I,J), and related nomenclature: (a) an internal node (I,J) and its maximum number of neighbour nodes; (b) quad 1, type 1 element; (c) quad 1, type 2 element; (d) quad 2, type 1 element; and (e) quad 2, type 2 element.

Chapter 4

The Multigrid Methods

4.1 Introduction

Multigrid methods can lead to significant increases in convergence rates for iterative solution techniques. In this thesis, a multigrid method is used in the context of the segregated solution algorithm for the CVFEM described in the previous chapter. Since the development of the multigrid technique is not original to this thesis, only a very limited description of the concepts of multigrid is included in this chapter; emphasis will be placed on the implementation of a multigrid algorithm in the context of the CVFEM. For a detailed introductory text on multigrid, the reader is referred to Briggs [11].

In this chapter, the concepts of the residual equation, coarse grid correction, prolongation, injection and V- and FMV-cycles will be introduced. Then the details of the multigrid implementation in the context of the CVFEM will be discussed.

4.2 The Residual Equation

Consider a system of linear equations:

$$A\vec{u} = \vec{f} \tag{4.1}$$

where $\vec{u}$ is the exact solution of this system, and $\vec{f}$ is the constant term of the system. This set of equations can represent any of the discretized equations discussed in the previous chapter. Clearly the exact solution to the problem $A\vec{u} = \vec{f}$ is unknown, while an approximation $\vec{v}$, which can be calculated by some iterative method, is known. There are two important measures of $\vec{v}$ as an approximation to $\vec{u}$. One is the algebraic error which is given by:

$$\vec{e} = \vec{u} - \vec{v} \tag{4.2}$$

Unfortunately, the algebraic error is also unknown, since the exact solution $\vec{u}$ is not available. However, a computable measure of how well $\vec{v}$ approximates $\vec{u}$ is the residual, which can be expressed as follows:

$$\vec{r} = \vec{f} - A\vec{v} \tag{4.3}$$

The residual is simply the amount by which the approximation $\vec{v}$ fails to satisfy the original problem $A\vec{u} = \vec{f}$. Its size may be measured by any of the standard vector norms. The two most commonly used norms for multigrid purposes are defined by:

$$\| \vec{e} \|_\infty = \max_{1 \le j \le N} | \vec{r}_j | \quad \text{and} \quad \| \vec{e} \|_2 = \left(\sum_{j=1}^{N} \vec{r}_j^{\,2} \right)^{\frac{1}{2}} \tag{4.4}$$

where N is the total number of nodes in the discretized domain.

Rearranging Eq. 4.3 as:

$$A\vec{v} = \vec{f} - \vec{r} \tag{4.5}$$

and subtracting the above equation from Eq. 4.1 gives:

$$A\,\vec{e} \;=\; \vec{r} \tag{4.6}$$

This is the so-called residual equation, which says that the error satisfies the same set of equations as the unknown $\vec{u}$ when $\vec{f}$ is replaced by $\vec{r}$. The residual equation, and its form, play a significant role in multigrid algorithms.

The residual equation, along with Eq. 4.2, can be used effectively to obtain a better solution. The procedure is as follows: assuming that an approximation $\vec{v}$ has been evaluated by some iterative method, it is possible to evaluate the residual $\vec{r}$ using Eq. 4.3. To improve the approximation $\vec{v}$, the residual equation, Eq. 4.6, is solved for $\vec{e}$ and then a new approximation can be obtained using the definition of the algebraic error:

$$\vec{u} \;=\; \vec{v} + \vec{e} \tag{4.7}$$

This is the essence of the residual correction method, which plays a very important role in the formulation of multigrid algorithms.

4.3 Coarse Grid Correction

It is well established [13] that many of the standard iterative solution methods, for example, Gauss-Seidel and Jacobi methods, possess a smoothing property. These methods are very effective in eliminating high frequency components of the error, while leaving the low frequency components relatively unchanged. Therefore, these methods illustrate a high convergence rate during the first few iterations, but the rate quickly decreases as the high frequency components are eliminated, and one is left with only low frequency components of the error.

One way to improve the convergence of an iterative method is to use a good initial guess. A simple technique for obtaining an improved initial guess is to perform some preliminary iterations on a coarse grid and then use these results as an initial guess on the original fine grid. Iteration on a coarser grid is less expensive since there are fewer unknowns to be evaluated. However, it is the following fact that makes coarse grid iteration more attractive: the smooth modes of the error on a fine grid are less smooth on a coarse grid. This conclusion can be easily seen from figure 4.1, which shows that a smooth wave on a grid with $N = 12$ is projected directly to a grid with $N = 6$ (for more rigorous verification, see [42]). This fact suggests that when iteration begins to stall, meaning the predominance of the smooth error modes, it is then advisable to move to a coarser grid, on which those smooth error modes appear more oscillatory and iteration on that grid should be more effective.

At this point, the idea of using a coarse grid and the residual equation, Eq. 4.6, can be incorporated to form a powerful iteration scheme – the coarse grid correction scheme, which is expressed as follows:

1. Iterate on $A\vec{\mathbf{u}} = \vec{\mathbf{f}}$ on a fine grid Ω^h to obtain an approximation $\vec{\mathbf{v}}^h$.

2. Evaluate the residual $\vec{\mathbf{r}} = \vec{\mathbf{f}} - A\vec{\mathbf{v}}^h$.

3. Iterate on the residual equation $A\vec{\mathbf{e}} = \vec{\mathbf{r}}$ on a coarse grid Ω^{2h} to obtain an approximation to the error $\vec{\mathbf{e}}^{2h}$.

4. Correct the solution approximation obtained on Ω^h with the error approximation obtained on Ω^{2h}: $\vec{\mathbf{v}}^h \leftarrow \vec{\mathbf{v}}^h + \vec{\mathbf{e}}^{2h}$.

The superscripts h and $2h$ in the above expressions indicate the grid on which the superscripted variable is evaluated. In this procedure one would iterate on the

fine grid until the convergence deteriorates. Then iterations would be performed on the residual equation using a coarser grid to obtain an approximation to the error itself. This error would be used to correct the approximation to $\vec{\mathbf{v}}$ initially obtained on the fine grid.

4.4 The Multigrid V- and FMV-Cycles

Using the residual equation and the coarse grid correction scheme, many forms of multigrid cycling schemes can be developed, such as the V-cycle scheme, the W-cycle scheme, and the full multigrid V-cycle (FMV) scheme. In the proposed CVFEM, the FMV and V schemes are employed.

The following notation is used to facilitate the description of the FMV and V schemes: the right-hand side vector of the residual equation, $\vec{\mathbf{r}}$, is represented by $\vec{\mathbf{f}}$, since it is just another right-hand side vector; and the solution of the residual equation, $\vec{\mathbf{e}}$, is expressed by $\vec{\mathbf{v}}$, since it is just a solution vector. With these changes, the pure V-cycle scheme is expressed in the following compact form by Briggs [11]:

$$\vec{\mathbf{v}}^h \leftarrow MV^h\left(\vec{\mathbf{v}}^h, \vec{\mathbf{f}}^h\right)$$

This implies the following algorithm:

1. Iterate n_1 times on $A^h\vec{\mathbf{v}}^h = \vec{\mathbf{f}}^h$ with a given initial guess $\vec{\mathbf{v}}^h$.

2. If Ω^h = coarsest grid, then go to 3, else,
   $\vec{\mathbf{f}}^{2h} \leftarrow I_h^{2h}\left(\vec{\mathbf{f}}^h - A^h\vec{\mathbf{v}}^h\right)$
   $\vec{\mathbf{v}}^{2h} \leftarrow 0$
   $\vec{\mathbf{v}}^{2h} \leftarrow MV^{2h}\left(\vec{\mathbf{v}}^{2h}, \vec{\mathbf{f}}^{2h}\right)$.

3. Correct $\vec{\mathbf{v}}^h \leftarrow \vec{\mathbf{v}}^h + I_{2h}^h \vec{\mathbf{v}}^{2h}$.

4. Iterate n_2 times on $A^h \vec{\mathbf{v}}^h = \vec{\mathbf{f}}^h$ with initial guess $\vec{\mathbf{v}}^h$.

The algorithm steps down from the finest grid to the coarsest grid, and then works its way back to the finest grid. Figure 4.2a shows the schedule for the grids in the order in which they are visited. The variable being solved on each grid level is indicated in Fig. 4.2a by u for the actual equation variable and e for the error. In the above algorithm, I_h^{2h} and I_{2h}^h are grid transfer operators which transfer data from fine to coarse, and coarse to fine grids, respectively.

Implied by this algorithm is that one would initially solve the given problem on the fine grid, then the residual is evaluated and transferred to a coarse grid. On the coarse grid one would solve the residual equation for the error $\vec{\mathbf{e}}$ on that grid. One would then determine the residual on this grid level and transfer it to the next coarse mesh, and again solve the residual equation. This descent is continued until the coarsest grid level is reached. Then one ascends to the fine grid level by correcting the error at each grid level, providing a better approximation, then iterating and correcting on the next finest grid level. This is repeated until the finest grid level is reached. Then one would iterate on this level with the new corrected initial value.

To take full advantage of the capabilities of multigrid, one would like to have the best possible initial guess at the beginning of the V-cycle. To do this one would use the FMV-cycle, as shown in Fig. 4.2b. In this algorithm one would actually start on the coarsest grid level, obtain a solution, transfer this solution to the next finest grid level, then solve as in a V-cycle, but at the end of every V-cycle, one would interpolate the solution to an initial guess on the next finest grid level. This is repeated until the finest grid level is reached.

Briggs [11] describes the FMV-cycle in the following manner:

$$\vec{\mathbf{v}}^h \leftarrow FMV^h\left(\vec{\mathbf{v}}^h, \vec{\mathbf{f}}^h\right)$$

1. If Ω^h = coarsest grid, then go to step 3, else,
   $\vec{\mathbf{f}}^{2h} \leftarrow I_h^{2h}\left(\vec{\mathbf{f}}^h - A^h\vec{\mathbf{v}}^h\right)$
   $\vec{\mathbf{v}}^{2h} \leftarrow 0$
   $\vec{\mathbf{v}}^{2h} \leftarrow FMV^{2h}\left(\vec{\mathbf{v}}^{2h}, \vec{\mathbf{f}}^{2h}\right)$.
2. Correct $\vec{\mathbf{v}}^h \leftarrow \vec{\mathbf{v}}^h + I_{2h}^h\vec{\mathbf{v}}^{2h}$.
3. $\vec{\mathbf{v}}^h \leftarrow MV^h\left(\vec{\mathbf{v}}^h, \vec{\mathbf{f}}^h\right)$ n_3 times.

Figure 4.2b shows the scheduling of grids for FMV with $n_3 = 1$. Each V-cycle is preceded by a smaller V-cycle designed to provide the best initial guess possible. The variable being solved on each grid level is indicated in Fig. 4.2a by u for the actual equation variable and e for the error.

To provide the best possible acceleration of a solution with multigrid using these two algorithms one would first perform an FMV-cycle and then continue with V-cycles. This is what is done in the algorithm in this thesis.

4.5 Multigrid Algorithm

In the CVFE-MG method presented in this thesis, the segregated solution algorithm, which has been discussed in the previous chapter, is used in the context of an FMV-V-cycle algorithm. The results generated by this CVFE-MG are then compared with the results obtained by the CVFEM presented in the previous chapter, when it is implemented on one grid.

4.5.1 Solution Algorithm

The coefficients in the discretized equations representing the actual problem, and the residual equations are the same, i.e. **A**. The only differences between the two sets of equations are the right hand sides, and the dependent variables. Therefore, the coefficients in both sets of equations are evaluated using the techniques described in Chapter 3. At each level in the multigrid algorithm, the segregated solution procedure is used to solve for u, v, p, or the errors in u, v, p, i.e. e^u, e^v, and e^p. The following is a brief description of the steps followed in the FMV-V-cycle algorithm used in this thesis.

The FMV-V-cycle algorithm starts from the coarsest grid level, and on this level, the actual dependent variables (u, v, p) are evaluated with an initial guess, $\vec{\mathbf{v}}^{8h}$, (refer to Fig. 4.2b). The newly obtained u, v, p-field is interpolated into the next finest level, Ω^{4h}. New values of u, v, p on Ω^{4h} are evaluated using the interpolated values as an initial guess. Then the residual of the dependent variables, $\vec{\mathbf{r}}^{4h}$, is calculated and injected into the coarsest level, Ω^{8h}, where the residual equations ($A\vec{\mathbf{e}}^{8h} = \vec{\mathbf{r}}^{8h}$) are solved to obtain the error, e^u, e^v, and e^p of the actual dependent variables, with an initial guess of zero. The error is then interpolated into the next finest level, Ω^{4h}, and used to correct the actual dependent variables there ($\vec{\mathbf{v}}^{4h} \leftarrow \vec{\mathbf{v}}^{4h} + \vec{\mathbf{e}}^{4h}$). With this better solution as an initial guess, the actual dependent variables, u, v and p are evaluated and interpolated into the next finest level, Ω^{2h}. New values of u, v, p on Ω^{2h} are evaluated using the interpolated values as an initial guess. Then, the residual at level Ω^{2h} is calculated and injected to level Ω^{4h}. On level Ω^{4h}, residual equations are solved with an initial guess of zero to obtain errors of the dependent variables, e^u, e^v, and e^p. The residual of these errors is injected to level Ω^{8h}, where the residual equations are solved for

the "errors" of the errors of the actual dependent variables with an initial guess of zero. These "errors" are interpolated to level Ω^{1h}, and used to correct the errors of the dependent variables, and the corrected values $\vec{e}^{1h}$ are used as a better initial guess to solve the residual equations at level Ω^{1h}. Then the newly obtained $\vec{e}^{1h}$ is interpolated to level Ω^{2h}, and used to correct the actual dependent variables u, v, p on level Ω^{2h}. The corrected dependent variables are used as a much better initial guess to solve the actual dependent variable equations on that level (Ω^{2h}), and the newly obtained value, $\vec{\mathbf{u}}^{2h}$, is interpolated to the finest level Ω^{h}, where it is used as an initial guess to evaluate u, v and p on the finest mesh. At this point, one obtains the actual dependent variable fields on the desired fine grid level. After that, a few V-cycles can be used as may be required. It should be noted that, at each grid level, the segregated solution algorithm described in section 3.7.1 is used to solve for u, v, p and the errors in these variables. This requires coefficient evaluations, as described in Chapter 3 at each grid level.

4.5.2 Intergrid Transfer

As mentioned above, the FMV-V-cycle algorithm requires data transfer between coarse and fine grids. Transferring vectors from a coarse grid to a fine grid is called prolongation or interpolation. Many interpolation methods can be used, however, for most multigrid purposes, the simplest linear interpolation is quite effective [11]. Therefore, a linear interpolation is used in this thesis.

The linear interpolation operator is denoted by I_{2h}^{h}. It takes coarse grid vectors and produces fine grid vectors according to the rule $\vec{\mathbf{v}}^{h} = I_{2h}^{h}\vec{\mathbf{v}}^{2h}$, where, for two-dimensional problems, the components of $\vec{\mathbf{v}}^{h}$ are given as follows:

$$
\begin{aligned}
v^h_{2i,2j} &= v^{2h}_{i,j} \\
v^h_{2i+1,2j} &= \frac{1}{2}\left(v^{2h}_{i,j} + v^{2h}_{i+1,j}\right) \\
v^h_{2i,2j+1} &= \frac{1}{2}\left(v^{2h}_{i,j} + v^{2h}_{i,j+1}\right) \\
v^h_{2i+1,2j+1} &= \frac{1}{4}\left(v^{2h}_{i,j} + v^{2h}_{i+1,j} + v^{2h}_{i,j+1} + v^{2h}_{i+1,j+1}\right)
\end{aligned} \tag{4.8}
$$

The subscripts on the right hand sides of Eq. 4.8 refer to the numbering scheme on the coarse mesh. The second class of intergrid transfer functions involves moving vectors from a fine grid to a coarse grid, which is called restriction or injection. Like interpolation methods, many restriction methods can be used in the multigrid algorithms. In the proposed CVFEM, a full weighting injection operator [11], which is denoted by I^{2h}_h, is used. Its function can be defined by $\vec{\mathbf{v}}^{2h} = I^{2h}_h \vec{\mathbf{v}}^h$, where,

$$
\begin{aligned}
v^{2h}_{i,j} &= v^h_{2i,2j} + (v^h_{2i+1,2j} + v^h_{2i,2j+1} + v^h_{2i-1,2j} + v^h_{2i,2j-1})/2 \\
&+ (v^h_{2i+1,2j+1} + v^h_{2i-1,2j+1} + v^h_{2i-1,2j-1} + v^h_{2i+1,2j-1})/4
\end{aligned} \tag{4.9}
$$

The subscript on the left hand side of Eq. 4.9 refers to the numbering scheme on the coarse mesh.

4.5.3 Some Details about the Programs

As discussed in section 4.5.1, at the end of the FMV and the beginning of every V-cycle, the latest actual dependent variables u, v and p are obtained. To take full advantage of this up to date solution, the coefficients of the momentum and continuity equations are evaluated using these newly obtained values to calculate the residual. This method has been proven to be very effective in increasing the efficiency of the proposed CVFE-MG.

Although under-relaxation parameters, α_u and α_v, have been used for momentum equations, the results may oscillate or even diverge when a very coarse grid is used. In this case, performing a few iterations of the solution algorithm at the end of every V-cycle, before calculating and injecting residuals to the coarser grid, was found to be an effective means of promoting convergence. This treatment was more efficient than using too much under-relaxation or increasing the level of the coarsest grid, as both led to slower convergence for the proposed CVFE-MG.

In every V-cycle, the actual dependent variables, u, v and p are only evaluated at the finest grid level. At other levels, u, v and p, which are needed to calculate the coefficients of momentum and continuity equations, are injected from the finest grid. The "mass conserving" velocities are injected in the same manner. This injecting scheme is more stable than injecting the "mass conserving" velocities from every next finest grid and interpolating them from every next coarsest grid.

It is obvious that two sets of boundary conditions are needed in the FMV-V-cycle algorithm. One is for the actual dependent variables, u, v and p, which has been discussed in the previous chapter, the other is for the residual equations. If a specified value boundary is used, the errors of the actual dependent variables at the boundary are zero, therefore, it is also a specified value boundary for errors. For specified flux and outflow boundaries, the errors on the boundaries are unknown, therefore, when injecting residuals from fine to coarse grids, residual injections both inside and along the boundaries are needed.

4.6 Conclusion

This chapter has presented a brief review of the concepts of multigrid, and details of the implementation of FMV- and V-cycle multigrid algorithms in the context of the segregated CVFEM have been discussed. In the following chapter, the efficiency of this CVFE-MG will be compared with that of the CVFEM applied to one grid, when both methods are used to solve two test problems.

Figure 4.1: A wave on Ω^h (N=12) is projected onto Ω^{2h} (N=6) [11].

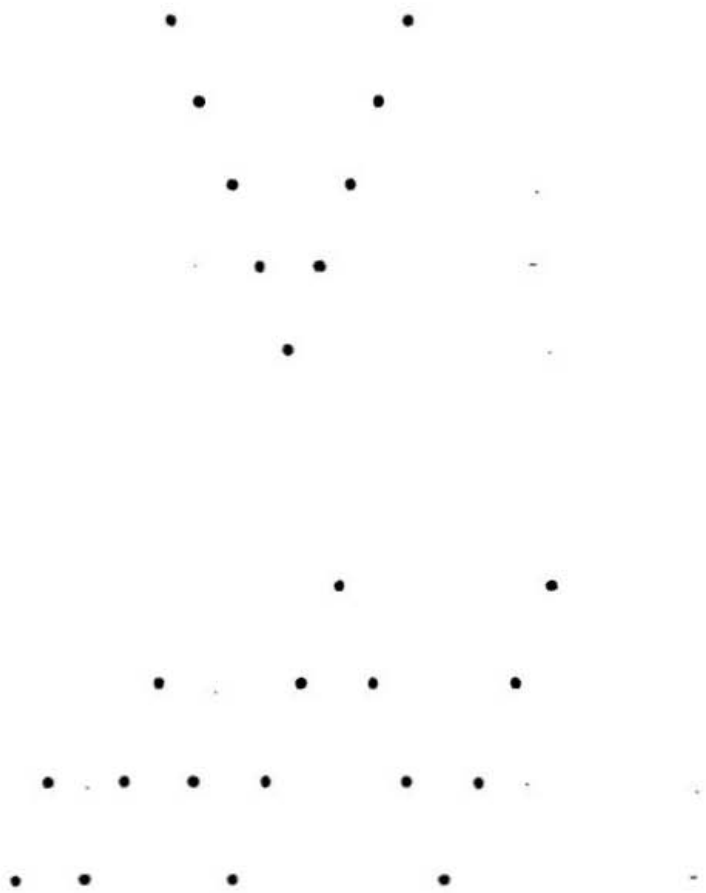

Figure 4.2: Schedule of grids for (a) V-cycle and (b) FMV scheme [11].

Chapter 5

Testing of the Proposed CVFEM

5.1 Introduction

The two-dimensional CVFEM presented in Chapter 3 and the multigrid solution algorithm proposed in Chapter 4 have been subjected to intensive testing and evaluation. The results of two test problems are presented and discussed in this chapter. These test problems are: (1) steady, laminar recirculation of an incompressible Newtonian fluid contained in a square enclosure with a sliding lid (i.e. square driven cavity); and (2) laminar flow over a rearward facing step. All computations were performed on the DEC 4000/610 computer at the Center for Computer Aided Engineering of Memorial University of Newfoundland.

The remainder of this chapter is divided into three sections. In section 5.2, the square driven cavity test problem is presented, in section 5.3, the rearward facing step problem is discussed, and in section 5.4, the results are summarized. The proposed CVFE-MG results are compared with numerical data available in the literature, and, in particular, the efficiency of the CVFE-MG is compared with that of the CVFEM described in Chapter 3 when it is implemented on one grid (CVFE-OG).

5.2 Square Driven Cavity

5.2.1 Problem Statement

In this problem, the steady, two-dimensional, laminar recirculation of an incompressible Newtonian fluid contained in a square enclosure is considered. The motion of the fluid is driven by a sliding lid. A schematic of this problem is given in Fig. 5.1a. A square enclosure of side L has its lower left corner located at the origin of the Cartesian co-ordinate system. All walls are fixed, except for the lid, which moves in the positive x-direction with a constant velocity U_w.

The equations which govern this fluid flow problem are the x- and y-momentum, and continuity equations. Using the following non-dimensional parameters:

$$\begin{aligned} x^* &= \frac{x}{L}; \quad y^* = \frac{y}{L}; \quad u^* = \frac{u}{U_w}; \\ v^* &= \frac{v}{U_w}; \quad p^* = \frac{p}{\rho U_w^2}; \quad Re_w = \frac{\rho U_w L}{\mu} \end{aligned} \tag{5.1}$$

the governing equations may be expressed in the following non-dimensional forms [18]:

x-momentum:

$$u^* \frac{\partial u^*}{\partial x^*} + v^* \frac{\partial u^*}{\partial y^*} = -\frac{\partial p^*}{\partial x^*} + \frac{1}{Re_w}\left(\frac{\partial^2 u^*}{\partial x^{*2}} + \frac{\partial^2 u^*}{\partial y^{*2}}\right) \tag{5.2}$$

y-momentum:

$$u^* \frac{\partial v^*}{\partial x^*} + v^* \frac{\partial v^*}{\partial y^*} = -\frac{\partial p^*}{\partial y^*} + \frac{1}{Re_w}\left(\frac{\partial^2 v^*}{\partial x^{*2}} + \frac{\partial^2 v^*}{\partial y^{*2}}\right) \tag{5.3}$$

continuity:

$$\frac{\partial u^*}{\partial x^*} + \frac{\partial v^*}{\partial y^*} = 0 \tag{5.4}$$

with the boundary conditions:

$$\begin{aligned} v^* &= 0 \text{ on all walls;} \\ u^* &= \begin{cases} 1 \text{ at } y^* = 1,\ 0 < x^* < 1; \\ 0 \text{ elsewhere.} \end{cases} \\ p^* &= 0 \text{ at } x^* = y^* = 0.5 \end{aligned} \tag{5.5}$$

The singularities at the corners of the lid are handled by setting the velocity to zero there. The only free parameter in this problem is the Reynolds number, Re_w.

This problem is often used in the testing of numerical methods for recirculating flows [18, 31, 39]. Ghia et al. [16] used a stream function-vorticity finite-difference formulation and a multigrid method with a 129×129 node grid to solve this problem. They published velocity profiles along the domain centerlines, and stream function values for the different vortices contained within the cavity, for Reynolds numbers ranging from 100 to 10,000.

5.2.2 Numerical Details

For this problem, a uniform fine grid of 33×33 was used to discretize the calculation domain. Five uniform grid levels were used in the multigrid algorithm; the finest mesh was 33×33 and each grid level doubled the mesh size until the coarsest mesh (3×3) was reached. All grids used the diagonal configuration shown in Fig. 5.1b. The results produced for Reynolds numbers of 100 and 400 will be presented in this discussion. For the grids used, and at these Reynolds numbers, the optimum values of the under-relaxation parameters α_u and α_v were 0.5. The most efficient CVFE-MG implementation employed 5 iterations of the segregated solution algorithm at the end of every V-cycle for $Re_w = 100$ and $Re_w = 400$.

Iterations in the TDMA solver were halted when the ratio between the current residual and the initial residual, at the commencement of iterations, was less than 0.5 for the momentum equations, and 0.7 for the continuity equations. The overall iterations in the segregated multigrid solution algorithm were terminated when the maximum error in u, v and p, in the whole calculation domain, was less than 10^{-3} . Here, the maximum error is the maximum absolute value of the difference between the current solution and the "converged" solutions, which were obtained by continuing iteration until the change in any u, v or p in the calculation domain, between successive iterations, was less than 10^{-5}.

The initial conditions for this problem were treated as follows: velocities at the boundaries were set equal to the exact values, and velocities inside the domain were set equal to zero. Pressure was set equal to zero everywhere in the domain.

5.2.3 Results

u'- and v'- velocity Profiles

Plots of u'-velocity along the vertical centerline and v'-velocity along the horizontal centerline of the cavity for Reynolds numbers of 100 are given in Figs. 5.2a and 5.2b, respectively. Similar plots for Reynolds number of 400 are presented in Fig. 5.3. As can be seen from Fig. 5.2, at $Re_w = 100$, the results are in good agreement with the numerical results of Ghia et al. [16]. At $Re_w = 400$, Fig. 5.3, however, the two methods provide different results: the proposed CVFE-MG does not capture the maximum values of these velocities. In the CVFEM used in this thesis, convection terms are interpolated using an upwinding function, and diffusion terms are interpolated linearly, for all grid Reynolds numbers. Therefore,

at higher Reynolds numbers, where convection dominates, the influence of the diffusion term will be overestimated and tend to reduce predicted maxima. The upwinding scheme is also first-order accurate and will not capture maxima as well as the second-order scheme used in Ghia et al. [16]. Also, the upwind scheme used does not take into account the directionality of the flow very well, and this can lead to false diffusion, or smearing of the solution. This effect would be more obvious at higher Reynolds numbers. Finally, the grid used here is 33×33, which is much coarser than the grid used in [16] which is 129×129.

Streamlines

Plots of streamlines generated by the proposed CVFE-MG method are presented in Figs. 5.4a and 5.4b for Reynolds numbers of 100 and 400, respectively. The plot for $Re_w = 100$, Fig. 5.4a, illustrates that the center of the vortex is displaced towards the upper right corner, due to the domination of viscous forces at this Reynolds number. At $Re_w = 400$, Fig. 5.4b, however, inertia forces become dominant, and the vortex center approaches the central region of the enclosure. Both streamline plots show the characteristic secondary recirculation zones at the bottom corners of the enclosure.

Execution Time

Plots of the maximum errors in u^*, v^*, and p^* for the CVFE-MG and CVFE-OG solutions versus execution time for $Re_w = 100$ are presented in Figs. 5.5a, 5.5b and 5.5c, respectively. As can be seen from these figures, solutions converge much faster using multigrid than one grid. For convenience of comparison, semi-log plots

of Fig. 5.5 are given in Fig. 5.6. For this square driven cavity problem, the solutions reach an acceptable level of convergence when the maximum error is less than 10^{-2}. By this criterion, the CVFE-MG requires 8.66s and the CVFE-OG requires 64.32s of CPU time, which makes the multigrid method 7.43 times faster, see Table 5.1.

Plots of residuals versus execution time for $Re_w = 100$ are presented in Fig. 5.7: figures 5.7a and 5.7b show the average residual of x- and y- momentum equations, respectively, and Fig. 5.7c shows the average residual of the continuity equation. From Figs. 5.7a and 5.7b, it is obvious that the residuals for both x- and y- momentum equations decreases more quickly using multigrid than one grid. For the residual of continuity equation in Fig. 5.7c, however, there is not much difference between multigrid and one grid methods. This is expected, as for this square driven cavity problem, pressure gradients are very small except around the upper left and right corners of the cavity, thus the capabilities of multigrid method are not fully demonstrated in the solution of the continuity equation.

Plots of the maximum errors of u^*, v^*, and p^* versus execution time are presented in Figs. 5.8a, 5.8b and 5.8c, respectively, and semi-log plots of Fig. 5.8 are given in Fig. 5.9 for $Re_w = 400$. Plots of average residuals of x-, y- momentum and continuity equations are presented in Figs. 5.10a, 5.10b and 5.10c, respectively. It can be seen from these figures, that the CVFE-MG again provides accelerated convergence, however, the magnitude of the increase in convergence rate is reduced. By the same convergence criterion as for $Re_w = 100$, the multigrid method is 3.80 times more efficient than the corresponding one grid method, requiring 17.90s as opposed to 68.03s, see Table 5.1.

As shown in Table 5.1, the CVFE-MG does not produce as large a reduction in execution time at $Re_w = 400$ as at $Re_w = 100$. As Reynolds number increases

the discretized equations become strongly non-linear, and the "mass conserving" velocity field will have a significant effect on the coefficients. It is speculated that the method used to transfer the "mass conserving" velocities between fine and coarse grids, as described in Section 4.5.2, may be improved. This would be an area for further research. One possible means of improving this part of the algorithm would be to provide continuous correction of the u, v, p solution on the fine mesh, throughout the V-cycle. This would provide more up to date fields to be used in the coefficients at all grid levels.

5.3 Rearward Facing Step

5.3.1 Problem Statement

In this problem, the steady, two-dimensional, laminar incompressible Newtonian fluid flow over a rearward facing step is considered. The domain is rectangular and extends 3H in the x-direction and is H high. The top half of the left boundary is an inflow boundary, with a specified inlet velocity of V_{in}. The top boundary is a symmetry plane, and the right boundary is an outflow boundary. The lower half of the left boundary, and the bottom surface of the domain are no flow, no slip boundaries. The geometry and velocity vectors for this problem are shown in Fig. 5.11a. The inlet velocity, V_{in}, is uniform.

The equations which govern this problem are the x-, y-momentum and continuity equations. Using the non-dimensional parameters:

$$x^* = \frac{x}{H}; \quad y^* = \frac{y}{H}; \quad u^* = \frac{u}{V_{in}};$$
$$v^* = \frac{v}{V_{in}}; \quad p^* = \frac{p}{\rho V_{in}^2}; \quad Re = \frac{\rho V_{in} H}{\mu} \tag{5.6}$$

the governing equations can be written in the forms given by Eqs. 5.2, 5.3 and 5.4, with the boundary conditions:

$$
\begin{aligned}
u^* &= \begin{cases} 1 & 0.5 < y^* \leq 1,\ x^* = 0; \\ 0 & 0 \leq y^* \leq 0.5,\ x^* = 0; \text{ and on the bottom boundary;} \end{cases} \\
\frac{\partial u^*}{\partial y^*} &= \frac{\partial v^*}{\partial y^*} = 0 \quad y^* = 1 \\
\frac{\partial u^*}{\partial x^*} &= \frac{\partial v^*}{\partial x^*} = 0 \quad x^* = 3 \qquad (5.7) \\
v^* &= 0 \quad \text{on the left and bottom boundaries;} \\
p^* &= 0 \quad \text{at the middle point of the right boundary.}
\end{aligned}
$$

This problem is used to test the capabilities of the CVFE-MG to solve problems involving inflow, outflow and symmetry boundary conditions, in the presence of a recirculating flow. The only free parameter in this problem is the Reynolds number.

5.3.2 Numerical Details

For this problem, a uniform fine grid of 33×33 was used to discretize the domain. Five uniform grid levels were used in the CVFE-MG, with the coarsest mesh consisting of 3×3 nodes, and each grid refinement doubled the number of nodes until the finest mesh, 33×33 nodes, was reached. All meshes used the diagonal configuration as shown in Fig. 5.1b. Results produced for a Reynolds number of 100 are presented here. For the grids used, and at this Reynolds number, the optimum values of the under-relaxation parameters, α_u and α_v, were 0.3, for the CVFE-MG and 0.4 for the CVFE-OG. The most efficient CVFE-MG implementation employed 3 iterations of the segregated solution algorithm at the end of every V-cycle. The stopping criteria in the TDMA solver, and overall convergence cri-

teria were the same as those used in the square driven cavity problem, see section 5.2.2.

The initial conditions were as follows: velocities at the left and bottom boundaries were set equal to the exact values; and velocities inside the domain were set equal to zero. Pressure was set equal to zero everywhere.

5.3.3 Results

Velocity Vectors

Plots of velocity vectors generated by the proposed CVFE-MG are presented in Fig. 5.11a for Reynolds number of 100. The arrows in the figure illustrate both the direction and relative magnitude of the velocity vector at each node. The expected recirculation zone is shown at the bottom left corner. An enlarged picture of the recirculation zone is presented in Fig. 5.11b.

Execution Time

Plots of the maximum errors in u^*, v^* and p^* between the solutions obtained by the proposed CVFE-MG and CVFE-OG and their respective "converged" solutions versus execution time for $Re = 100$ are presented in Figs. 5.12a, 5.12b and 5.12c, respectively. It can be seen that similar results to the square driven cavity problem were obtained, demonstrating that the proposed CVFE-MG is more efficient than the CVFE-OG for this outflow problem. For the convenience of comparison, semi-log plots of Fig. 5.12 are given in Fig. 5.13. For this rearward facing step problem, the solutions reach an acceptable level of convergence when the maximum error in u^*, v^* and p^* is less than 10^{-2}. By this criterion, the CVFE-MG requires 54.94s and

the CVFE-OG requires 119.90s of CPU time, which makes the multigrid method 2.18 times faster, as shown in Table 5.2. Plots of average residuals of the x- and y- momentum and continuity equations versus execution time for $Re = 100$ are presented in Figs. 5.14a, 5.14b and 5.14c, respectively.

The multigrid method was effective in accelerating the solution to this problem, however, the outflow and symmetry boundary conditions have made it less effective than in the square driven cavity problem. The CVFE-MG was also applied to two-dimensional Poiseuille and Couette flow problems and it was again found to be twice as fast as the CVFE-OG for these simpler flow problems.

5.4 Summary

The two problems presented in this chapter have demonstrated that the proposed CVFE-MG can generate solutions that correctly predict the physical behaviour of laminar flows, and that the execution time of CVFE-MG is significantly less than that of the CVFE-OG method. Variations in the behaviour of the CVFE-MG with Reynolds number are to be investigated in further research.

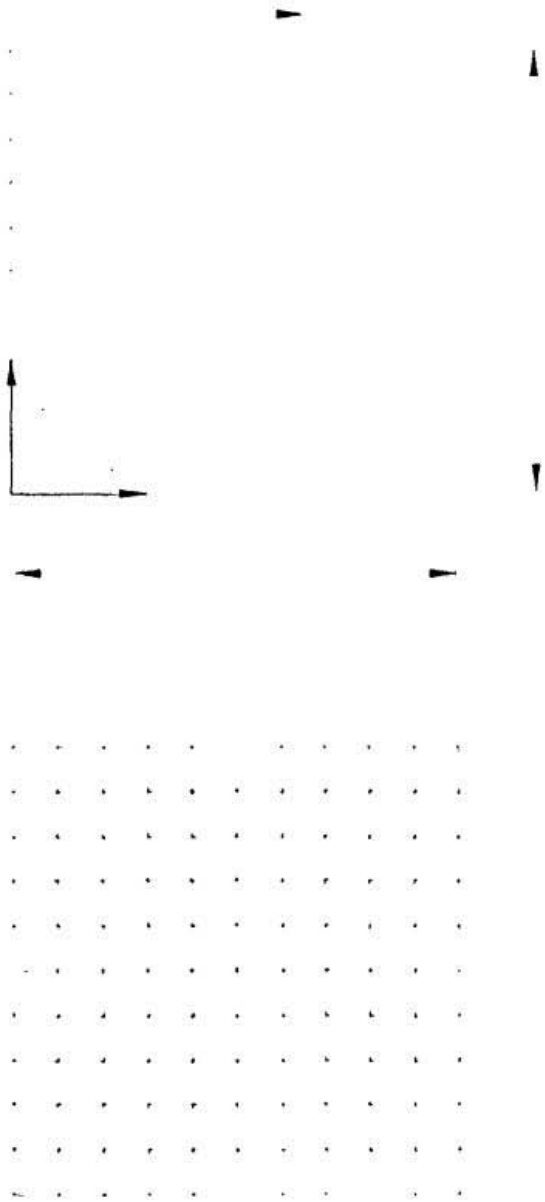

Figure 5.1: Square driven cavity: (a) problem schematic; and (b) uniform 11×11 node grid showing the diagonal configuration.

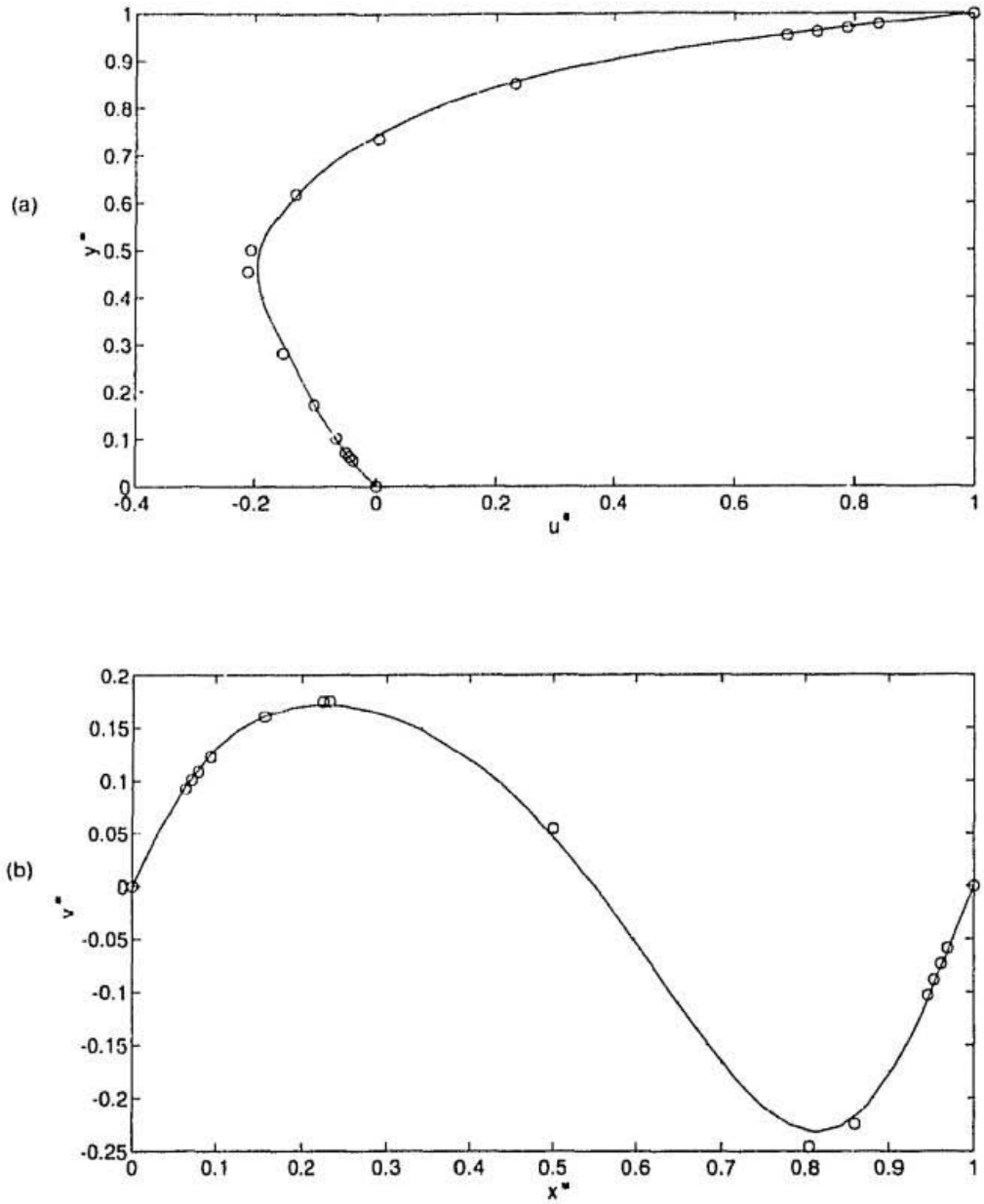

Figure 5.2: Square driven cavity: Velocity profiles for $Re_w = 100$: (a) u^*-velocity at the vertical centerline of the cavity; (b) v^*-velocity at the horizontal centerline of the cavity. (· CVFE-MG; o Ghia, et al. [16])

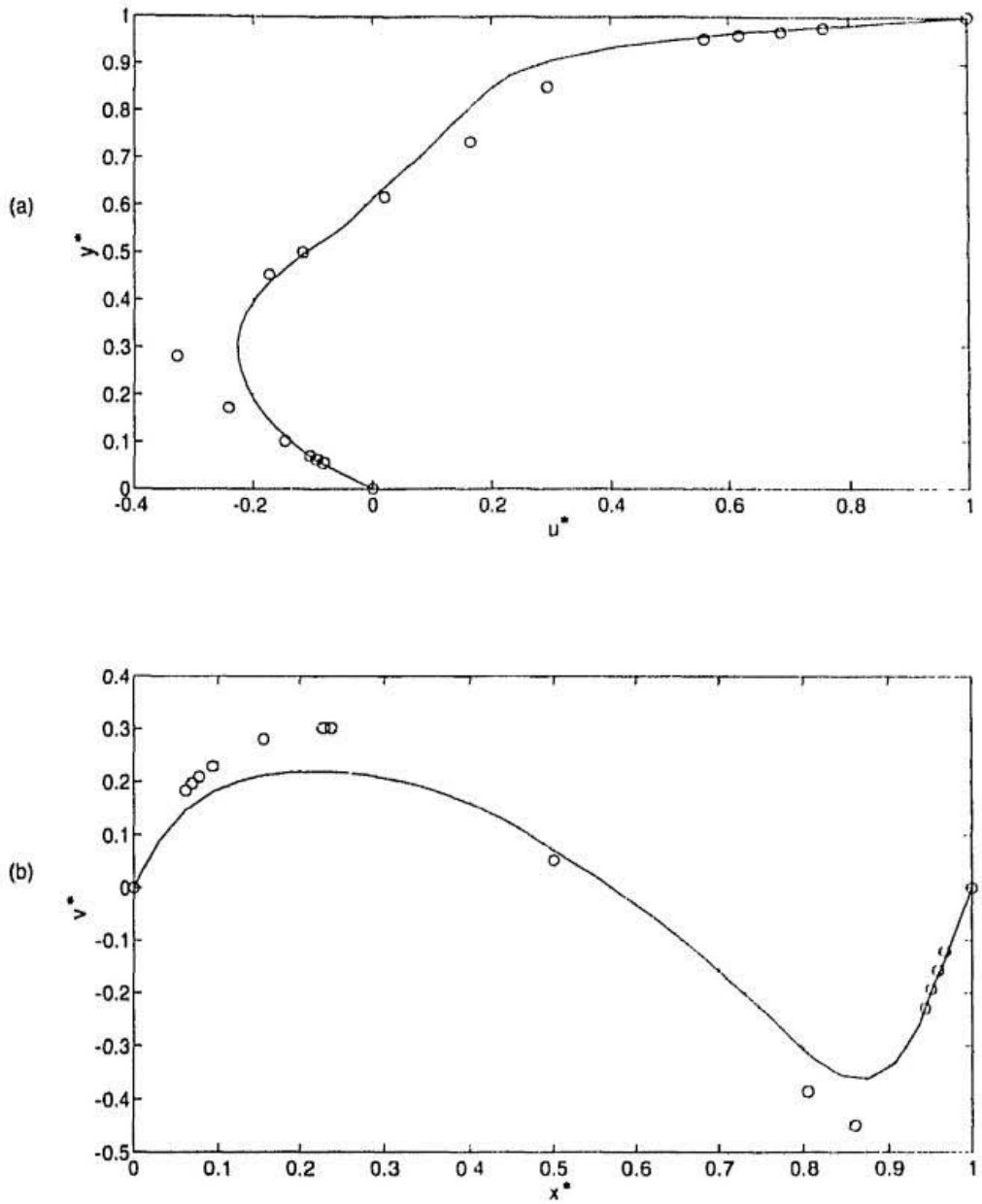

Figure 5.3: Square driven cavity: Velocity profiles for $Re_w = 400$: (a) u^*-velocity at the vertical centerline of the cavity; (b) v^*-velocity at the horizontal centerline of the cavity. (— CVFE-MG; o Ghia, et al. [16])

(a)

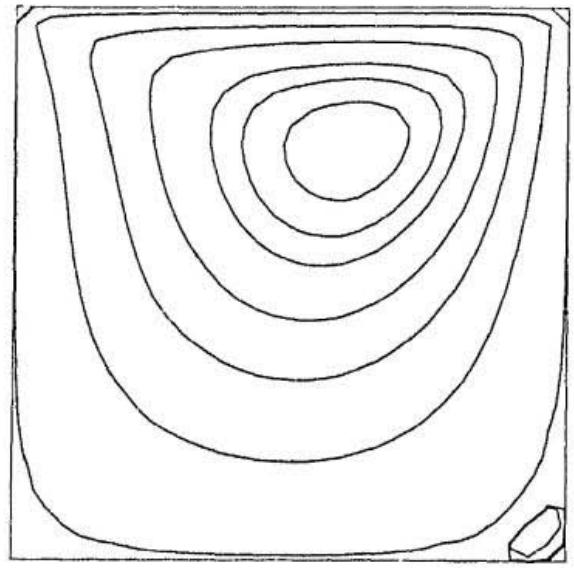

(b)

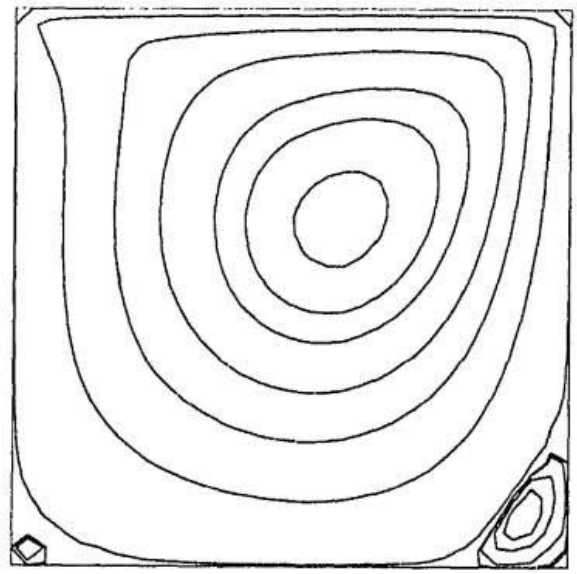

Figure 5.4: Square driven cavity: Streamline plots obtained with the proposed CVFE-MG for: (a) $Re_w = 100$ and (b) $Re_w = 400$.

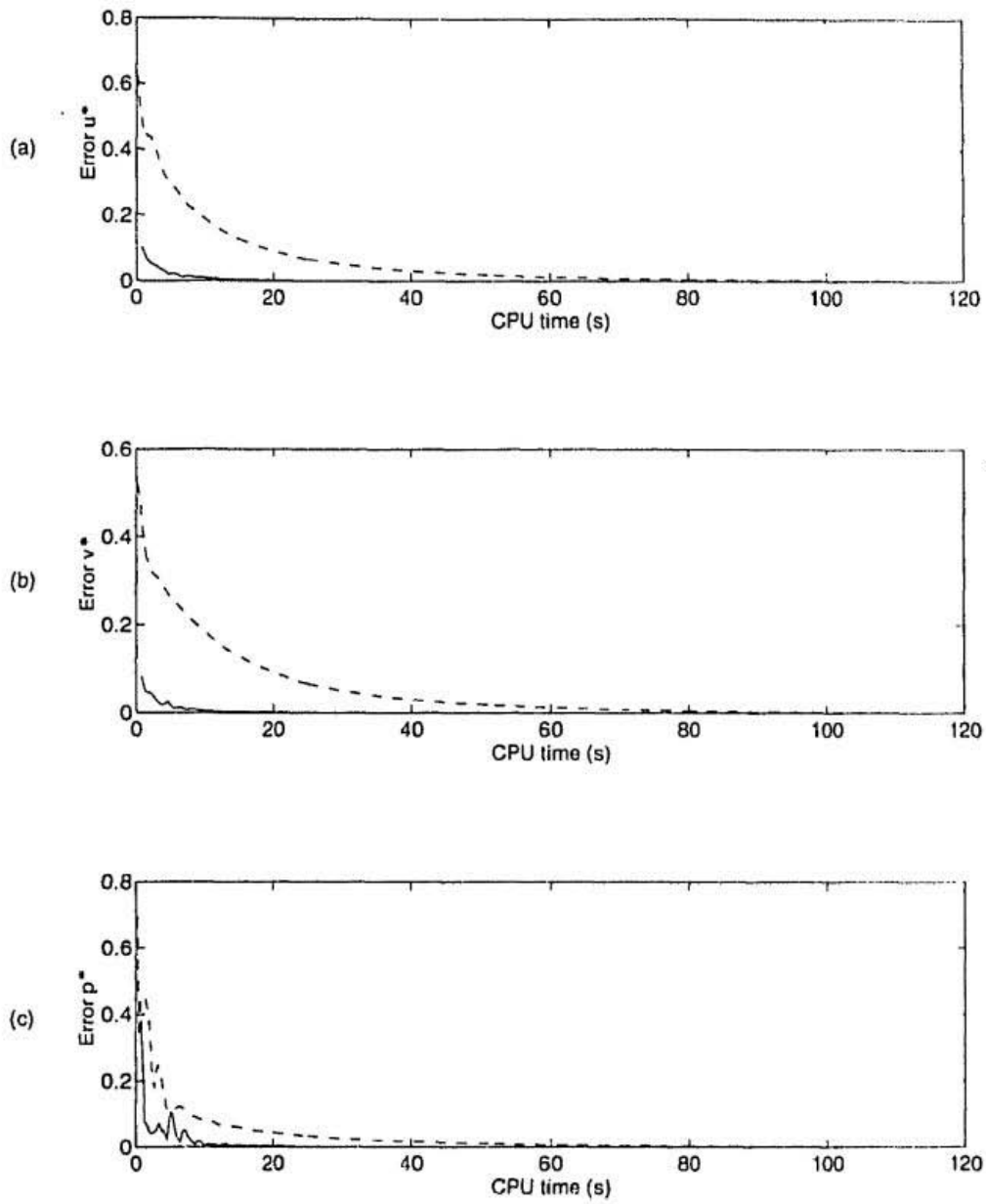

Figure 5.5: Square driven cavity: Plots of the maximum errors against execution time for $Re_w = 100$: (a) u^*-velocity; (b) v^*-velocity and (c) pressure p^*.
(-- CVFE-MG; ___ CVFE-OG)

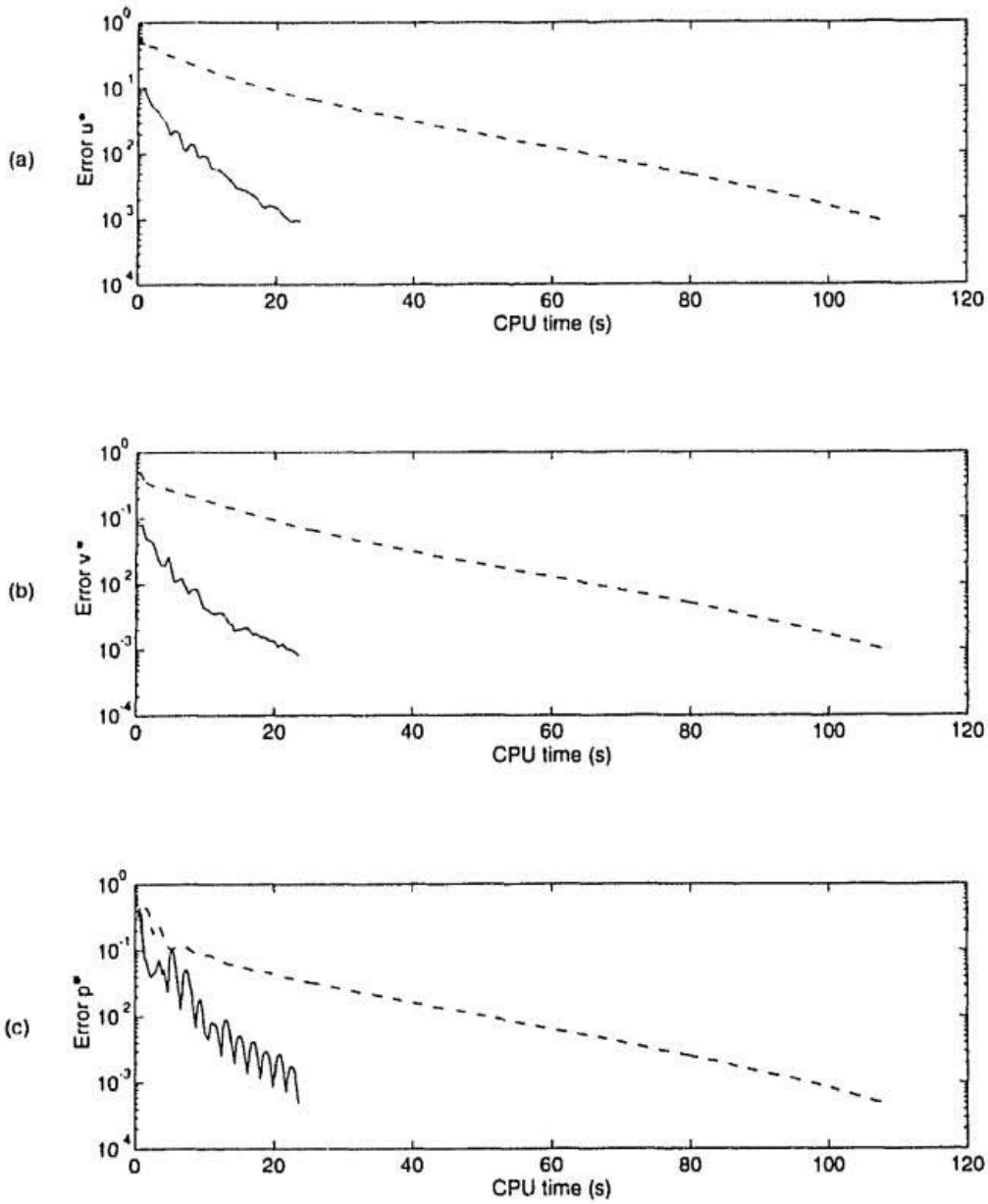

Figure 5.6: Square driven cavity: Semi-log plots of the maximum errors against execution time for $Re_w = 100$: (a) u^*-velocity; (b) v^*-velocity and (c) pressure p^*. (CVFE-MG; --- CVFE-OG)

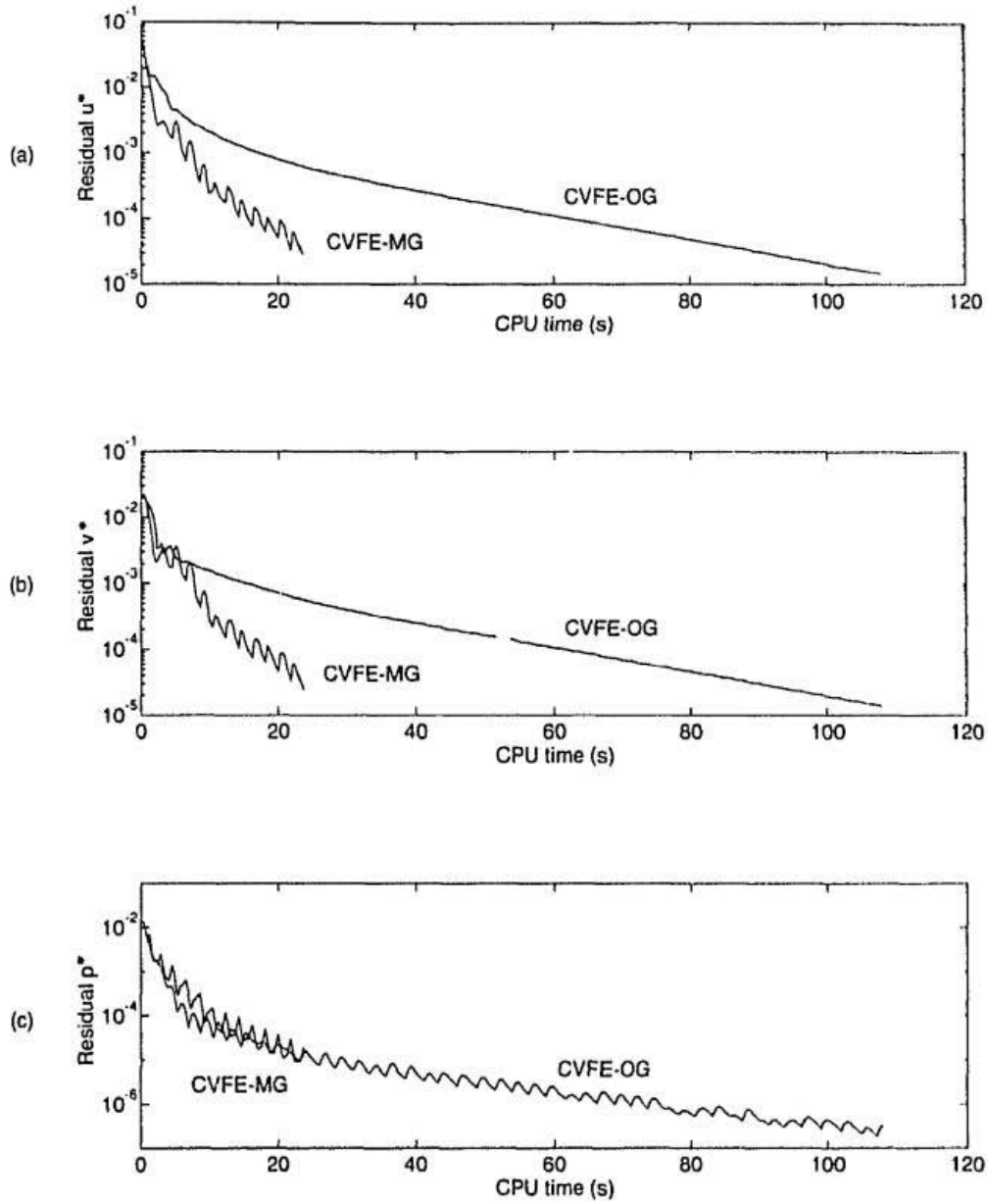

Figure 5.7: Square driven cavity: Plots of average residual against execution time for $Re_w = 100$: (a) u^*-velocity; (b) v^*-velocity and (c) pressure p^*.

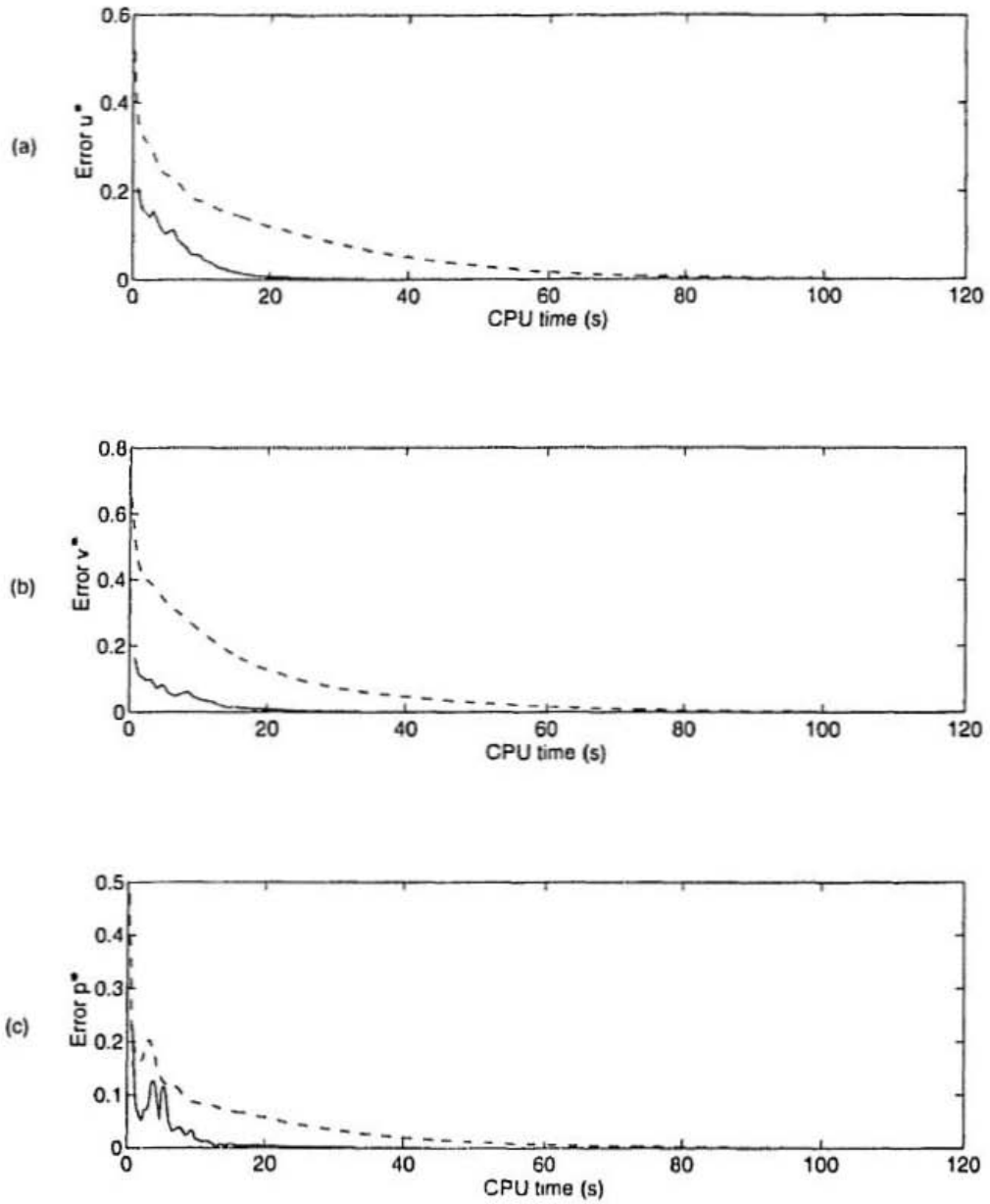

Figure 5.8: Square driven cavity: Plots of the maximum errors against execution time for $Re_w = 400$: (a) u^*-velocity; (b) v^*-velocity and (c) p essure p^*.
(CVFE-MG; ___ CVFE-OG)

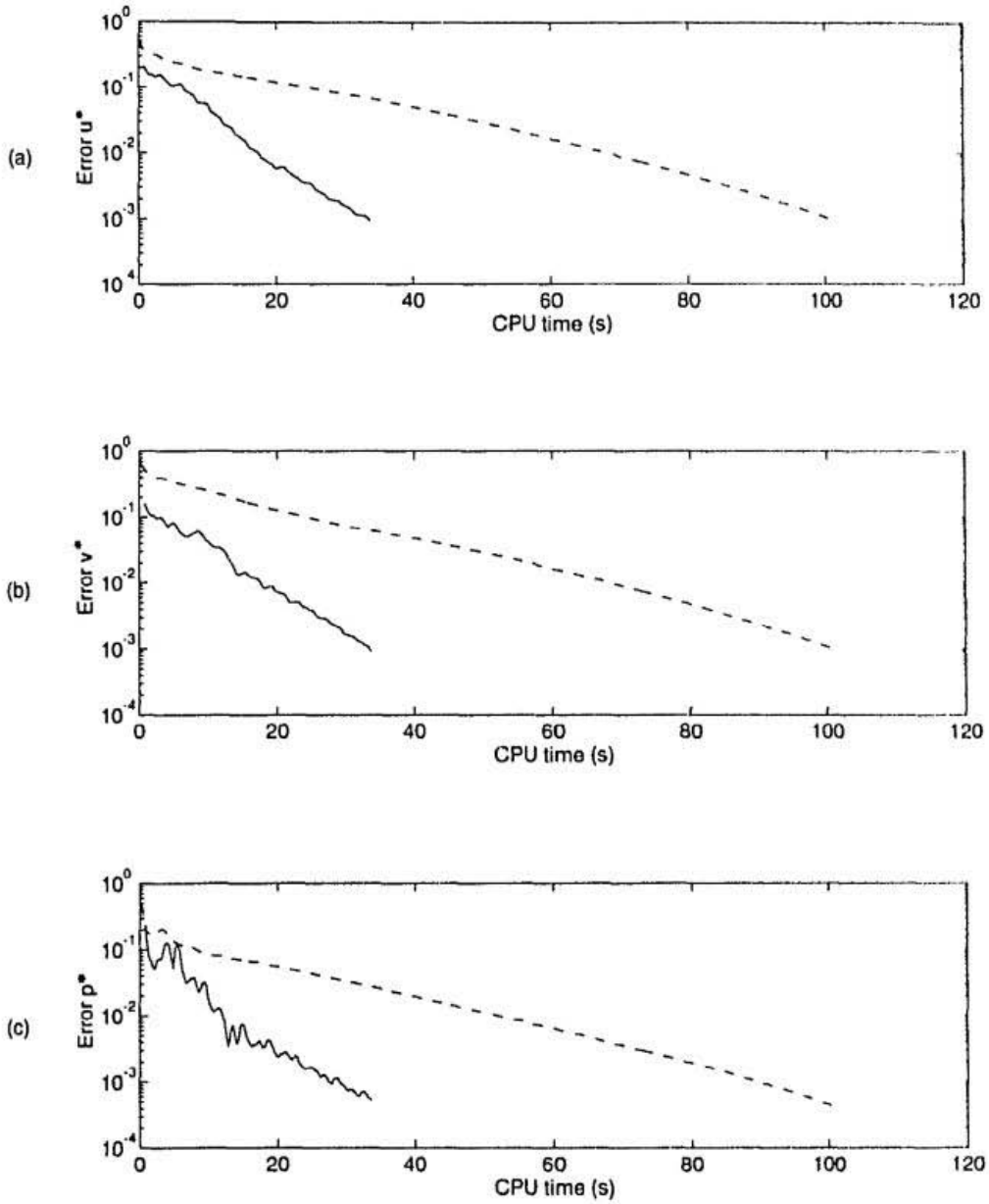

Figure 5.9: Square driven cavity: Semi-log plots of the maximum errors against execution time for $Re_w = 400$: (a) u^*-velocity; (b) v^*-velocity and (c) pressure p^*. (— CVFE-MG; --- CVFE-OG)

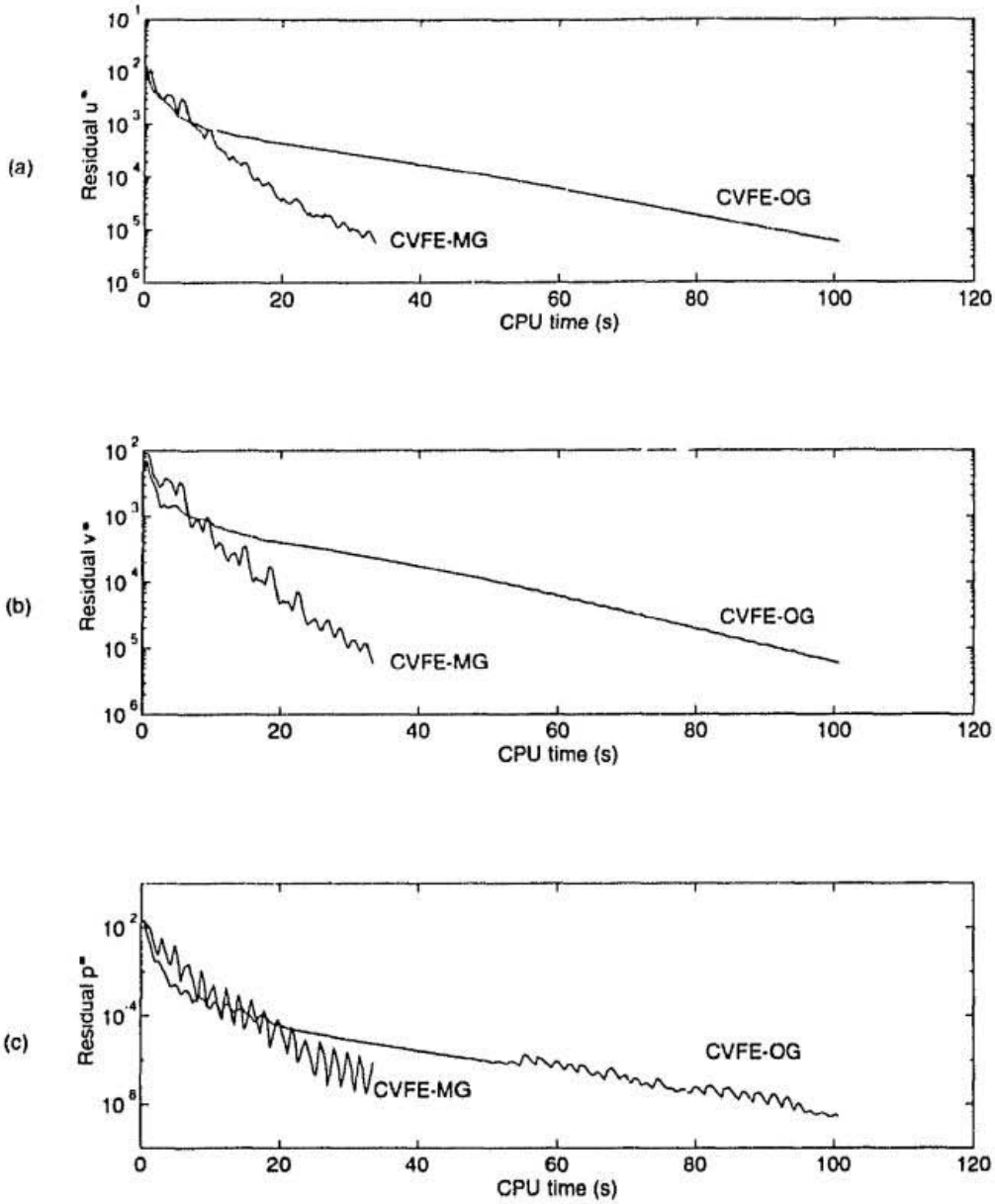

Figure 5.10: Square driven cavity: Plots of average residual against execution time for $Re_n = 400$: (a) u^*-velocity; (b) v^*-velocity and (c) pressure p^*.

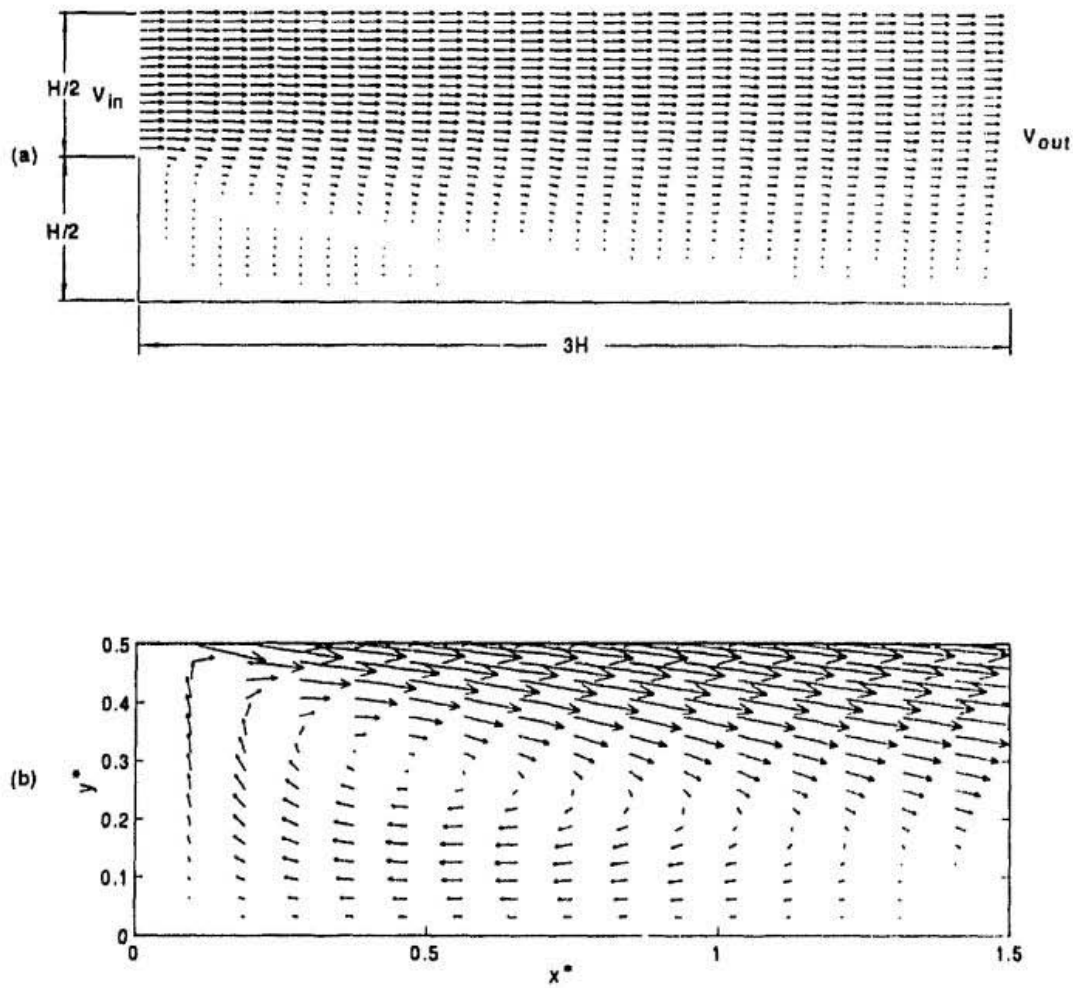

Figure 5.11: Rearward facing step: (a) problei i schematic and velocity vectors for $Re = 100$: (b) enlarged portion of the recirculation zone for $Re = 100$.

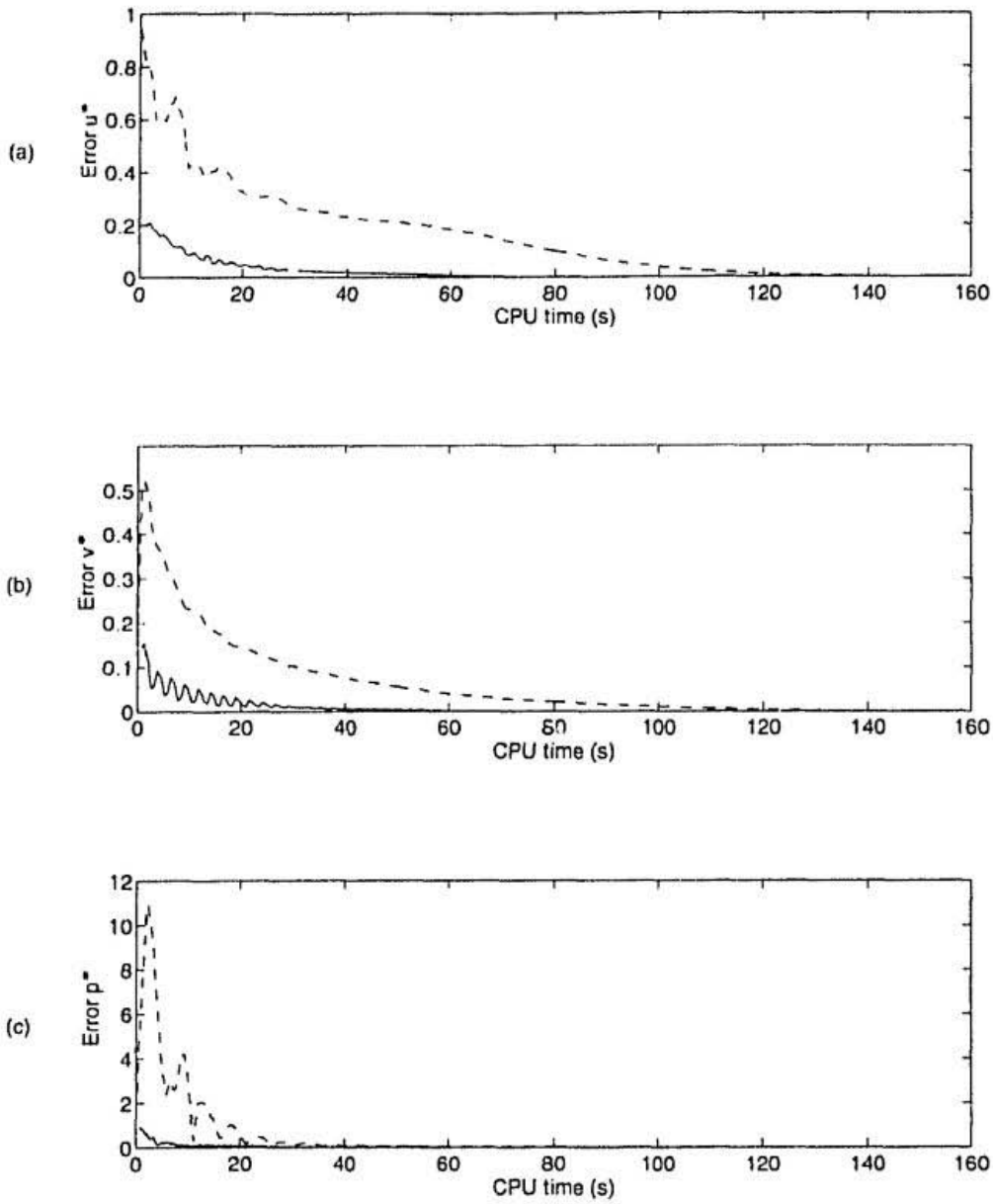

Figure 5.12: Rearward facing step: Plots of the maximum errors against execution time for $Re_w = 100$: (a) u^*-velocity; (b) v^*-velocity and (c) pressure p^*.
(CVFE-MG; --- CVFE-OG)

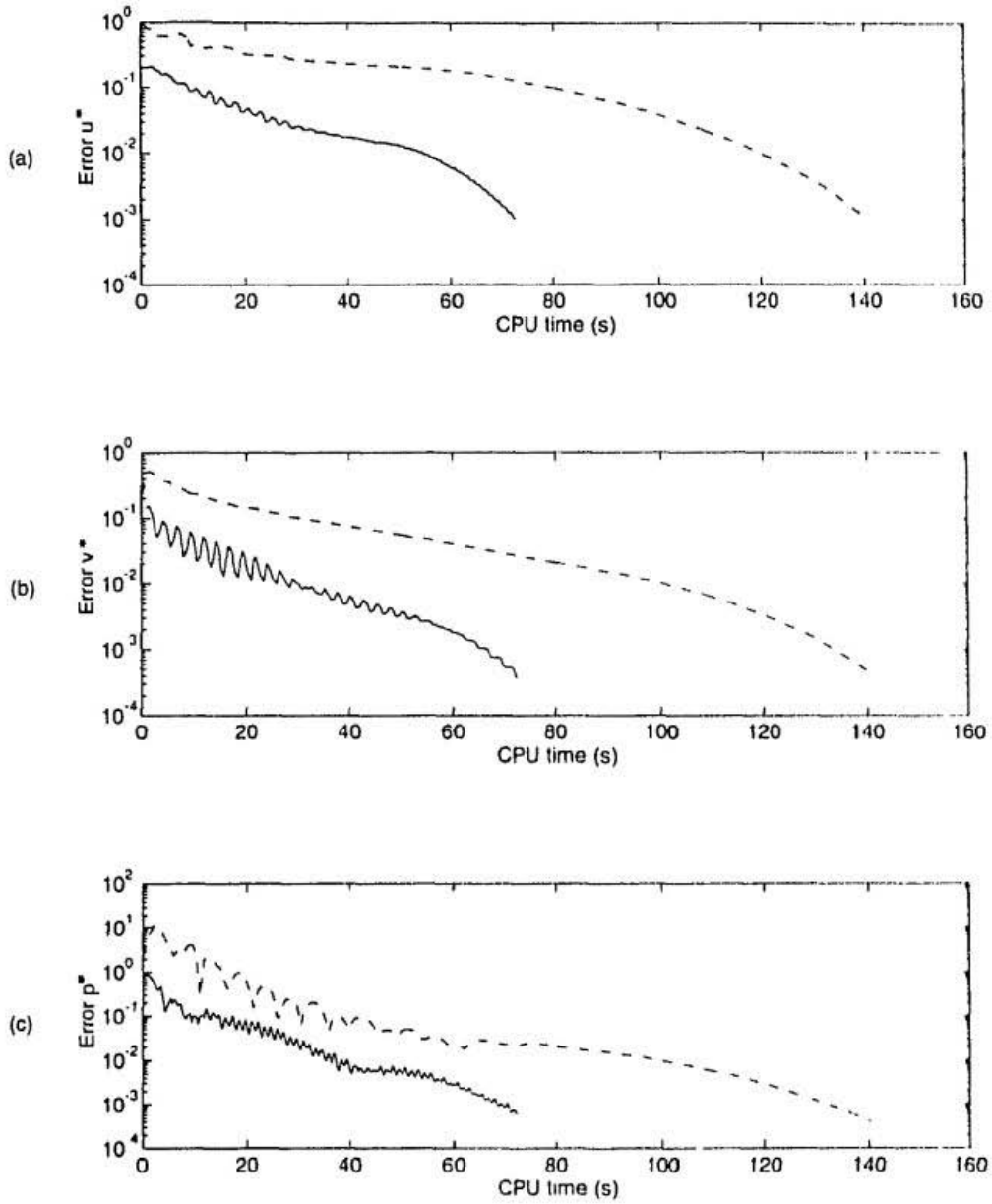

Figure 5.13: Rearward facing step: Semi-log plots of the maximum errors against execution time for $Re_w = 100$: (a) u^*-velocity; (b) v^*-velocity and (c) pressure p^*. (— CVFE-MG; __ CVFE-OG)

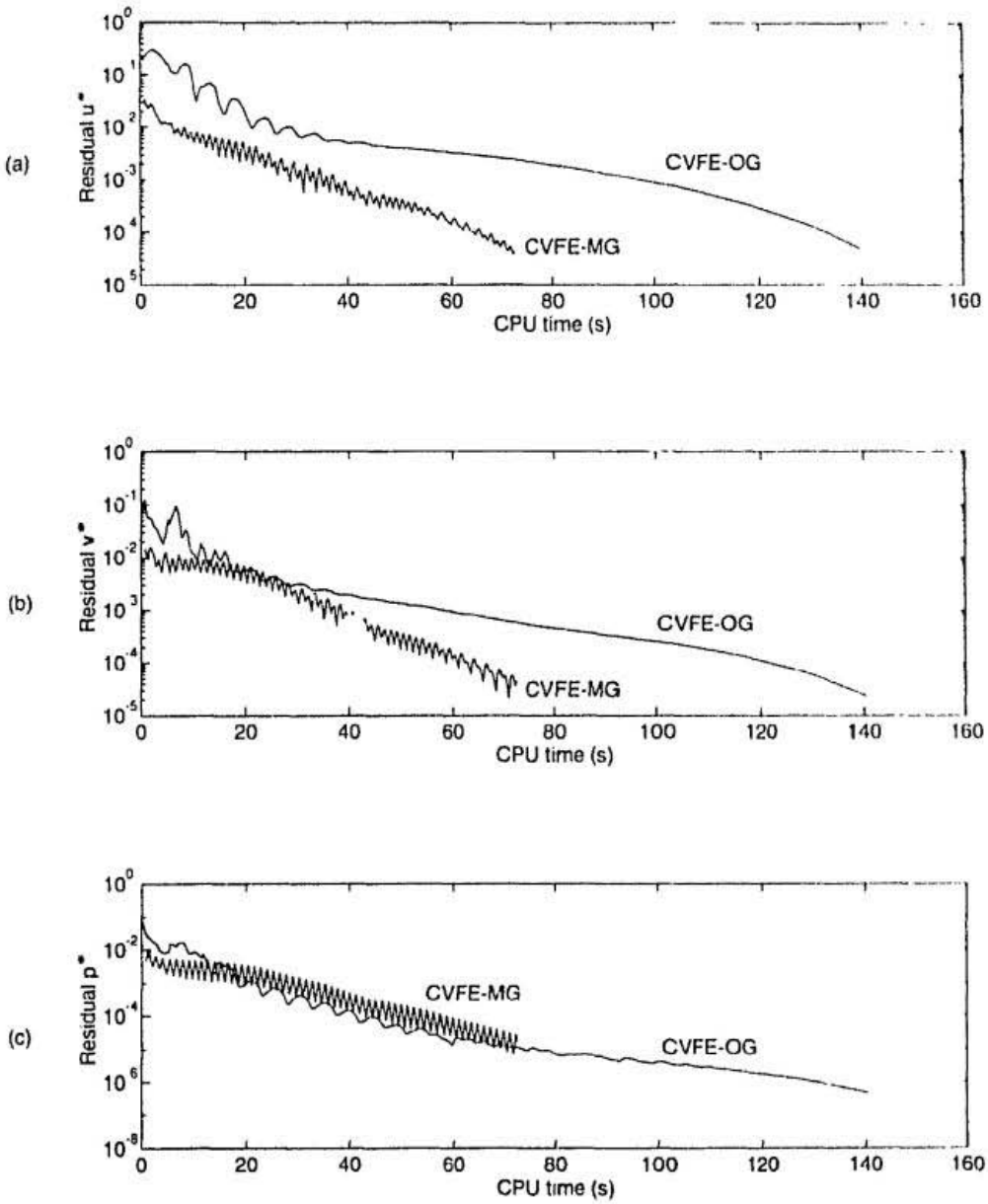

Figure 5.14: Rearward facing step: Plots of average residual against execution time for $Re_w = 100$: (a) u^*-velocity; (b) v^*-velocity and (c) pressure p^*.

	multigrid	one grid	ratio
Reynolds number	100	100	
Execution Time (s)	8.66	64.32	7.43
Iterations or V-cycles	5	249	
Reynolds number	400	400	
Execution Time (s)	17.90	68.03	3.80
Iterations or V-cycles	10	249	

Table 5.1: Square driven cavity: comparison of execution time and iterations between CVFE-MG and CVFE-OG for convergence (maximum error u^*, v^* and $p^* < 10^{-2}$).

	multigrid	one grid	ratio
Reynolds number	100	100	
Execution Time (s)	54.94	119.90	2.18
Iterations or V-cycles	44	354	

Table 5.2: Rearward facing step: comparison of execution time and iterations between CVFE-MG and CVFE-OG for convergence (maximum error u^*, v^* and $p^* < 10^{-2}$).

Chapter 6

Conclusion

6.1 Review of the Thesis and its Contributions

The formulation and implementation of an equal-order colocated control volume finite element-multigrid (CVFE-MG) method for steady, two-dimensional, viscous incompressible flows has been presented in this thesis. The proposed method was formulated using the velocity components and pressure as the dependent variables. The pressure and the diffused scalars were interpolated linearly; the convected scalars were interpolated using mass weighted interpolation which guaranteed positive contributions to the coefficients in the algebraic discretization equation; and the transporting velocities were interpolated using a linear interpolation of pseudo-velocities and pressure coefficients, in which the pressure gradients appeared explicitly. It was this explicit inclusion of the pressure gradients that prevented the appearance of spurious oscillations of velocity and pressure.

In the proposed CVFE-MG, the nonlinear, coupled algebraic equations, which were obtained from the discretization of the x- and y-momentum and continuity equations, were solved by a segregated solution algorithm with multigrid techniques. Both FMV- and V-cycle multigrid algorithms were employed. The proposed CVFE-MG was applied to two test problems: square driven cavity; and

rearward facing step. For the square driven cavity problem, at Reynolds number of 100, the CVFE-MG results were in good agreement with the results in [16]. At Reynolds number of 400, however, the CVFE-MG underpredicted the maxima in the velocity profiles. This under prediction was caused by the interpolation schemes used in the CVFEM. The upwinding scheme used could induce false diffusion, and the linear interpolation of diffused scalars at all grid Reynolds numbers would overestimate the influence of diffusion at high Reynolds numbers. Both of these factors would tend to smear maxima and minima in a solution. The CVFE-MG provided realistic prediction of the fluid flow over the rearward facing step. This problem demonstrated the ability of the method to solve outflow problems with symmetry boundary conditions, in the presence of recirculating flow.

The CVFE-MG was found to be more efficient than solution with the same CVFEM using one grid (CVFE-OG). It was found that the CVFE-MG could obtain solutions 2.18 to 7.43 times faster than the CVFE-OG for the problems presented in this thesis. The acceleration of the convergence rate was reduced as Reynolds number increased, and thus the nonlinearity of the coupled equations increased. Also, the presence of symmetry and outflow boundaries reduced the effectiveness of the multigrid algorithm.

6.2 Proposed Extensions of this Work

As mentioned above, the effectiveness of the multigrid algorithm was reduced as Reynolds number increased. In the V-cycles, the actual dependent variables u, v and p were only evaluated at the finest level. At other levels, u, v and p, which were needed to calculate the coefficients of the momentum and continuity

equations, were injected from the finest grid. At high Reynolds numbers, velocity gradients are large, and the intergrid transfer used here was not very efficient, since the most updated values were not immediately used. One suggested way to solve this problem is that after obtaining the errors of the actual dependent variables u, v and p at the second finest level, one would interpolate the errors into the finest level immediately and correct these dependent variables at the finest level, and then inject the "corrected" values to other coarse levels for the use of coefficient calculation.

The successful implementation of multigrid algorithms in the context of a primitive variables, viscous flow CVFEM will lead to continued research into the optimization of these methods. Areas of research to be considered are improvements to the interpolation schemes, and extensions to three-dimensions, and unsteady problems.

References

[1] Bachvalov, N.S., On the Convergence of a Relaxation Method with Natural Constraints on the Elliptic Operator, *USSR Comput. Math. and Math. Phys.*, Vol.6, pp. 101-135, 1966.

[2] Baker, A.J., *Computation of Fluid Flow by the Finite Element Method*, Hemisphere Publishing Corporation, Washington, 1983.

[3] Baliga, B.R., *A Control-Volume Based Finite Element Method for Convective Heat and Mass Transfer*, Ph D. Thesis, Dept. of Mech. Eng., University of Minnesota, 1978.

[4] Baliga, B.R. and Patankar, S.V., A New Finite Element Formulation for Convection-Diffusion Problems, *Numerical Heat Transfer*, Vol.3, pp.393-409, 1980.

[5] Baliga, B.R. and Patankar, S.V., A Control Volume Finite Element Method for Two-Dimensional Fluid Flow and Heat Transfer, *Numerical Heat Transfer*, Vol.6, pp.245-261, 1983.

[6] Baliga, B.R., Pham, T.T. and Patankar, S.V., Solution of Some Two-Dimensional Incompressible Fluid Flow and Heat Transfer Problems Using Control Volume Finite Element Method, *Numerical Heat Transfer*, Vol.6, pp.263-282, 1983.

[7] Baliga, B.R. and Patankar, S.V., Elliptic Systems: Finite Element Method II, in Minkowycz, W.J., Sparrow, E.M., Schneider, G.E. and Pletcher, R.H.(eds), *Handbook of Numerical Heat Transfer*, Chap.11, pp.421-461, Wiley, New York, 1988.

[8] Becker, C., Ferziger, J.H., Peric, M. and Scheuerer, G., *Vieweg Verlag*, Braunschweig, 1989.

[9] Brandt, A., Multi-Level Adaptive Technique (MLAT) for Fast Numerical Solution to Boundary Value Problems, *Proc. 3rd Int. Conf. on Numerical Methods in Fluid Mechanics*, Vol.1, H. Cabannes and R. Temam(eds), Springer, Berlin, pp. 82-89, 1973.

[10] Brandt, A., Multi-level Adaptive Solutions to Boundary Value Problems, *Math. Comput.*, Vol.31, pp. 333-390, 1977.

[11] Briggs, W.L., *A Multigrid Tutorial*, Socity for Industrial and Applied Mathematics, Philadelphia, 1987.

[12] Chung, T.J., *Finite Element Analysis of Fluid Dynamics*, McGraw Hill Book Co., Toronto, 1978.

[13] Fedorenko, R.P., The Speed of Convergence of One Iterative Process, *USSR Comput. Math. and Math. Phys.*, Vol.4, pp. 227-235, 1964.

[14] Frederickson, P.O. and McBryan O.A., Recent Developmnts for the PSMG Multiscale Method, *Multigrid Methods III*, Hackbusch, W. and Trottenberg, U. (eds), ISNM 98, 1991.

[15] Finlayson, B.A., *The Method of Weighted Residuals and Variational Principles*, Academic Press, New York, 1972.

[16] Ghia, U., Ghia, K.N. and Shin, C.T., High Re Solutions for Incompressible Flow Using Navier-Stokes Equations and a Multi-Grid Method, *Journal of Computational Physics*, Vol.48, pp. 387-411, 1982.

[17] Hackbusch, W., *Ein Iteratives Verfahren zur Schnellen Auflösung Elliptischer Randwertprobleme*, Universität Köln, Report, pp. 12-76, 1976.

[18] Hookey, N.A., *Evaluation and Enhancements of Control Volume Finite Element Methods for Two-Dimensional Fluid Flow and Heat Transfer*, M.Eng. Thesis, Dept. of Mech. Eng., McGill University, 1986.

[19] Hookey, N.A., Baliga, B.R. and Prakash, C., Evaluation and Enhancements of Some Control Volume Finite-Element Methods - Part 1: Convection-Diffusion Problems, *Numerical Heat Transfer*, Vol.14, pp. 255-272, 1988.

[20] Hookey, N.A. and Baliga, B.R., Evaluation and Enhancements of Some Control Volume Finite-Element Methods - part 2: Fluid Flow Problems, *Numerical Heat Transfer*, Vol.14, pp. 273-293, 1988.

[21] Hookey, N.A., *A Control Volume Finite Element Method for Two Dimensional Viscous Compressible Fluid Flow*, Ph.D. Thesis, Dept. of Mech. Eng., McGill University, 1989.

[22] Hookey, N.A., Simulation of Viscous Fluid Flows using a Multigrid-Control Volume Finite Element Method, *Colorado Conference on Iterative Methods*, Breckenridge, Colorado, April, 1994.

[23] Huebner, K.H. and Thornton, E.A., *The Finite Element Method for Engineers*, John Wiley and Sons, New York, 1982.

[24] LeDain-Muir, B., *A Control Volume Finite-Element Method for Three-Dimensional Elliptic Fluid Flow and Heat Transfer*, M.Eng. Thesis, McGill University, 1983.

[25] LeDain-Muir, B. and Baliga, B.R., Solution of Three-Dimensional Convection-Diffusion Problems Using Tetrahedral Elements and Flow-Oriented Upwinding Interpolation Functions, *Numerical Heat Transfer*, Vol.9, pp.143-162, 1986.

[26] Lonsdale, G., *Solution of a Rotating Navier-Stokes Problem by a Non-Linear Multigrid Algorithm*, Report No. 105, Dept. of Mathematics, University of Manchester, 1985.

[27] McCormick, S.F., *Multilevel Adaptive Methods for Partial Differential Equations*, Society for Industrial and Applied Mathematics, Philadelphia, 1989.

[28] McCormick, S.F., *Multigrid Methods (Frontiers in Applied Mathematics 3)*, Society for Industrial and Applied Mathematics, Philadelphia, 1987.

[29] Patankar, S.V., *Numerical Heat Transfer and Fluid Flow*, Hemisphere Publishing Co., 1980.

[30] Prakash, C., *A Finite-Element Method for Predicting Flow through Ducts with Arbitrary Cross Sections*, Ph.D. Thesis, University of Minnesota, 1981.

[31] Prakash, C. and Patankar, S.V., A Control Volume-Based Finite-Element Method for Solving the Navier-Stokes Equations using Equal-Order Velocity-Pressure Interpolation, *Numerical Heat Transfer*, Vol.8, pp. 259-280, 1985.

[32] Prakash, C., An Improved Control Volume Finite-Element Method for Heat and Mass Transfer, and for Fluid Flow Using Equal-Order Velocity-Pressure Interpolation, *Numerical Heat Transfer*, Vol.9, pp. 253-276, 1986.

[33] Prakash, C., Examination of the Upwind (Donor-Cell) Formulation in Control Volume Finite-Element Methods for Fluid Flow and Heat Transfer, *Numerical Heat Transfer*, Vol.11, pp. 401-416, 1987.

[34] Prakash, C. and Baliga, B.R., Control-Volume-Based Numerical Methods for Fluid Flow: Similarities and Differences, in Chung, T.J. and Karr, G.R.(eds), *Finite Element Analysis in Fluids*, UAH Press, Huntsville, Alabama, 1989.

[35] Raithby, G.D., Skew Upstream Differencing Schemes for Problems Involving Fluid Flow, *Comp. Meth. in App. Mech. and Eng.*, Vol.9, pp. 153-164, 1976.

[36] Ramadhyani, S. and Patankar, S.V., Solution of the Convection Diffusion Equation by a Finite-Element Method Using Quadrilateral Elements, *Numerical Heat Transfer*, Vol.8, pp. 595-612, 1985.

[37] Saabas, H.J., *A Control Volume Finite Element Method for Three-Dimensional, Incompressible, Viscous Fluid Flow*, Ph.D. Thesis, Dept. of Mech. Eng., McGill University, 1991.

[38] Schneider, G.E. and Raw, M.J., A Skewed Positive Influence Coefficient Upwinding Procedure for Control Volume Based Finite Element Convection Diffusion Computation, *Numerical Heat Transfer*, Vol.9, pp. 1-26, 1986.

[39] Schneider, G.E. and Raw, M.J., Control Volume Finite Element Method for Heat Transfer and Fluid Flow Using Colocated Variables - 1. Computational Procedure, *Numerical Heat Transfer*, Vol.11, pp. 363-390, 1987.

[40] Schneider, G.E., Elliptic System: Finite Element Method I, in Minkowycz, W.J., Sparrow, E.M., Schneider, G.E. and Pletcher, R.H.,(eds.), *Handdbook of Numerical Heat Transfer*, Chap. 10, pp. 379-420, Wiley, New York, 1988.

[41] Vanka, S.P., Block-Implicit Multigrid Calculation of Flows, *Comp. Meth. Appl. Mech. Eng.*, Vol.59, pp. 29-48, 1986.

[42] Wesseling, W., *An Introduction to Multigrid Methods*, Pure and Applied Mathematics, John Wiley & Sons Ltd., 1992.

[43] White, F.M., *Viscous Fluid Flow*, McGraw-Hill Book Co. Ltd., New York, 1974.

[44] Zienkiewicz, O.C., *The Finite Element Method*, McGraw-Hill Book Co. Ltd., London, 1977.

Appendix A

Interpolation Functions for the Proposed Two-Dimensional CVFEM

A.1 Interpolation of Pressure

In the proposed two-dimensional CVFEM, pressure is interpolated linearly within an element:

$$p = a_p x + b_p y + c_p \tag{A.1}$$

Substitution of the nodal conditions:

$$\begin{aligned} p = p_1 \quad & at \quad x = x_1 \quad and \quad y = y_1 \\ p = p_2 \quad & at \quad x = x_2 \quad and \quad y = y_2 \\ p = p_3 \quad & at \quad x = x_3 \quad and \quad y = y_3 \end{aligned} \tag{A.2}$$

into Eq. A.1 produces the following set of simultaneous, linear algebraic equations:

$$\begin{aligned} p_1 &= a_p x_1 + b_p y_1 + c_p \\ p_2 &= a_p x_2 + b_p y_2 + c_p \\ p_3 &= a_p x_3 + b_p y_3 + c_p \end{aligned} \tag{A.3}$$

Using Cramer's Rule to solve these equations results in the following expressions for the coefficients a_p, b_p, and c_p :

$$a_p = \frac{1}{det}\left[(y_2 - y_3)p_1 + (y_3 - y_1)p_2 + (y_1 - y_2)p_3\right] \tag{A.4}$$

$$b_p = -\frac{1}{det}\left[(x_2 - x_3)\,p_1 + (x_3 - x_1)\,p_2 + (x_1 - x_2)\,p_3\right] \quad (A.5)$$

$$c_p = \frac{1}{det}\left[(x_2y_3 - x_3y_2)\,p_1 + (x_3y_1 - x_1y_3)\,p_2 + (x_1y_2 - x_2y_1)\,p_3\right] \quad (A.6)$$

where

$$det = x_1y_2 + x_2y_3 + x_3y_1 - y_1x_2 - y_2x_3 - y_3x_1 \quad (A.7)$$

Defining the following variables:

$$\begin{aligned} xmul_1 &= x_2 - x_3, \quad ymul_1 = y_2 - y_3, \quad xymul_1 = x_2y_3 - x_3y_2 \\ xmul_2 &= x_3 - x_1, \quad ymul_2 = y_3 - y_1, \quad xymul_2 = x_3y_1 - x_1y_3 \\ xmul_3 &= x_1 - x_2, \quad ymul_3 = y_1 - y_2, \quad xymul_3 = x_1y_2 - x_2y_1 \end{aligned} \quad (A.8)$$

allows the expressions for the coefficients to be rewritten more compactly as:

$$a_p = \frac{1}{det}\sum_{i=1}^{3} ymul_i\,p_i \quad (A.9)$$

$$b_p = -\frac{1}{det}\sum_{i=1}^{3} xmul_i\,p_i \quad (A.10)$$

$$c_p = \frac{1}{det}\sum_{i=1}^{3} xymul_i\,p_i \quad (A.11)$$

Then the pressure gradients may be expressed as follows:

$$\frac{\partial p}{\partial x} = a_p = \frac{1}{det}\sum_{i=1}^{3} ymul_i\,p_i \quad (A.12)$$

$$\frac{\partial p}{\partial y} = b_p = -\frac{1}{det}\sum_{i=1}^{3} xmul_i\,p_i \quad (A.13)$$

A.2 Interpolation of a Diffused Scalar

In the proposed two-dimensional CVFEM, linear interpolation is used to obtain algebraic approximations to the diffusion flux across the control volume faces contained within an element.

The interpolation function for the diffused scalar, ϕ^d, is given by:

$$\phi^d = a^d_\phi x + b^d_\phi y + c^d_\phi \tag{A.14}$$

The coefficients a^d_ϕ, b^d_ϕ, and c^d_ϕ are determined in the same manner as the coefficients in the interpolation function for pressure. Hence,

$$a^d_\phi = \frac{1}{det} \sum_{i=1}^{3} ymul_i \, \phi_i \tag{A.15}$$

$$b^d_\phi = -\frac{1}{det} \sum_{i=1}^{3} xmul_i \, \phi_i \tag{A.16}$$

$$c^d_\phi = \frac{1}{det} \sum_{i=1}^{3} xymul_i \, \phi_i \tag{A.17}$$

where $ymul_i$, $xmul_i$, $xymul_i$, and det have been defined in Eqs. A.7 and A.8.

Then the gradients of ϕ^d may be expressed as:

$$\frac{\partial \phi^d}{\partial x} = a^d_\phi = \frac{1}{det} \sum_{i=1}^{3} ymul_i \, \phi_i \tag{A.18}$$

$$\frac{\partial \phi^d}{\partial y} = b^d_\phi = -\frac{1}{det} \sum_{i=1}^{3} xmul_i \, \phi_i \tag{A.19}$$

A.3 Interpolation of a Convected Scalar

In the proposed CVFEM, the convected scalar, ϕ^c, which appears in the $\rho \vec{v} \phi$ term, is interpolated with mass weighted (MAW) functions. The mass flux across a particular subcontrol volume surface within an element is taken as positive when the velocity vector at the integration point is in the same direction as the assumed normal to the surface. With respect to Fig. 3.3a, the mass flux across face 1 is given by:

$$\dot{m}_1 = \rho \, \vec{v}^1 \cdot \vec{n}^1 \tag{A.20}$$

A similar expression can be written for the mass flux across the other subcontrol volume face within an element. On each of the two control volume faces (denoted by the index k), a value of the convected scalar, that is assumed to prevail over

that face, can be defined. This is the integration point value, and it is given the symbol ϕ_k^c, whereas the nodal values are represented by $\Phi_i's$. The following rules can be used to determine ϕ_k^c.

For quad 1, type 1 element and quad 2, type 2 element (Figs.3.4b & e)

For control volume face 1:

$$\text{If } \dot{m}_1 > 0 \quad \phi_1^c = f_1\phi_2^c + (1 - f_1)\,\Phi_3 \tag{A.21}$$

$$\text{If } \dot{m}_1 < 0 \quad \phi_1^c = \Phi_1 \tag{A.22}$$

where

$$f_1 = min\left[max\left(\frac{\dot{m}_2}{\dot{m}_1}, 0\right), 1\right] \tag{A.23}$$

For control volume face 2:

$$\text{If } \dot{m}_2 > 0 \quad \phi_2^c = \Phi_2 \tag{A.24}$$

$$\text{If } \dot{m}_2 < 0 \quad \phi_2^c = f_2\phi_1^c + (1 - f_2)\,\Phi_3 \tag{A.25}$$

where

$$f_2 = min\left[max\left(\frac{\dot{m}_1}{\dot{m}_2}, 0\right), 1\right] \tag{A.26}$$

For quad 1, type 2 element and quad 2, type 1 element (Figs.3.4c & d)

For control volume face 1:

$$\text{If } \dot{m}_1 > 0 \quad \phi_1^c = \Phi_1 \tag{A.27}$$

$$\text{If } \dot{m}_1 < 0 \quad \phi_1^c = f_1\phi_2^c + (1 - f_1)\,\Phi_3 \tag{A.28}$$

where

$$f_1 = min\left[max\left(\frac{\dot{m}_2}{\dot{m}_1}, 0\right), 1\right] \tag{A.29}$$

For control volume face 2:

$$\text{If } \dot{m}_2 > 0 \quad \phi_2^c = f_2\phi_1^c + (1 - f_2)\,\Phi_3 \tag{A.30}$$

$$\text{If } \dot{m}_2 < 0 \quad \phi_2^c = \Phi_2 \tag{A.31}.$$

where

$$f_2 = min\left[max\left(\frac{\dot{m}_1}{\dot{m}_2}, 0\right), 1\right] \tag{A.32}$$

Using Eqs. A.21 to A.26 or Eqs. A.27 to A.32, the following equations can be obtained for the appropriate element:

$$\begin{bmatrix} a_{11} & a_{12} \\ a_{21} & a_{22} \end{bmatrix} \begin{Bmatrix} \phi_1^c \\ \phi_2^c \end{Bmatrix} = \begin{bmatrix} b_{11} & b_{12} & b_{13} \\ b_{21} & b_{22} & b_{23} \end{bmatrix} \begin{Bmatrix} \Phi_1 \\ \Phi_2 \\ \Phi_3 \end{Bmatrix} \tag{A.33}$$

Solving these equations, the integration point values can be determined as:

$$\phi_1^c = \frac{1}{det_a}[(a_{22}b_{11} - a_{12}b_{21})\Phi_1 + (a_{22}b_{12} - a_{12}b_{22})\Phi_2 + (a_{22}b_{13} - a_{12}b_{23})\Phi_3] \tag{A.34}$$

$$\phi_2^c = \frac{1}{det_a}[(a_{11}b_{21} - a_{21}b_{11})\Phi_1 + (a_{11}b_{22} - a_{21}b_{12})\Phi_2 + (a_{11}b_{23} - a_{21}b_{13})\Phi_3] \tag{A.35}$$

where

$$det_a = a_{11}a_{22} - a_{12}a_{21} \tag{A.36}$$

Defining the following variables:

$$CM_i^1 = \frac{1}{det_a}(a_{22}b_{1i} - a_{12}b_{2i}) \tag{A.37}$$

$$CM_i^2 = \frac{1}{det_a}(a_{11}b_{2i} - a_{21}b_{1i}) \tag{A.38}$$

allows the integration point value, ϕ_k^c, to be rewritten more compactly as:

$$\phi_k^c = \sum_{i=1}^{3} CM_i^k \Phi_i \; : \qquad k = 1, 2 \tag{A.39}$$

It should be noted that ϕ_k^c can be easily obtained directly from Eqs. A.21 to A.26 or Eqs. A.27 to A.32 without solving Eq. A.33, if there are only two control volume faces within each element.

A.4 Interpolation of Mass Conserving Velocity

As discussed in Chapter 3, the "mass conserving" velocities at each node within an element can be determined by:

$$u_i^m = \hat{u}_i - d_i^u \left(\frac{\partial p}{\partial x}\right)_e \tag{A.40}$$

$$v_i^m = \hat{v}_i - d_i^v \left(\frac{\partial p}{\partial y}\right)_e \tag{A.41}$$

In the proposed CVFEM, each "mass conserving" velocity component is interpolated within an element by assuming a linear variation of the corresponding pseudo-velocities, $\hat{u}_i$ and $\hat{v}_i$, and pressure coefficients, d_i^u and d_i^v. The interpolation functions are as follows:

$$\hat{u}_i = a_u\, x + b_u\, y + c_u \tag{A.42}$$

$$d_i^u = a_{d^u}\, x + b_{d^u}\, y + c_{d^u} \tag{A.43}$$

$$\hat{v}_i = a_v\, x + b_v\, y + c_v \tag{A.44}$$

$$d_i^v = a_{d^v}\, x + b_{d^v}\, y + c_{d^v} \tag{A.45}$$

The coefficients in Eqs. A.42 to A.45 can be obtained in the same manner as the coefficients in the pressure interpolation function. Hence,

$$a_u = \frac{1}{det} \sum_{i=1}^{3} ymul_i\, \hat{u}_i \tag{A.46}$$

$$b_u = -\frac{1}{det} \sum_{i=1}^{3} xmul_i\, \hat{u}_i \tag{A.47}$$

$$c_u = \frac{1}{det} \sum_{i=1}^{3} xymul_i\, \hat{u}_i \tag{A.48}$$

$$a_{d^u} = \frac{1}{det} \sum_{i=1}^{3} ymul_i\, d_i^u \tag{A.49}$$

$$b_{d^u} = -\frac{1}{det} \sum_{i=1}^{3} xmul_i\, d_i^u \tag{A.50}$$

$$c_{d^u} = \frac{1}{det} \sum_{i=1}^{3} xymul_i\, d_i^u \tag{A.51}$$

$$a_v = \frac{1}{det} \sum_{i=1}^{3} ymul_i\, \hat{v}_i \tag{A.52}$$

$$b_v = -\frac{1}{det}\sum_{i=1}^{3} xmul_i\, \hat{r}_i \tag{A.53}$$

$$c_v = \frac{1}{det}\sum_{i=1}^{3} xymul_i\, \hat{r}_i \tag{A.54}$$

$$a_{dv} = \frac{1}{det}\sum_{i=1}^{3} ymul_i\, d_i^v \tag{A.55}$$

$$b_{dv} = -\frac{1}{det}\sum_{i=1}^{3} xmul_i\, d_i^v \tag{A.56}$$

$$c_{dv} = \frac{1}{det}\sum_{i=1}^{3} xymul_i\, d_i^v \tag{A.57}$$

where $ymul_i$, $xmul_i$, $xymul_i$ and det have been defined in Eqs. A.7 and A.8.

Appendix B

Integration of Fluxes in the Proposed Two-Dimensional CVFEM

B.1 Introduction

In chapter 3, the governing equations for steady, two-dimensional, viscous, incompressible flows were written in the following conservative forms:

$$\vec{\nabla} \cdot \vec{J} = S \tag{B.1}$$

$$\vec{\nabla} \cdot \vec{g} = 0 \tag{B.2}$$

where $\vec{J}$ is the combined convection-diffusion flux vector, S is the source term, and $\vec{g}$ is the mass flux vector. Equation B.1 represents the x-momentum equation when:

$$\vec{J} = \rho \vec{v} u - \mu \vec{\nabla} u \tag{B.3}$$

$$S = S^u - \frac{\partial p}{\partial x} \tag{B.4}$$

the y-momentum equation when:

$$\vec{J} = \rho \vec{v} v - \mu \vec{\nabla} v \tag{B.5}$$

$$S = S^v - \frac{\partial p}{\partial y} \tag{B.6}$$

and other conservation equations when:

$$\vec{J} = \rho \vec{v} \phi - \Gamma \vec{\nabla} \phi \tag{B.7}$$

$$S = S^\phi \tag{B.8}$$

Applying Gauss' Divergence Theorem to a control volume V, which is fixed in space, the integral forms of Eqs. B.1 and B.2 can be obtained:

$$\int_{\partial V} \vec{J} \cdot \vec{n}\, ds = \int_V S\, dV \tag{B.9}$$

$$\int_{\partial V} \vec{g} \cdot \vec{n}\, ds = 0 \tag{B.10}$$

where ∂V is the surface of the control volume, and $\vec{n}$ is a unit outward vector normal to the differential area ds.

With reference to the polygonal control volume associated with a typical node 3 within the calculation domain, either an internal node as in Fig. 3.2a , or a boundary node as in Fig. 3.2b , Eqs. B.9 and B.10 can be cast in the following forms:

$$\left[\int_{M_3}^{M_1} \vec{J} \cdot \vec{n}^1\, ds - \int_{M_3}^{M_2} \vec{J} \cdot \vec{n}^2\, ds - \int_V S\, dV\right]$$
$$+ \ [\text{similar contributions from other elements associated with node 3}]$$
$$+ \ [\text{boundary contributions, if applicable}] = 0 \tag{B.11}$$

$$\left[\int_{M_3}^{M_1} \vec{g} \cdot \vec{n}^1\, ds - \int_{M_3}^{M_2} \vec{g} \cdot \vec{n}^2\, ds\right]$$
$$+ \ [\text{similar contributions from other elements associated with node 3}]$$
$$+ \ [\text{boundary contributions, if applicable}] = 0 \tag{B.12}$$

To derive the element contribution to the control volume integral conservation equations, B.11 and B.12, it is necessary to integrate the appropriate flux across the two control volume faces in an element. The procedures used in the proposed method to perform these integrations are described in this appendix. All nomenclature used in this appendix is defined in Fig. 3.4.

B.2 Momentum Equations

B.2.1 x-Momentum Equation

The integrated flux of x-momentum across a control volume face k is expressed in the following manner:

$$[\text{Integrated flux across control volume face } k] = \int_{face\,k} \vec{J}^k \cdot \vec{n}^k\, ds \tag{B.13}$$

where

$$\vec{J}^k = \rho \vec{v} u - \mu \vec{\nabla} u \tag{B.14}$$

The combined convection-diffusion flux vector, $\vec{J}^k$, can be separated into its component parts in the x and y directions:

$$\vec{J}^k = J_x^k \, \vec{i} + J_y^k \, \vec{j} \tag{B.15}$$

where

$$J_x^k = \rho u u - \mu \frac{\partial u}{\partial x} \tag{B.16}$$

$$J_y^k = \rho v u - \mu \frac{\partial u}{\partial y} \tag{B.17}$$

Substituting the MAW interpolation function, Eq. A.39, for the convected scalar u, and the linear interpolation function, Eqs. A.18 and A.19, for the gradients of the diffused scalar u, into Eqs. B.16 and B.17 allows J_x^k and J_y^k to be written in the following forms:

$$J_x^k = \rho^k u^k \left(\sum_{i=1}^{3} CM_i^k \; u_i \right) - \frac{\mu}{det} \left(\sum_{i=1}^{3} ymul_i \; u_i \right) \tag{B.18}$$

$$J_y^k = \rho^k v^k \left(\sum_{i=1}^{3} CM_i^k \; u_i \right) + \frac{\mu}{det} \left(\sum_{i=1}^{3} xmul_i \; u_i \right) \tag{B.19}$$

It should be noted that u^k and v^k are the components of "mass conserving" velocity. The unit normal $\vec{n}^k$ in Eq. B.13 can be defined as:

$$\vec{n}^k = \left(n_x^k \, \vec{i} + n_y^k \, \vec{j} \right) / l^k \tag{B.20}$$

where

$$n_x^k = \left(y_M^k - y_{M_3} \right) \tag{B.21}$$

$$n_y^k = \left(x_{M_3} - x_M^k \right) \tag{B.22}$$

$$l^k = \left[\left(x_M^k - x_{M_3} \right)^2 + \left(y_M^k - y_{M_3} \right)^2 \right]^{\frac{1}{2}} \tag{B.23}$$

Therefore, Eq. B.13 can be expressed as follows:

$$\int_{face\,k} \vec{J}^k \cdot \vec{n}^k \, ds = \frac{1}{l^k} \int_{face\,k} \left(J_x^k \; n_x^k + J_y^k \; n_y^k \right) ds \tag{B.24}$$

Substituting Eqs. B.18 to B.20 into Eq. B.24, and using Simpson's Rule to approximate the integration gives:

$$\begin{aligned}\int_{face\,k} \vec{J}^k \cdot \vec{n}^k \, ds &= \frac{n_x^k}{6}\left(\rho_M^k u_M^k + 4\rho_H^k u_H^k + \rho_{M_3} u_{M_3}\right)\left(\sum_{i=1}^{3} CM_i^k \, u_i\right) \\ &+ \frac{n_y^k}{6}\left(\rho_M^k v_M^k + 4\rho_H^k v_H^k + \rho_{M_3} v_{M_3}\right)\left(\sum_{i=1}^{3} CM_i^k \, u_i\right) \\ &- \frac{\mu\, n_x^k}{det}\left(\sum_{i=1}^{3} ymul_i \, u_i\right) + \frac{\mu\, n_y^k}{det}\left(\sum_{i=1}^{3} xmul_i \, u_i\right) \qquad \text{(B.25)}\end{aligned}$$

The subscripts H and M indicate that the subscripted quantity is evaluated at the positions shown in Fig. 3.4, for face k. This expression may be simplified by defining the following "average" variables for control volume face k:

$$(U)_{av}^k = \left(\rho_M^k u_M^k + 4\rho_H^k u_H^k + \rho_{M_3} u_{M_3}\right) / 6 \qquad \text{(B.26)}$$

$$(V)_{av}^k = \left(\rho_M^k v_M^k + 4\rho_H^k v_H^k + \rho_{M_3} v_{M_3}\right) / 6 \qquad \text{(B.27)}$$

Using these variables, Eq. B.25 can be written as:

$$\begin{aligned}\int_{face\,k} \vec{J}^k \cdot \vec{n}^k \, ds &= \left[n_x^k \, (U)_{av}^k + n_y^k \, (V)_{av}^k\right]\left(\sum_{i=1}^{3} CM_i^k \, u_i\right) \\ &+ \frac{\mu}{det}\left[n_y^k \left(\sum_{i=1}^{3} xmul_i \, u_i\right) - n_x^k \left(\sum_{i=1}^{3} ymul_i \, u_i\right)\right] \qquad \text{(B.28)}\end{aligned}$$

The above equation can be simplified, and rewritten in terms of nodal velocities:

$$\int_{face\,k} \vec{J}^k \cdot \vec{n}^k \, ds = C_1^k \, u_1 + C_2^k \, u_2 + C_3^k \, u_3 \qquad \text{(B.29)}$$

where

$$C_i^k = \left[n_x^k \, (U)_{av}^k + n_y^k \, (V)_{av}^k\right] CM_i^k + \frac{\mu}{det}\left(n_y^k \, xmul_i - n_x^k \, ymul_i\right) \qquad \text{(B.30)}$$

For incompressible flow, an element source term $\mathcal{S}^u$ can be expressed as:

$$\mathcal{S}^u = S^u - \frac{\partial p}{\partial x} \qquad \text{(B.31)}$$

The integration of $\mathcal{S}^u$ over a subcontrol volume V_j is given by the following expression:

$$\int_{V_j} \mathcal{S}^u \, dV = A_j \left[\left(S_c^u\right)_j + \left(S_p^u\right)_j u_j - \frac{1}{det}\sum_{i=1}^{3} ymul_i \, p_i\right] \qquad \text{(B.32)}$$

where

$A_j = A_e/4$ or $A_e/2$, depending on the domain discretization, and,

$A_e = | x_1y_2 + x_2y_3 + x_3y_1 - y_1x_2 - y_2x_3 - y_3x_1 | /2$, the area of the element.

B.2.2 y-Momentum Equation

The integrated flux of y-momentum across a control volume face k is expressed in the following manner:

$$[\text{Integrated flux across control volume face } k] = \int_{face\,k} \vec{J}^k \cdot \vec{n}^k ds \qquad \text{(B.33)}$$

which can be simplified to

$$\int_{face\,k} \vec{J}^k \cdot \vec{n}^k \, ds \;=\; C_1^k v_1 + C_2^k v_2 + C_3^k v_3 \qquad \text{(B.34)}$$

Since the convection-diffusion fluxes for the x and y momentum equations are quite similar, the derivations of the integrated fluxes of the x and y momentum are nearly identical. The only differences result from the different pressure gradients and source terms used in the two momentum equations. The C_i^k terms, Eq. B.30, will therefore remain the same. However, the volume integration of the appropriate source terms, $\mathcal{S}^v$ should be reevaluated:

$$\int_{V_j} \mathcal{S}^v \, dV \;=\; A_j \left[\left(S_c^v\right)_j + \left(S_p^v\right)_j v_j + \frac{1}{det} \sum_{i=1}^{3} xmul_i \, p_i \right] \qquad \text{(B.35)}$$

B.3 Continuity Equation

The integrated mass flux across a control volume face k is expressed in the following manner:

$$[\text{Integrated mass flux across control volume face } k] = \int_{face\,k} \vec{g}^k \cdot \vec{n}^k ds \qquad \text{(B.36)}$$

where

$$\vec{g}^k \;=\; \rho \vec{v} \qquad \text{(B.37)}$$

Substituting Eq. B.20 into Eq. B.36 gives:

$$\int_{face\,k} \vec{g}^k \cdot \vec{n}^k \, ds \;=\; \frac{1}{l^k} \int_{face\,k} \rho^k \left(u^k \, n_x^k + v^k \, n_y^k \right) ds \qquad \text{(B.38)}$$

where u^k and v^k are the components of "mass conserving" velocity. Using Simpson's Rule to approximate the integration gives:

$$\begin{aligned} \int_{face\,k} \vec{g}^k \cdot \vec{n}^k \, ds \;&=\; \frac{n_x^k}{6} \left(\rho_M^k u_M^k + 4\rho_H^k u_H^k + \rho_{M_3} u_{M_3} \right) \\ &+\; \frac{n_y^k}{6} \left(\rho_M^k v_M^k + 4\rho_H^k v_H^k + \rho_{M_3} v_{M_3} \right) \end{aligned} \qquad \text{(B.39)}$$

The subscripts H and M indicate that the subscripted quantity is evaluated at the positions shown in Fig. 3.4, for face k. This expression may be simplified by defining the following "average" variables for control volume face k:

$$\left(\dot{U} \right)_{av}^k \;=\; \left[\rho_M^k \dot{u}_M^k + 4\rho_H^k \dot{u}_H^k + \rho_{M_3} \dot{u}_{M_3} \right] / 6 \qquad \text{(B.40)}$$

$$(D^u)_{av}^k \;=\; \left[\rho_M^k (d^u)_M^k + 4\rho_H^k (d^u)_H^k + \rho_{M_3} d_{M_3}^u \right] / 6 \qquad \text{(B.41)}$$

$$\left(\dot{V} \right)_{av}^k \;=\; \left[\rho_M^k \dot{v}_M^k + 4\rho_H^k \dot{v}_H^k + \rho_{M_3} \dot{v}_{M_3} \right] / 6 \qquad \text{(B.42)}$$

$$(D^v)_{av}^k \;=\; \left[\rho_M^k (d^v)_M^k + 4\rho_H^k (d^v)_H^k + \rho_{M_3} d_{M_3}^v \right] / 6 \qquad \text{(B.43)}$$

Thus, Eq. B.39 can be written as:

$$\begin{aligned} \int_{face\,k} \vec{g}^k \cdot \vec{n}^k \, ds \;&=\; n_x^k \left[\left(\dot{U} \right)_{av}^k - (D^u)_{av}^k \left(\frac{\partial p}{\partial x} \right)_r \right] \\ &+\; n_y^k \left[\left(\dot{V} \right)_{av}^k - (D^v)_{av}^k \left(\frac{\partial p}{\partial y} \right)_r \right] \end{aligned} \qquad \text{(B.44)}$$

Using linear interpolation for pressure, the elemental pressure gradients in the above equation can be written in terms of the nodal pressures, as indicated in Eqs. A.12 and A.13. Consequently, Eq. B.44 can be written as follows:

$$\begin{aligned} \int_{face\,k} \vec{g}^k \cdot \vec{n}^k \, ds \;&=\; n_x^k \left[\left(\dot{U} \right)_{av}^k - \frac{(D^u)_{av}^k}{det} \sum_{i=1}^{3} ymul_i \, p_i \right] \\ &+\; n_y^k \left[\left(\dot{V} \right)_{av}^k + \frac{(D^v)_{av}^k}{det} \sum_{i=1}^{3} xmul_i \, p_i \right] \end{aligned} \qquad \text{(B.45)}$$

The above equation can be simplified and rewritten in terms of nodal pressures:

$$\int_{face\,k} \vec{g}^k \cdot \vec{n}^k \, ds \;=\; E_1^k \, p_1 + E_2^k \, p_2 + E_3^k \, p_3 + B^k \qquad \text{(B.46)}$$

where

$$E_i^k = \frac{1}{det}\left[n_y^k\,(D^v)_{av}^k\;xmul_i - n_x^k\,(D^u)_{av}^k\;ymul_i\right] \tag{B.47}$$

$$B^k = n_x^k\left(\dot{U}\right)_{av}^k + n_y^k\left(\dot{V}\right)_{av}^k \tag{B.48}$$

Appendix C

Assembly of the Discretized Equations in the Proposed Two-Dimensional CVFEM

C.1 Introduction

The integrated fluxes of momentum and mass across a control volume face k in an element and the integrated source terms, which were discussed in Appendix B, are used to compile the complete discretized forms of the integral conservation equations for a control volume. The assembly of the final forms of the discretized equations are described in this appendix.

In the assembly of these discretized equations, reference is made to the nomenclature in Fig. 3.4. The polygonal control volume constructed around an internal node (i, j) in a calculation domain, and all of the elements that may be associated with this control volume are shown in Fig. 3.4a. It should be noted that the maximum number of connections a node may have with its neighbours are shown in this figure. Figures 3.4b to 3.4e, show the four types of elements that are used in Fig. 3.4a, with their corresponding node numbering schemes. These four elements result from the two possible orientations of the diagonal.

C.2 Assembly of the Momentum Equations

C.2.1 x-Momentum Equation

For the x-momentum equation, the integral of the flux across a control volume face k within an element is written as follows in Appendix B:

$$\int_{face\ k} \vec{f}^k \cdot \vec{n}^k \, ds \;=\; C_1^k \, u_1 + C_2^k \, u_2 + C_3^k \, u_3 \qquad (C.1)$$

and the elemental contribution to the volume integration of the source term for the control volume around node j is given by:

$$\int_{V_j} S^u \, dV \;=\; A_j \left[(S_c^u)_j + \left(S_p^u\right)_j u_j - \frac{1}{det} \sum_{i=1}^{3} ymul_i \, p_i \right] \qquad (C.2)$$

which can be rewritten more compactly as:

$$\int_{V_j} S^u \, dV \;=\; A_j \, \left(S_p^u\right)_j \, u_j + D_j^u \qquad (C.3)$$

where

$$D_j^u \;=\; A_j \left[(S_c^u)_j - \frac{1}{det} \sum_{i=1}^{3} ymul_i \, p_i \right] \qquad (C.4)$$

The assembly of the final form of the discretized x-momentum equation is done in an element-by-element manner. When each element is considered separately, the appropriate C_i^k terms are derived for each node i and each control volume face k, and this gives six C_i^k terms per element. With reference to the nomenclature in Fig. 3.4, new coefficients can be defined in each element that simplify the assembly of the control volume integral conservation equation. The algebraic discretized equations can finally be written such that only the center-point contributions will remain on the left hand side of the equations, the other related node contributions will be kept on the right hand side of the equations.

For the quad 1, type 1 element in Fig. 3.4b, the following coefficients can be evaluated when node 1 is node (i, j), node 2 is node $(i+1, j+1)$, and node 3 is node $(i+1, j)$:

With respect to node $(i+1, j)$:

$$A^c_{u(i+1,j)} \;=\; A^c_{u(i+1,j)} + C_3^1 - C_3^2 - A_3 S^u_{p3} \qquad (C.5)$$

$$A^n_{u(i+1,j)} = A^n_{u(i+1,j)} - C^1_2 + C^2_2 \tag{C.6}$$

$$A^w_{u(i+1,j)} = A^w_{u(i+1,j)} - C^1_1 + C^2_1 \tag{C.7}$$

$$A^{con}_{u(i+1,j)} = A^{con}_{u(i+1,j)} + D^u_3 \tag{C.8}$$

The coefficients appear on both sides of these equations, because contributions will also be made from other elements, and previous contributions must be maintained. The contributions to the center-point coefficient $A^c_{u(i+1,j)}$ are the portion of the net transport of x-momentum out of the subcontrol volume surrounding node $(i+1, j)$, associated with u_3 in Fig. 3.4b. The contributions to the other coefficients are the portion of the net transport of x-momentum into the subcontrol volume due to the corresponding nodes. In Fig. 3.4b the portion associated with u_1 is added to $A^w_{u(i+1,j)}$, and the portion associated with u_2 is added to $A^n_{u(i+1,j)}$. The source-related terms, Eq. C.3, are then added to the appropriate coefficients to complete the assembly for node $(i+1, j)$ in the quad 1, type 1 element of Fig. 3.4b. Similar procedures are used to assemble the coefficients at the other nodes in the element.

With respect to node (i, j):

$$A^c_{u(i,j)} = A^c_{u(i,j)} - C^1_1 - A_1 S^u_{p_1} \tag{C.9}$$

$$A^e_{u(i,j)} = A^e_{u(i,j)} + C^1_3 \tag{C.10}$$

$$A^{ne}_{u(i,j)} = A^{ne}_{u(i,j)} + C^1_2 \tag{C.11}$$

$$A^{con}_{u(i,j)} = A^{con}_{u(i,j)} + D^u_1 \tag{C.12}$$

With respect to node $(i+1, j+1)$:

$$A^c_{u(i+1,j+1)} = A^c_{u(i+1,j+1)} + C^2_2 - A_2 S^u_{p_2} \tag{C.13}$$

$$A^{sw}_{u(i+1,j+1)} = A^{sw}_{u(i+1,j+1)} - C^2_1 \tag{C.14}$$

$$A^s_{u(i+1,j+1)} = A^s_{u(i+1,j+1)} - C^2_3 \tag{C.15}$$

$$A^{con}_{u(i+1,j+1)} = A^{con}_{u(i+1,j+1)} + D^u_2 \tag{C.16}$$

For the quad 1, type 2 element in Fig. 3.4c, the following coefficients can be evaluated when node 1 is node (i, j), node 2 is node $(i+1, j+1)$, and node 3 is node $(i, j+1)$:

With respect to node (i, j):

$$A^{c}_{u(i,j)} = A^{c}_{u(i,j)} + C^{1}_{1} - A_1 S^{u}_{p_1} \quad \text{(C.17)}$$

$$A^{nr}_{u(i,j)} = A^{nr}_{u(i,j)} - C^{1}_{2} \quad \text{(C.18)}$$

$$A^{n}_{u(i,j)} = A^{n}_{u(i,j)} - C^{1}_{3} \quad \text{(C.19)}$$

$$A^{con}_{u(i,j)} = A^{con}_{u(i,j)} + D^{u}_{1} \quad \text{(C.20)}$$

With respect to node $(i+1, j+1)$:

$$A^{c}_{u(i+1,j+1)} = A^{c}_{u(i+1,j+1)} - C^{2}_{2} - A_2 S^{u}_{p_2} \quad \text{(C.21)}$$

$$A^{w}_{u(i+1,j+1)} = A^{w}_{u(i+1,j+1)} + C^{2}_{3} \quad \text{(C.22)}$$

$$A^{sw}_{u(i+1,j+1)} = A^{sw}_{u(i+1,j+1)} + C^{2}_{1} \quad \text{(C.23)}$$

$$A^{con}_{u(i+1,j+1)} = A^{con}_{u(i+1,j+1)} + D^{u}_{2} \quad \text{(C.24)}$$

With respect to node $(i, j+1)$:

$$A^{c}_{u(i,j+1)} = A^{c}_{u(i,j+1)} - C^{1}_{3} + C^{2}_{3} - A_3 S^{u}_{p_3} \quad \text{(C.25)}$$

$$A^{s}_{u(i,j+1)} = A^{s}_{u(i,j+1)} + C^{1}_{1} - C^{2}_{1} \quad \text{(C.26)}$$

$$A^{r}_{u(i,j+1)} = A^{r}_{u(i,j+1)} + C^{1}_{2} - C^{2}_{2} \quad \text{(C.27)}$$

$$A^{con}_{u(i,j+1)} = A^{con}_{u(i,j+1)} + D^{u}_{3} \quad \text{(C.28)}$$

For the quad 2, type 1 element in Fig. 3.4d, the following coefficients can be evaluated when node 1 is node $(i+1, j)$, node 2 is node $(i, j+1)$, and node 3 is node (i, j):

With respect to node $(i+1, j)$:

$$A^{c}_{u(i+1,j)} = A^{c}_{u(i+1,j)} + C^{1}_{1} - A_1 S^{u}_{p_1} \quad \text{(C.29)}$$

$$A^{nw}_{u(i+1,j)} = A^{nw}_{u(i+1,j)} - C^{1}_{2} \quad \text{(C.30)}$$

$$A^{w}_{u(i+1,j)} = A^{w}_{u(i+1,j)} - C^{1}_{3} \quad \text{(C.31)}$$

$$A^{con}_{u(i+1,j)} = A^{con}_{u(i+1,j)} + D^{u}_{1} \quad \text{(C.32)}$$

With respect to node $(i, j+1)$:

$$A^{c}_{u(i,j+1)} = A^{c}_{u(i,j+1)} - C^{2}_{2} - A_2 S^{u}_{p_2} \quad \text{(C.33)}$$

$$A^{s}_{u(i,j+1)} = A^{s}_{u(i,j+1)} + C^{2}_{3} \quad \text{(C.34)}$$

$$A^{se}_{u(i,j+1)} = A^{se}_{u(i,j+1)} + C^{2}_{1} \quad \text{(C.35)}$$

$$A^{con}_{u(i,j+1)} = A^{con}_{u(i,j+1)} + D^{u}_{2} \quad \text{(C.36)}$$

With respect to node (i, j):

$$A^c_{u(i,j)} = A^c_{u(i,j)} - C^1_3 + C^2_3 - A_3 S^u_{p3} \quad (C.37)$$

$$A^e_{u(i,j)} = A^e_{u(i,j)} + C^1_1 - C^2_1 \quad (C.38)$$

$$A^n_{u(i,j)} = A^n_{u(i,j)} + C^1_2 - C^2_2 \quad (C.39)$$

$$A^{con}_{u(i,j)} = A^{con}_{u(i,j)} + D^u_3 \quad (C.40)$$

For the quad 2, type 2 element in Fig. 3.4e, the following coefficients can be evaluated when node 1 is node $(i+1, j)$, node 2 is node $(i, j+1)$, and node 3 is node $(i+1, j+1)$:
With respect to node $(i+1, j)$:

$$A^c_{u(i+1,j)} = A^c_{u(i+1,j)} - C^1_1 - A_1 S^u_{p1} \quad (C.41)$$

$$A^n_{u(i+1,j)} = A^n_{u(i+1,j)} + C^1_3 \quad (C.42)$$

$$A^{nw}_{u(i+1,j)} = A^{nw}_{u(i+1,j)} + C^1_2 \quad (C.43)$$

$$A^{con}_{u(i+1,j)} = A^{con}_{u(i+1,j)} + D^u_1 \quad (C.44)$$

With respect to node $(i+1, j+1)$:

$$A^c_{u(i+1,j+1)} = A^c_{u(i+1,j+1)} + C^1_3 - C^2_3 - A_3 S^u_{p3} \quad (C.45)$$

$$A^w_{u(i+1,j+1)} = A^w_{u(i+1,j+1)} - C^1_2 + C^2_2 \quad (C.46)$$

$$A^s_{u(i+1,j+1)} = A^s_{u(i+1,j+1)} - C^1_1 + C^2_1 \quad (C.47)$$

$$A^{con}_{u(i+1,j+1)} = A^{con}_{u(i+1,j+1)} + D^u_3 \quad (C.48)$$

With respect to node $(i, j+1)$:

$$A^c_{u(i,j+1)} = A^c_{u(i,j+1)} + C^2_2 - A_2 S^u_{p2} \quad (C.49)$$

$$A^{se}_{u(i,j+1)} = A^{se}_{u(i,j+1)} - C^2_1 \quad (C.50)$$

$$A^e_{u(i,j+1)} = A^e_{u(i,j+1)} - C^2_3 \quad (C.51)$$

$$A^{con}_{u(i,j+1)} = A^{con}_{u(i,j+1)} + D^u_2 \quad (C.52)$$

When these coefficients have been evaluated and assembled for every element in the calculation domain, the final form of the discretized x-momentum equation for each node is obtained as follows:

$$
\begin{aligned}
A^c_{u(i,j)} * u_{(i,j)} &= A^e_{u(i,j)} * u_{(i+1,j)} + A^{ne}_{u(i,j)} * u_{(i+1,j+1)} + A^n_{u(i,j)} * u_{(i,j+1)} \\
&+ A^{nw}_{u(i,j)} * u_{(i-1,j+1)} + A^w_{u(i,j)} * u_{(i-1,j)} + A^{sw}_{u(i,j)} * u_{(i-1,j-1)} \\
&+ A^s_{u(i,j)} * u_{(i,j-1)} + A^{se}_{u(i,j)} * u_{(i+1,j-1)} + A^{con}_{u(i,j)} \qquad \text{(C.53)}
\end{aligned}
$$

C.2.2 y-Momentum Equation

For the y-momentum equation, the integral of the flux across a control volume face k within an element is written as follows in Appendix B:

$$
\int_{face\,k} \vec{J}^k \cdot \vec{n}^k \, ds = C_1^k v_1 + C_2^k v_2 + C_3^k v_3 \qquad \text{(C.54)}
$$

and the elemental contribution to the volume integration of the source for the control volume around node j is given by:

$$
\int_{V_j} \mathcal{S}^v \, dV = A_j \left[(S_c^v)_j + \left(S_p^v\right)_j v_j + \frac{1}{det} \sum_{i=1}^{3} xmul_i \, p_i \right] \qquad \text{(C.55)}
$$

which can be rewritten more compactly as:

$$
\int_{V_j} \mathcal{S}^v \, dV = A_j \left(S_p^v\right)_j v_j + D_j^v \qquad \text{(C.56)}
$$

where

$$
D_j^v = A_j \left[(S_c^v)_j + \frac{1}{det} \sum_{i=1}^{3} xmul_i \, p_i \right] \qquad \text{(C.57)}
$$

As discussed in Appendix B, the C_i^k terms in the expression for the integrated flux across a control volume face k, Eq. C.54, are identical for both the x- and y-momentum equations. Therefore, the coefficients involving only C_i^k terms are identical for both x- and y-momentum equations and these coefficients do not need to be reevaluated. These coefficients include A_v^e, A_v^{ne}, A_v^n, A_v^{nw}, A_v^w, A_v^{sw}, A_v^s, and A_v^{se}. The remaining coefficients must be evaluated, because they include either pressure gradient or source terms which are unique to the y-momentum equation.

These coefficients are specified using the same procedures as for the x-momentum equation.

For the quad 1, type 1 element in Fig. 3.4b, the following coefficients can be evaluated when node 1 is node (i, j), node 2 is node $(i+1, j+1)$, and node 3 is node $(i+1, j)$:

With respect to node (i, j):

$$A^c_{v(i,j)} = A^c_{v(i,j)} - C^1_1 - A_1 S^v_{p_1} \tag{C.58}$$

$$A^{con}_{v(i,j)} = A^{con}_{v(i,j)} + D^v_1 \tag{C.59}$$

With respect to node $(i+1, j)$:

$$A^c_{v(i+1,j)} = A^c_{v(i+1,j)} + C^1_3 - C^2_3 - A_3 S^v_{p_3} \tag{C.60}$$

$$A^{con}_{v(i+1,j)} = A^{con}_{v(i+1,j)} + D^v_3 \tag{C.61}$$

With respect to node $(i+1, j+1)$:

$$A^c_{v(i+1,j+1)} = A^c_{v(i+1,j+1)} + C^2_2 - A_2 S^v_{p_2} \tag{C.62}$$

$$A^{con}_{v(i+1,j+1)} = A^{con}_{v(i+1,j+1)} + D^v_2 \tag{C.63}$$

For the quad 1, type 2 element in Fig. 3.4c, the following coefficients can be evaluated when node 1 is node (i, j), node 2 is node $(i+1, j+1)$, and node 3 is node $(i, j+1)$:

With respect to node (i, j):

$$A^c_{v(i,j)} = A^c_{v(i,j)} + C^1_1 - A_1 S^v_{p_1} \tag{C.64}$$

$$A^{con}_{v(i,j)} = A^{con}_{v(i,j)} + D^v_1 \tag{C.65}$$

With respect to node $(i+1, j+1)$:

$$A^c_{v(i+1,j+1)} = A^c_{v(i+1,j+1)} - C^2_2 - A_2 S^v_{p_2} \tag{C.66}$$

$$A^{con}_{v(i+1,j+1)} = A^{con}_{v(i+1,j+1)} + D^v_2 \tag{C.67}$$

With respect to node $(i, j+1)$:

$$A^c_{v(i,j+1)} = A^c_{v(i,j+1)} - C^1_3 + C^2_3 - A_3 S^v_{p_3} \tag{C.68}$$

$$A^{con}_{v(i,j+1)} = A^{con}_{v(i,j+1)} + D^v_3 \tag{C.69}$$

For the quad 2, type 1 element in Fig. 3.4d, the following coefficients can be evaluated when node 1 is node $(i+1, j)$, node 2 is node $(i, j+1)$, and node 3 is node (i, j):
With respect to node $(i+1, j)$:

$$A^c_{v(i+1,j)} = A^c_{v(i+1,j)} + C^1_1 - A_1 S^v_{p_1} \tag{C.70}$$

$$A^{con}_{v(i+1,j)} = A^{con}_{v(i+1,j)} + D^v_1 \tag{C.71}$$

With respect to node $(i, j+1)$:

$$A^c_{v(i,j+1)} = A^c_{v(i,j+1)} - C^2_2 - A_2 S^v_{p_2} \tag{C.72}$$

$$A^{con}_{v(i,j+1)} = A^{con}_{v(i,j+1)} + D^v_2 \tag{C.73}$$

With respect to node (i, j):

$$A^c_{v(i,j)} = A^c_{v(i,j)} - C^1_3 + C^2_3 - A_3 S^v_{p_3} \tag{C.74}$$

$$A^{con}_{v(i,j)} = A^{con}_{v(i,j)} + D^v_3 \tag{C.75}$$

For the quad 2, type 2 element in Fig. 3.4e, the following coefficients can be evaluated when node 1 is node $(i+1, j)$, node 2 is node $(i, j+1)$, and node 3 is node $(i+1, j+1)$:
With respect to node $(i+1, j)$:

$$A^c_{v(i+1,j)} = A^c_{v(i+1,j)} - C^1_1 - A_1 S^v_{p_1} \tag{C.76}$$

$$A^{con}_{v(i+1,j)} = A^{con}_{v(i+1,j)} + D^v_1 \tag{C.77}$$

With respect to node $(i+1, j+1)$:

$$A^c_{v(i+1,j+1)} = A^c_{v(i+1,j+1)} + C^1_3 - C^2_3 - A_3 S^v_{p_3} \tag{C.78}$$

$$A^{con}_{v(i+1,j+1)} = A^{con}_{v(i+1,j+1)} + D^v_3 \tag{C.79}$$

With respect to node $(i, j+1)$:

$$A^c_{v(i,j+1)} = A^c_{v(i,j+1)} + C^2_2 - A_2 S^v_{p_2} \tag{C.80}$$

$$A^{con}_{v(i,j+1)} = A^{con}_{v(i,j+1)} + D^v_2 \tag{C.81}$$

When these coefficients have been evaluated and assembled for every element in the calculation domain, the final form of the discretized y-momentum equation for each node is obtained as follows:

$$\begin{aligned} A^c_{v(i,j)} * v_{(i,j)} &= A^e_{v(i,j)} * v_{(i+1,j)} + A^{ne}_{v(i,j)} * v_{(i+1,j+1)} + A^n_{v(i,j)} * v_{(i,j+1)} \\ &+ A^{nw}_{v(i,j)} * v_{(i-1,j+1)} + A^w_{v(i,j)} * v_{(i-1,j)} + A^{sw}_{v(i,j)} * v_{(i-1,j-1)} \\ &+ A^s_{v(i,j)} * v_{(i,j-1)} + A^{se}_{v(i,j)} * v_{(i+1,j-1)} + A^{con}_{v(i,j)} \end{aligned} \tag{C.82}$$

C.3 Assembly of the Continuity Equations

In Appendix B, the integral of the mass flux across a control volume face k within an element is written as follows:

$$\int_{face\,k} \vec{g}^k \cdot \vec{n}^k \, ds = E^k_1 p_1 + E^k_2 p_2 + E^k_3 p_3 + B^k \tag{C.83}$$

Equation C.83 for the continuity equation is similar in form to equation C.1 for the x-momentum equation, therefore, the discretized form of the continuity equation may be assembled in the same manner as the discretized momentum equations.

For the quad 1, type 1 element in Fig. 3.4b, the following coefficients can be evaluated when node 1 is node (i, j), node 2 is node $(i+1, j+1)$, and node 3 is node $(i+1, j)$:

With respect to node (i, j):

$$A^c_{p(i,j)} = A^c_{p(i,j)} - E^1_1 \tag{C.84}$$

$$A^e_{p(i,j)} = A^e_{p(i,j)} + E^1_3 \tag{C.85}$$

$$A^{ne}_{p(i,j)} = A^{ne}_{p(i,j)} + E^1_2 \tag{C.86}$$

$$A^{con}_{p(i,j)} = A^{con}_{p(i,j)} + B^1 \tag{C.87}$$

With respect to node $(i+1, j)$:

$$A^c_{p(i+1,j)} = A^c_{p(i+1,j)} + E^1_3 - E^2_3 \tag{C.88}$$

$$A^n_{p(i+1,j)} = A^n_{p(i+1,j)} - E^1_2 + E^2_2 \tag{C.89}$$

$$A^w_{p(i+1,j)} = A^w_{p(i+1,j)} - E^1_1 + E^2_1 \tag{C.90}$$

$$A^{con}_{p(i+1,j)} = A^{con}_{p(i+1,j)} - B^1 + B^2 \tag{C.91}$$

With respect to node $(i+1, j+1)$:

$$A^{c}_{p(i+1,j+1)} = A^{c}_{p(i+1,j+1)} + E^{2}_{2} \tag{C.92}$$

$$A^{sw}_{p(i+1,j+1)} = A^{sw}_{p(i+1,j+1)} - E^{2}_{1} \tag{C.93}$$

$$A^{s}_{p(i+1,j+1)} = A^{s}_{p(i+1,j+1)} - E^{2}_{3} \tag{C.94}$$

$$A^{con}_{p(i+1,j+1)} = A^{con}_{p(i+1,j+1)} - B^{2} \tag{C.95}$$

For the quad 1, type 2 element in Fig. 3.4c, the following coefficients can be evaluated when node 1 is node (i, j), node 2 is node $(i+1, j+1)$, and node 3 is node $(i, j+1)$:
With respect to node (i, j):

$$A^{c}_{p(i,j)} = A^{c}_{p(i,j)} + E^{1}_{1} \tag{C.96}$$

$$A^{ne}_{p(i,j)} = A^{ne}_{p(i,j)} - E^{1}_{2} \tag{C.97}$$

$$A^{n}_{p(i,j)} = A^{n}_{p(i,j)} - E^{1}_{3} \tag{C.98}$$

$$A^{con}_{p(i,j)} = A^{con}_{p(i,j)} - B^{1} \tag{C.99}$$

With respect to node $(i+1, j+1)$:

$$A^{c}_{p(i+1,j+1)} = A^{c}_{p(i+1,j+1)} - E^{2}_{2} \tag{C.100}$$

$$A^{w}_{p(i+1,j+1)} = A^{w}_{p(i+1,j+1)} + E^{2}_{3} \tag{C.101}$$

$$A^{sw}_{p(i+1,j+1)} = A^{sw}_{p(i+1,j+1)} + E^{2}_{1} \tag{C.102}$$

$$A^{con}_{p(i+1,j+1)} = A^{con}_{p(i+1,j+1)} + B^{2} \tag{C.103}$$

With respect to node $(i, j+1)$:

$$A^{c}_{p(i,j+1)} = A^{c}_{p(i,j+1)} - E^{1}_{3} + E^{2}_{3} \tag{C.104}$$

$$A^{s}_{p(i,j+1)} = A^{s}_{p(i,j+1)} + E^{1}_{1} - E^{2}_{1} \tag{C.105}$$

$$A^{e}_{p(i,j+1)} = A^{e}_{p(i,j+1)} + E^{1}_{2} - E^{2}_{2} \tag{C.106}$$

$$A^{con}_{p(i,j+1)} = A^{con}_{p(i,j+1)} + B^{1} - B^{2} \tag{C.107}$$

For the quad 2, type 1 element in Fig. 3.4d, the following coefficients can be evaluated when node 1 is node $(i+1, j)$, node 2 is node $(i, j+1)$, and node 3 is node (i, j):

With respect to node $(i+1, j)$:

$$A^{c}_{p(i+1,j)} = A^{c}_{p(i+1,j)} + E^{1}_{1} \tag{C.108}$$

$$A^{nw}_{p(i+1,j)} = A^{nw}_{p(i+1,j)} - E^{1}_{2} \tag{C.109}$$

$$A^{w}_{p(i+1,j)} = A^{w}_{p(i+1,j)} - E^{1}_{3} \tag{C.110}$$

$$A^{con}_{p(i+1,j)} = A^{con}_{p(i+1,j)} - B^{1} \tag{C.111}$$

With respect to node $(i, j+1)$:

$$A^{c}_{p(i,j+1)} = A^{c}_{p(i,j+1)} - E^{2}_{2} \tag{C.112}$$

$$A^{s}_{p(i,j+1)} = A^{s}_{p(i,j+1)} + E^{2}_{3} \tag{C.113}$$

$$A^{se}_{p(i,j+1)} = A^{se}_{p(i,j+1)} + E^{2}_{1} \tag{C.114}$$

$$A^{con}_{p(i,j+1)} = A^{con}_{p(i,j+1)} + B^{2} \tag{C.115}$$

With respect to node (i, j):

$$A^{c}_{p(i,j)} = A^{c}_{p(i,j)} - E^{1}_{3} + E^{2}_{3} \tag{C.116}$$

$$A^{e}_{p(i,j)} = A^{e}_{p(i,j)} + E^{1}_{1} - E^{2}_{1} \tag{C.117}$$

$$A^{n}_{p(i,j)} = A^{n}_{p(i,j)} + E^{1}_{2} - E^{2}_{2} \tag{C.118}$$

$$A^{con}_{p(i,j)} = A^{con}_{p(i,j)} + B^{1} - B^{2} \tag{C.119}$$

For the quad 2, type 2 element in Fig. 3.4e, the following coefficients can be evaluated when node 1 is node $(i+1, j)$, node 2 is node $(i, j+1)$, and node 3 is node $(i+1, j+1)$:

With respect to node $(i+1, j)$:

$$A^{c}_{p(i+1,j)} = A^{c}_{p(i+1,j)} - E^{1}_{1} \tag{C.120}$$

$$A^{n}_{p(i+1,j)} = A^{n}_{p(i+1,j)} + E^{1}_{3} \tag{C.121}$$

$$A^{nw}_{p(i+1,j)} = A^{nw}_{p(i+1,j)} + E^{1}_{2} \tag{C.122}$$

$$A^{con}_{p(i+1,j)} = A^{con}_{p(i+1,j)} + B^{1} \tag{C.123}$$

With respect to node $(i+1, j+1)$:

$$A^{c}_{p(i+1,j+1)} = A^{c}_{p(i+1,j+1)} + E^{1}_{3} - E^{2}_{3} \tag{C.124}$$

$$A^{w}_{p(i+1,j+1)} = A^{w}_{p(i+1,j+1)} - E^{1}_{2} + E^{2}_{2} \tag{C.125}$$

$$A^{s}_{p(i+1,j+1)} = A^{s}_{p(i+1,j+1)} - E^{1}_{1} + E^{2}_{1} \tag{C.126}$$

$$A^{con}_{p(i+1,j+1)} = A^{con}_{p(i+1,j+1)} - B^{1} + B^{2} \tag{C.127}$$

With respect to node $(i, j+1)$:

$$A^{c}_{p(i,j+1)} = A^{c}_{p(i,j+1)} + E_2^2 \tag{C.128}$$

$$A^{se}_{p(i,j+1)} = A^{se}_{p(i,j+1)} - E_1^2 \tag{C.129}$$

$$A^{e}_{p(i,j+1)} = A^{e}_{p(i,j+1)} - E_3^2 \tag{C.130}$$

$$A^{con}_{p(i,j+1)} = A^{con}_{p(i,j+1)} - B^2 \tag{C.131}$$

When these coefficients have been evaluated and assembled for every element in the calculation domain, the final form of the discretized continuity equation for each node is obtained as follows:

$$\begin{aligned} A^{c}_{p(i,j)} * p_{(i,j)} &= A^{e}_{p(i,j)} * p_{(i+1,j)} + A^{ne}_{p(i,j)} * p_{(i+1,j+1)} + A^{n}_{p(i,j)} * p_{(i,j+1)} \\ &+ A^{nw}_{p(i,j)} * p_{(i-1,j+1)} + A^{w}_{p(i,j)} * p_{(i-1,j)} + A^{sw}_{p(i,j)} * p_{(i-1,j-1)} \\ &+ A^{s}_{p(i,j)} * p_{(i,j-1)} + A^{se}_{p(i,j)} * p_{(i+1,j-1)} + A^{con}_{p(i,j)} \end{aligned} \tag{C.132}$$